Impact and water jet impact of high performance thermoplastics

Gentilcore, G.

Award date:
1992

Awarding institution:
University of Bath

Impact and Water Jet Impact of High Performance Thermoplastics.

submitted by G.Gentilcore

for the degree of PhD

of the University of Bath

1992.

ProQuest LLC
789 East Eisenhower Parkway
P.O. Box 1346
Ann Arbor, MI 48106-1346

Summary of dissertation.

The impact and liquid impact properties of three engineering thermoplastics (PEEK, PEK and PET) have been investigated by using the liquid jet impact technique and a method for quantitatively analysing the damage, namely, a Charpy type impact tester.

The liquid impact performance and some associated fracture properties have been investigated. A loss of toughness of PEEK (more prominent at higher levels of crystallinity) and PET occurs under single and multiple liquid impact. For PEK however, a loss in toughness was only observed at high liquid impact velocities after numerous impacts. These differences especially between PEEK and PEK were not apparent in characterising the polymers by using mechanical and viscoelastic measurements except when investigating the notched impact performance. Again PEK was shown to offer a greater resistance to fracture and it has been proposed that this occurs as a result of the addition of a processing aid (PTFE in fine powder form), which may act in a similar manner to the rubber modification of a glassy plastic.

Two types of failure mode have been observed where damage resulting from a single impact results in the formation of a cone crack surrounding a central damage zone resembling a half penny type crack. In the case of multiple impact, what has been referred to as 'crumbling' has been observed. The formation of this crumbled zone has been used to explain the induction period before the onset of erosion when measuring performance using the whirling arm techniques.

Components in service, that are subjected to liquid impact may simultaneously be subjected to elevated temperatures. The use of the Charpy type tester in analysing the post-liquid impact on increasing temperatures has revealed no loss in toughness after the impact event, although the extent of surface damage seen as plastic deformation has increased significantly. No evidence of thermal shock was observed at the temperatures chosen for investigation.

Acknowledgements

The work presented in this dissertation was performed under the supervision of Prof. B. Harris to whom I am very grateful for his interest, advice and constant support throughout the course of this work.

I would also like to thank Dr. J. M. Senior of the Department of Health, for giving me his time as well as support and encouragement in acting as my industrial supervisor.

In addition I would like to thank Raychem Ltd and Scimat Ltd for financial support and technical assistance.

Last but not least I would like to take this opportunity to thank my wife for her patience and invaluable support.

The work presented here is original except where otherwise stated and includes nothing which is the result of work done in collaboration. This dissertation has not been submitted for a degree at any other university.

April 1992

CONTENTS

6.Conclusions and suggestions for future work.

CHAPTER 1
LIQUID IMPACT EROSION

1.0.0 Introduction.

The use of reinforced plastics in aerospace components has been an important step forward in the design of aircraft and missiles because of the good balance of properties achieved coupled with a marked decrease in the weight of the component.

During flight the components are subjected to many natural hazards such as atmospheric radiation, wind gusts, wind shear, lightening strike, static electricity and impacts from ice, hailstones, birds and other forms of debris. An aspect of the impact phenomenon which has attracted a great deal of attention is the impact of the component by a liquid, from raindrops or moisture present in clouds, for example. Because of the mode of failure of the component by an impacting and erosive process, the special problem of liquid impact erosion is an important design criterion for the aerospace engineer.

The importance of liquid impact erosion first became apparent in 1945 (1,2), where United States Air Force personnel reported severe damage of a glass fibre reinforced plastic radar housing of a B-29 Superfortress when flown through a particularly heavy rainfall, on missions from the Mariana Islands to Japan. Further investigations established that water drops free from any abrasive particles on collision with such materials would result in damage.

Much of the pioneer work was carried out by the Cornell Aeronautical Laboratories (3), who were sponsored by the United States Air Force. A Convair

Delta Dart F-106A aircraft was flown through thunderstorms at supersonic speeds and damage by liquid impact was detected on the following parts; rivet heads, leading edges of wings, aluminium nose cone, cockpit canopy frame and of course the radome.

The problems encountered when flying through rain are enhanced with increased flight speed and with aerodynamic heating of the component associated with supersonic flight.

1.0.1 Materials used for aircraft and missile components.

Classes of materials used where liquid impact erosion is a major concern include (4);

a) Elastomeric coatings and reinforced plastics for radome and antenna covers. Radome erosion problems are primarily subsonic, because aircraft try to avoid supersonic flight in rain enviroments. However, in more advanced systems, and particularly in the case of missiles, this is not always possible. Protective coatings which are elastomeric (low modulus, high elongation) have been found to provide the best protection. The most common types of coatings are polyurethane or fluorocarbon based. These are generally 0.3 to 0.4mm (5) in thickness and are usually applied as a spray over reinforced plastic components.

b) Ceramic (fused silica to alumina) radomes or caps are used with or in lieu of plastic radomes. These are limited because of their inherent brittleness, thermal mismatch problems and structural weaknesses. The ceramics are used when flight speeds are of the order of mach 3.0 and above, and are the only

solution to the severe problems of erosion and temperature limitations of standard constructions (6).

c) Optically guided missiles use glass radomes and if these become pitted or frosted by erosion, visual acquisition of the target will be hampered. Further erosion may lead to catastrophic failure.

d) Infra-red window housings, such as those using zinc selenide for the 8-12 μm infra red range (7), lose their transmission characteristics because of internal cracking and extensive surface damage.

e) Transparent materials such as acrylics and polycarbonates, which are used as aircraft canopies and windshields, also lose transmission as a result of frosting of the component.

f) Ablative plastics such as Teflon, graphite and composites such as quartz reinforced silica and carbon fibre reinforced carbon are used for ballistic missiles. On re-entry, and at the high velocities subsequent to re-entry, erosion occurs as actual removal of material which can lead to serious malfunctions.

Table 1.1 (4), outlines the enviromental conditions under which various systems, of which some have been described above, are required to perform.

1.0.2 Radomes.

Although all forward facing components of aircraft are at risk, the radome itself is generally the component at the forefront of research because of its position on the aircraft.

A radome can be described as a cover for radar transmitting and receiving antennae which allows

microwave transmission and reception with minimum distortion and loss, whilst providing adequate enviromental protection. The basic design of a radome falls into two categories, the solid wall, such as the Concorde nose radome, and the sandwich wall, as used by the Sea Harrier, see figure 1.2.

The solid wall radome is generally of narrow band or single frequency and is stronger and heavier than the sandwich construction. The lighter weight sandwich radome is generally utilised for civil aircraft, but because of its broadband frequency range has important applications to military aircraft and missiles.

The use of polymers in the construction of radomes has been common for many years (6). Typically, high performance thermosetting resins are used as the matrix with various forms of fibre reinforcement (8), (see table 1.3). Hitherto, thermoplastic materials have found few applications and are limited to small radomes at modest temperature regimes. Nevertheless thermoplastics have excited the industry because of their ease of application and attractive dielectric properties, and, especially, because of the increased thermal performances available.

1.0.3. Present work.

The thermoplastics which are generating most interest are the polyarylates such as polyethersulphone (PES), polyetherimide (PEI) and, in particular, polyetheretherketone (PEEK). Raychem Ltd, a high technology company noted for its high

performance cross-linked wire and cable and heat shrinkable products, have a number of patents for the synthesis of a whole range of high temperature, semi-crystalline thermoplastic polymers. One of these patents illustrates the procedure for the manufacture of polyetherketone (PEK). This patent has now been sold to BASF who are marketing the polymer under the tradename of "Ultrapek".

The work detailed in this dissertation is centred upon the mechanical properties of PEK and, their importance to liquid impact erosion processes. As opportunities exist in the aerospace market, a material which has been generating a great deal of interest, namely PEEK, manufactured by ICI under the tradename of "Victrex" PEEK, will be used as a comparator. As these polymers are relatively new, it was considered important to judge these against a well studied thermoplastic and so polyethylene terephthalate was introduced into the experimental investigations.

The phenomenon of liquid impact erosion is found not only to occur with forward facing components of aircraft flying through rain enviroments but is also a major problem where aircraft or vehicles generate their own rainstorms, such as rotor blades of helicopters and hovercrafts. Similar damage is observed when vapour bubbles in a turbulent liquid stream collapse at the component surface. This `cavitation' effect is a major concern for the Naval engineer in the design of ships propellers.

Table 1.1 (4). Enviromental exposure of aerospace components.

Component	Enviroment
Fibre reinforced aircraft radomes	Subsonic rain
Fibre reinforced or ceramic missile radomes	Supersonic rain and higher temperatures
Transparent plastic canopies and windshields	Subsonic rain and ice
Aircraft leading edges	Subsonic rain
Re-entry vehicle nose tips, heat shields and antenna windows	Hypersonic rain, dust and ice

Table 1.3. Types of fibre reinforcement used for resins in the construction of a radome, (9).

Resin	Reinforcement
Polyester Epoxy Polyimide	E glass filament wound
Polyester Epoxy Polyimide	E glass cloth
Polyester Epoxy Polimide	Quartz cloth
Polyester Epoxy Polyimide	Kevlar (Aromatic polyamide)

1.1.0. The liquid impact erosion process.

The first consideration to be made of the factors influencing the impact of a liquid with a solid and, more importantly, of plastic components subjected to rain, must be of rainfall itself. The rainfall parameters can be split into two areas; the intensity of the rain and the nature of the raindrops themselves.

(i) Rainfall intensity.

A wide range of rainfall intensities occur and the severity of rain encountered by the component, whatever the material used, is critical if it is to be effective as a protective structure. The following table illustrates these rainfall ranges.

Type of rainfall	Intensity
Drizzle	0-0.1 in/hr
Moderate to heavy	0.1-0.5 in/hr
Tropical rain and thunderstorms	0.5-1.0 in/hr

(ii) Raindrops.

The shape and size of a drop will influence the the extent of damage when it collides with the component. Raindrop shapes have been found to (10) oscillate about a preferred shape, usually oblate through spherical to prolate spheroid. The shape depends upon the size of the drop and factors such as wind conditions. The size of the drop covers a wide distribution, usually in the range of 0.25-7.0mm in diameter. The larger the raindrop present in the rainfall distribution the greater the extent of damage. The raindrops will be distorted by aerodynamic effects, ie the raindrop will flatten resulting in a larger diameter when passing through

Figure 1.2. The construction of a Radome.

(i) Solid wall radome - a continuous fibre reinforcement of a resin matrix.

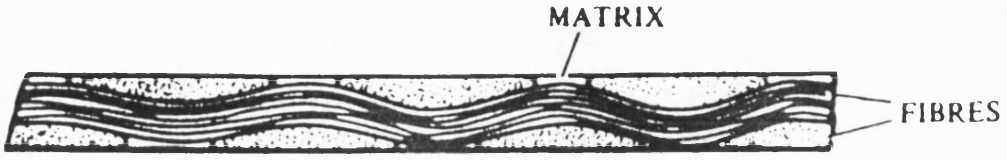

(ii) Sandwich radome - constructed using a low dielectric constant core, usually a foamed or honeycomb structure between thin fibre reinforced skins.

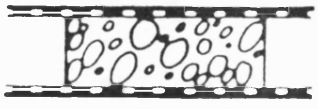
SYNTACTIC CORE

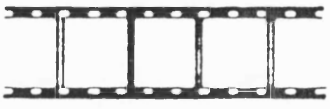
HONEYCOMB CORE

the shockwave of a rapidly moving body.

1.1.1. Impact between a liquid and a solid.

When a liquid mass impacts on a solid body, two distinct regimes of behaviour exist;

(i) The initial stage during which very high pressures are generated as a result of the compressible behaviour of the liquid. This period of high pressure continues as long as the contact area between the impacting drop and the solid expand supersonically with respect to the shockwaves in the liquid. The duration of this period depends upon the impact velocity and the drop radius.

(ii) The second stage of the impact process is met when the shockwaves generated by the impact move up the free surface of the drop. Lateral jetting begins and the impact pressure drops to much lower values, usually as low as 10% of the original pressure. This drop in pressure occurs when incompressible flow within the water drop is reached.

These distinct regimes of behaviour can be described by the following equations. The initial high pressure stage, for impact of a compressible target leads to the waterhammer pressure which is given by (11);

$$P = v.[p_1C_1p_2C_2 \div (p_1C_1 + p_2C_2)] \qquad 1.$$

where v is the impacting velocity and $p_{1,2}$ and $C_{1,2}$ are the densities and shock wave velocities of the liquid and solid respectively. In the case of a rigid target this equation reduces to (12);

$$P = p_1C_1v \qquad 2.$$

For most structural materials $p_2C_2 >> p_1C_1$ and thus equation 2 will give a sufficiently accurate determination of the pressure.

The initial compressible flow stage is followed by the incompressible flow stage. Here the pressure drops to the Bernoulli stagnation pressure;

$$P_B = \tfrac{1}{2}p_1v^2 \qquad 3.$$

It is during this stage that jetting occurs. The water hammer equation can be used directly to find the maximum pressure when a jet (from liquid jet apparatus) collides with a rigid surface (13). Although there is no physical restraint to prevent sideways flow in a jet, a finite time will elapse before release waves move in to the centre of the column.

The value of P found experimentally for a water jet with a velocity of 720m/s and a compression wave velocity of 1500m/s was 95 kg/mm^2 (13), compared to a theoretical value of 110 kg/mm^2. The experimental value was found to be smaller as a result of the jet geometry. The end of the jet is curved and so is not parallel to the target surface (an assumption made for the above equations), but agreement between the two values is reasonable.

The decay of the peak load should approximately equal the time taken for the release waves to move in from the boundaries of the jet and set up radial flow. The decay times are found to be of the order of 2-3 μs, whereas theoretically the decay time should be of the order of 1.5 μs (13). Again this

difference was a result of the jet geometry in comparison to a rain drop.

The tangential flow, or the flow of liquid along the surface of the target solid was found to be 2-3 times that of the impact velocity. Theory suggests that for a flat-ended jet striking perpendicularly, the velocity of flow along the surface of the solid, should equal the impacting velocity. The increase in velocity is again attributed to the geometry of the jet head by virtue of the fact that as the flow velocity from under the sloping surface is the sum of the velocity at which the junction of the liquid and jet move outwards. For a two dimensional case of flow using the simpler geometry of a wedge fronted jet, the radial velocity V_R, from under the wedge is given by (13);

$$V_R = V \cot(\tfrac{1}{2}\alpha) \qquad 4.$$

where V is the impacting velocity and α is the angle which the sloping face of the jet makes with the surface. As this angle tends towards zero, the momentum and mass of the liquid tends towards zero.

The contact between a spherical drop and a solid is made at one point and then the contact area grows as the impact process continues. The shockfront generated by the impact is domed and there is a radial component of particle motion followed by a gross lateral spreading flow. The effect of the 'roundness' of the drop and the dependence of pressure upon the shockwave velocity are significant. The water hammer equation underestimates the actual peak impact pressure by a factor of approximately three (14). It was later found that the pressures

generated during liquid drop impingement are even higher than previousely estimated and that these pressures could be higher than the yield stress of some of the toughest materials (15).

The pressures are uniform and do equal pCv at the first instant of contact, but their magnitude at the perimeter increases as the impact progresses and the angle of contact between the liquid and the solid increase (16), see figure 1.4.

This increase will occur when the ring expansion becomes subsonic with respect to the velocity of sound in the compressed region, allowing the shockwave to become detached and travel into the body of the drop. The pressure in this compressed region is then relieved by high velocity lateral jetting and the maximum pressure obtained during the drop impact is found in a ring surrounding the centre of the impact zone. In practice the damage produced from impact with a water droplet is characterised by a ring of pronounced cracking and deformation, and will be discussed more fully below.

1.2.0. Damage mechanisms.

When a drop of water collides with a solid surface at high velocity, the resultant high pressures will result in damage of some form. The damage is caused by the shear and tensile forces produced as a result of the localised compression. The nature of the damage is dependent upon the angle with which the water drop impacts the target material (17), but for the purpose of this dissertation only impact at normal incidence ie 90° to the surface of

Figure 1.4. Schematic representation of a water drop impacting a rigid surface.

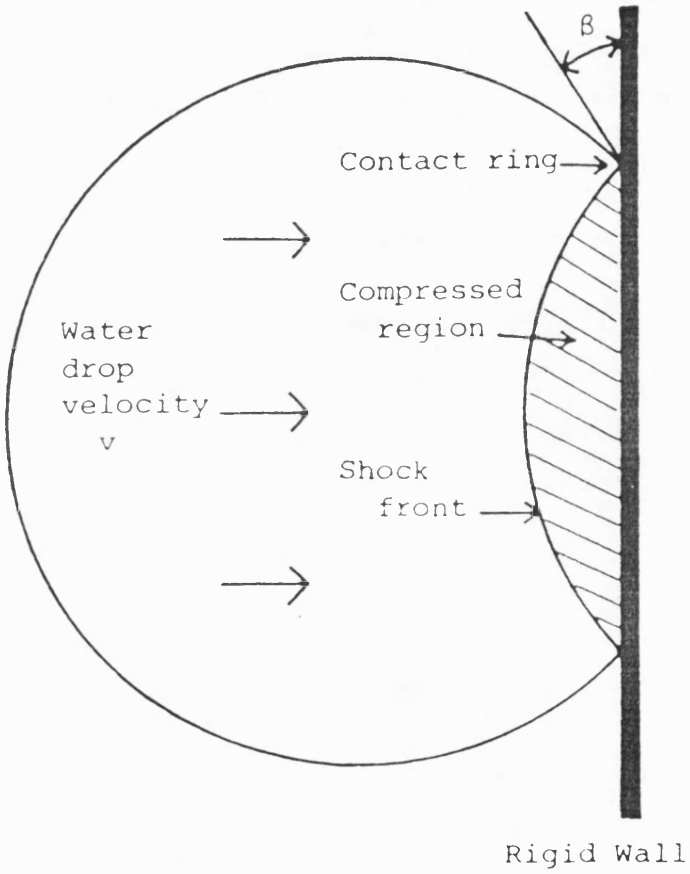

the solid will be considered.

The types of failure that have been observed are listed and described as follows;

(i) Circumferential surface fracture.

This mode of failure is generally observed in brittle materials but may also occur with polymers which are ductile at low strain rates but behave in a brittle manner at the strain rates encountered during an impact process. Circumferential fractures will occur when radial tensions, resulting from the high pressures generated during liquid impact, exceed the breaking strength of the material. In the area under direct pressure loading, all surface stresses are compressive and do not result in surface fractures. This explains the characteristic nature of damage from water drops observed as circumferential cracking surrounding an undamaged zone.

(ii) Subsurface flow and fracture.

This mode of failure is mainly observed in rigid polymers such as polymethylmethacrylate. It is essentially caused by plastic flow along the trajectories of maximum shear. When the short, intense stress pulse passes through the solid, the solid is unable to deform and relieve the stresses quickly enough and so the stresses are relieved by the formation of cracks.

(iii) Large scale plastic deformation.

Here permanent deformation of the impact zone is observed and the resultant surface depression is likened to pushing a steel ball bearing into the surface of the target solid.

(iv) Shear deformation around the periphery of the impact zone.

Two types of shear deformation occur.

a) Depending upon the mechanical strength of the target solid, the shearing action results in a wavy appearence in metals to a severely torn surface in polymers such as polyethylene.

b) Localised shearing along surface discontinuities such as cracks or scratches will result in the opening up of these surface defects enhancing the damage appearance.

(v) Failure because of reflection and interference of stress waves.

Reflection of the initial compression pulse in the free boundaries of the solid specimen can result in large fractures at points away from the impact zone. The waves are similar to those produced by detonating an explosive charge at the surface of a specimen and the resultant fracture patterns are almost identical.

A more detailed explanation of the characteristic ring cracks is proposed as a result of the interaction of Rayleigh surface stress waves with any flaws present on the target solid surface (18). The initiation of cracks or the propagation of new cracks or existing flaws is likened to the behaviour of a solid under an indentor such as the Vickers diamond used for hardness measurements (19). When a specimen is loaded, the initial contact prior to failure is either plastic or elastic, depending upon the type of indentor used, sharp , blunt or spherical. The pre-present surface flaws experience an ever increasing tensile stress until a flaw becomes critical and develops into a crack. This is independent of the flaw characteristic, provided that

the density of flaws is high. Spherical indentors can produce a work hardening or densification of the surface and can even result in plastic deformation causing a surface depression. On unloading lateral cracks may form because of elastic/plastic mismatches in the stress field and they will extend sideways towards the surface.

1.3.0. Test techniques available for the determination of erosion by a water drop.

The need to evaluate materials as protective coatings against enviromental damage and, in particular, against damage caused by rain, has developed a wide variety of techniques. If the presence of rainfall could be more accurately predicted, and its characteristics measured under test conditions, then there would be no substitute for in-flight testing. As this is not always possible or available to many engineers and scientists, the evaluation of materials is carried out under simulated rainfall conditions. The techniques used can be divided into two categories; multiple impact studies for the classification of materials and the components made from them and single impact studies, which are more academic in nature and are used to understand the mechanisms of failure of the materials.

1.3.1. Multiple impact measurements.

These measurements employ standard rainfall conditions as natural rainfall can only be broadly defined on the basis of intensity and drop size. By means of this technique, the information obtained will allow a prediction to be made of the service

life of the material or component under investigation. Experimental parameters can be set to observe the influence of velocity, drop size, intensity, impact angle and any constructional or design changes to the component.

There are two basic approaches to multiple impact testing: a whirling arm technique, where the test piece is rotated at high speed through a simulated rainfall (20) in which velocities of up to 1000m/s can be achieved and, secondly, a rocket sled technique, developed to overcome the limitations of the whirling arm, where only small sized test pieces can be used. Here the test specimen is accelerated by a rocket powered sled along a track into a simulated rainfall (21), at velocities approaching 1500m/s.

1.3.2. Single impact measurements.

More fundamental measurements of the erosion process and failure mechanisms can be investigated by using impact from a single water droplet, especially when used in combination with a fast frame camera. A more detailed account of measurements using this technique will be discussed in chapter 3.0, as this is the method employed for investigations presented in this dissertation.

1.3.3. Assessment of damage caused by liquid impact erosion.

There are no standard 'degrees of erosion', so that each component available for the intended application must be rated according to its individual functional requirement. For example the leading edge

of a wing may lose up to half its thickness before it is considered to be severely damaged while the loss of a few thousandths of an inch in thickness will impair the microwave characteristics of a radome, and superficial frosting of a windshield in flight can prove disastrous.

Rain erosion resistance can be defined as the time under standard conditions of speed and rainfall required to produce detectable or structural damage. Qualitatively, the progress of rain erosion can be monitored as weight loss measurements in combination with visual examination of the specimen with respect to its surface texture, amount of erosion or wear, penetration of erosion to a certain depth and detection of structural erosion. In general, measurements are published as the time taken to erode through the protective coating to the laminate, or an arbitary depth, but more commonly appear as weight loss measurements under the standard conditions.

Analysis of the mechanisms of erosion have been published which were based on single liquid impact studies in optically clear polymers such as polymethylmethacrylate or the use of various glasses (13,18,26), where the stress concentrations and stress patterns can be observed by high speed photography and the resultant damage can be carefully examined with microscope techniques. Quantitative information has been obtained from single impact studies by using the hydraulic test technique (7), and by quoting the `threshold velocity', which is the velocity below which no erosion damage can be detected, which is useful for both single and

multiple impact studies.

1.4.0. Liquid impact damage of materials.

This section will concentrate on the information available on the behaviour of polymers but will include some assessments of the damage of such materials as ceramics to place the section into context.

As an introduction to this section, table 1.5 contains a summary of the requirements for erosion resistant materials for the aerospace application. It gives a clear insight into the extremes of material performance required to meet the demanding pressures of an erosion resistant protective component.

Before even entering upon a discussion of choosing the material type for the intended application, certain design features need to be understood. The geometry of the component plays an important part, where the general rule of minimising the angle of impact applies. This has an overall effect of reducing the effective impact velocity. An exception to this rule has been observed (28), where it has been suggested that angles of 10-30° should be avoided since erosion damage can be increased. No explanation for this has been proposed.

The component must be produced in such a way as to give a very high quality of surface finish, by machining or polishing. This improvement in surface finish will limit the presence of flaws, which reduces initiation of damage sites and thereby

Table 1.5. Summary of erosion requirements (2)

System	Time @ speed	Max. temp
AIRCRAFT RADOME PROTECTION (DIELECTRIC TRANSMISSION REQUIRED)		
1. Present tactical support aircraft	120mins @ 220 m/s	110°C
2. Improved tactical support aircraft	30 mins up to Mach 2.o	260°C
3. Mach 3.0 interceptor	120mins @ Mach 0.9 + 60 @ 1.5	340°C
4. Mach 3.0 Transport	60mins @ Mach 1.0	340°C
TACTICAL MISSILE RADOMES AND I.R. DOMES		
5. High performance missile (up to Mach 6.0)	30secs @ Mach 6.0	1100°C
6. Optical missile	120mins @ 220 m/s	260°C
HELICOPTER ROTOR BLADE PROTECTION		
7. Military helicopter	10hrs in sand @ 240 m/s + 10hrs in rain @ 240 m/s	95°C
JET ENGINE PROTECTION		
8. Turbine engine compressors	60mins in dust, tip speeds up to Mach 1.25 + 60 mins in rain, speeds up to Mach 1.25	300°C
RE-ENTRY VEHICLE PROTECTION		
9. Nose tip, heat shield and antenna window	sufficiently low mass loss up to Mach 10 in rain or ice crystals	3300°C

increases erosion resistance. Many other features play an important role, such as choice of underlying structure, foamed or honeycomb, and these criteria must be fully understood in any investigation of the erosion resistance of materials. This dissertation is restricted to the investigation of the matrix materials, but it is necessary to mention that other factors are involved when tackling the problem of providing erosion resistant materials for aerospace applications, and indeed some applications may involve the use of an unreinforced plastic.

A summary of the types of materials used is listed below.

(i) Plastic laminates such as glass fibre reinforced epoxies give inadequate protection when used on their own. The resin used is not usually chosen for its erosion resistance but for its high-temperature performance and electrical properties. Additives can have a deleterious effect, for example the use of alumina or titanium dioxide to improve electrical properties (25). It is important in the construction process to control void formation and dry spots, and to ensure that the surface has a high concentration of the resin. As has already been mentioned some applications require unreinforced plastics, where very short flight times are encountered, such as those envisaged for short-range missiles. Polyethylene, with its very good dielectric properties, is a possibility as are polymers such as polyphenylene oxide and polyetheretherketone for their excellent rain erosion resistance.

(ii) The use of coatings to absorb some of the energy of impact is widely used in the industry. They are

generally elastomeric in nature but some inorganic coatings of a ceramic or electrodeposited metal have also been employed (1). A great deal of work has been carried out in providing a protective elastomeric coating mainly on the use of polyurethane or fluorocarbon based sprays and paints (4,22,23,24). It is important for the coating to have strong adhesion to the component and to obtain an optimum coating thickness, since too thin a coating will offer no real protection and too thick a coating will impair the electrical properties. The ability to carry out repair work quickly is advantageous for these coatings.

(iii) Glasses are nominally high-strength materials but are sensitive to notches and flaws, and are susceptible to time-dependent crack propagation. Usually a loss in optical clarity is observed before any loss in structural integrity. Some improvements have been made with chemically-toughened and heat treated glasses to give better resistance. Glasses used for infra-red transmission such as zinc selenide offer poor resistance while sapphire offers performance equalled only by ceramics and metals.

(iv) Ceramics and glass ceramics offer excellent overall performances, with high-temperature properties exceeding those of all the alternatives. They do suffer however from their inherently brittle behaviour.

(v) Metals provide good protection but are rarely used owing to their high strength to weight relationship, relative to that of glass fibre reinforced plastics and ceramics.

Table 1.6, illustrates the differing

Table 1.6. Rain erosion performance of materials using the whirling arm technique at a velocity of 225m/s with a rainfall intensity of 25mm/hour, (2).

Material	Erosion time	Comments
GFRP laminate	5-15 mins	Severe erosion removal of layers
GFRP laminate + PU protection	0.25mm/90-165mins 0.36mm/90-260mins	Eroded through coating in local-ised areas
Perspex	20 mins	
Polyethylene	270 mins	Eroded through varying degrees
Nylon 6	1080 mins	
Untoughened glass- White plate	2-12 mins	severe erosion
Toughened glass	17-37 mins	moderate pitting to severe cracks
Zinc selenide	4 mins	severe erosion
Sapphire-single crystal	1800 mins	Undamaged
Silicon nitride	360-1800 mins	moderate pitting to undamaged
Stainless steel	1800 mins	Undamaged

performances of the above mentioned materials, which were tested under standard conditions at the Royal Aircraft Establishment at Farnborough (2).

1.4.1. Engineering thermoplastics.

Both single impact and multiple impact studies have been carried out to evaluate the behaviour of thermoplastics, to ascertain the parameters involved in failure and the types of damage mechanisms which occur.

The advantage of using thermoplastics is that they are inherently ductile in nature compared to the more brittle thermosetting resins. This major difference is enhanced when fibre reinforcement is used (27), with the reinforced thermoplastic being less affected by erosion, although the stiffness donated by the reinforcing fibres will tend towards that of a more brittle structure. The variation in mechanical properties of composite materials because of the nature of the reinforcement and its interaction with the matrix resin, leads to a certain inhomogeneity of structure. This will provide initiation points for failure throughout the matrix under the triaxial stresses produced during impact, which may result in spallation, delamination and splitting. This can be overcome to some extent by using three-dimensional reinforcement, but stress concentrations would still occur which can result in a decrease in impact resistance over un-reinforced resins. Ductile failure observed in thermoplastics is characterised by its ability to absorb the impacting energy, so that strength reduction and weight loss are minimised.

An example of a thermoplastic which has proved to be of interest is polycarbonate (28). The polymer is formable, has a high impact strength and toughness at high temperature, and yet it is still susceptible to erosion, so where it has found a use, the need to provide a polyurethane protective coating still exists to allow an adequate service life (29).

As has already been mentioned the thermoplastics which are of greatest interest are the ones belonging to the polyarylate family. These can be split into two distinct categories;
(i) Amorphous- polyethersulphone (PES), polysulphone, polyetherimide (PEI).
(ii) Semi-crystalline- polyetherketone (PEK) and polyetheretherketone (PEEK).

PEEK has been found to offer excellent rain erosion resistance (6). Figure 1.7, shows a graphical representation of test data produced by the Royal Aircraft Establishment at Farnborough, Hants. It clearly demonstrates the excellent properties of PEEK, with virtually no weight loss after 100 minutes of testing (2). PEI, comes out quite favourably, giving values similar to those for glass reinforced PEEK and polyphenylene oxide (PPO). To place these figures into perspective, the values obtained for PES are similar to those for glass reinforced epoxies, although the advantages of using PES are ease of application and its ductile characteristics. Other investigations have also found PEEK to be superior to other thermoplastics (30), showing low weight losses and stating that, although the values obtained for reinforced PEEK are lower, this still presents advantages over other

systems. Single impact studies on PEEK have also revealed encouraging properties (31), where a threshold velocity of 230 m/s was found compared to 215 m/s for PES. The performance at elevated temperature was also investigated to determine the polymers response to aerodynamic heating. Here the threshold velocity values decreased on raising the temperature to 300°C, and the amount of damage associated with the water drop impact increased. This does not appear to be the case with multiple impact studies, where indications were that the erosion resistance increased on increasing the temperature up to the glass transition of the resin (2) in glass fibre reinforced systems.

Difficulty has been encountered when postulating what aspects of the mechanical properties of the polymer influence its resistance to water drop impact. Generally, if the polymer has a high impact strength and a high modulus, it should exhibit good water drop impact erosion resistance. Poisson's ratio has also been used as a parameter for the prediction of the polymers' resistance, the ratio having a modifying effect on the fracture behaviour of the polymer. The use of Poisson's ratio is important in the description of the materials elastic behaviour and, for example, as the ratio tends towards zero (32), the material will maintain a constant cross section when pushed or pulled.

Some investigation of the behaviour of PEK was also undertaken at the Royal Aircraft Establishment by means of the whirling arm technique. Samples of PEK (the same grade as that used in this thesis) ,

Figure 1.7. The rain erosion resistance of some engineering thermoplastics carried out at a velocity of 225 m/s with a rainfall intensity of 25 mm/hour, (6).

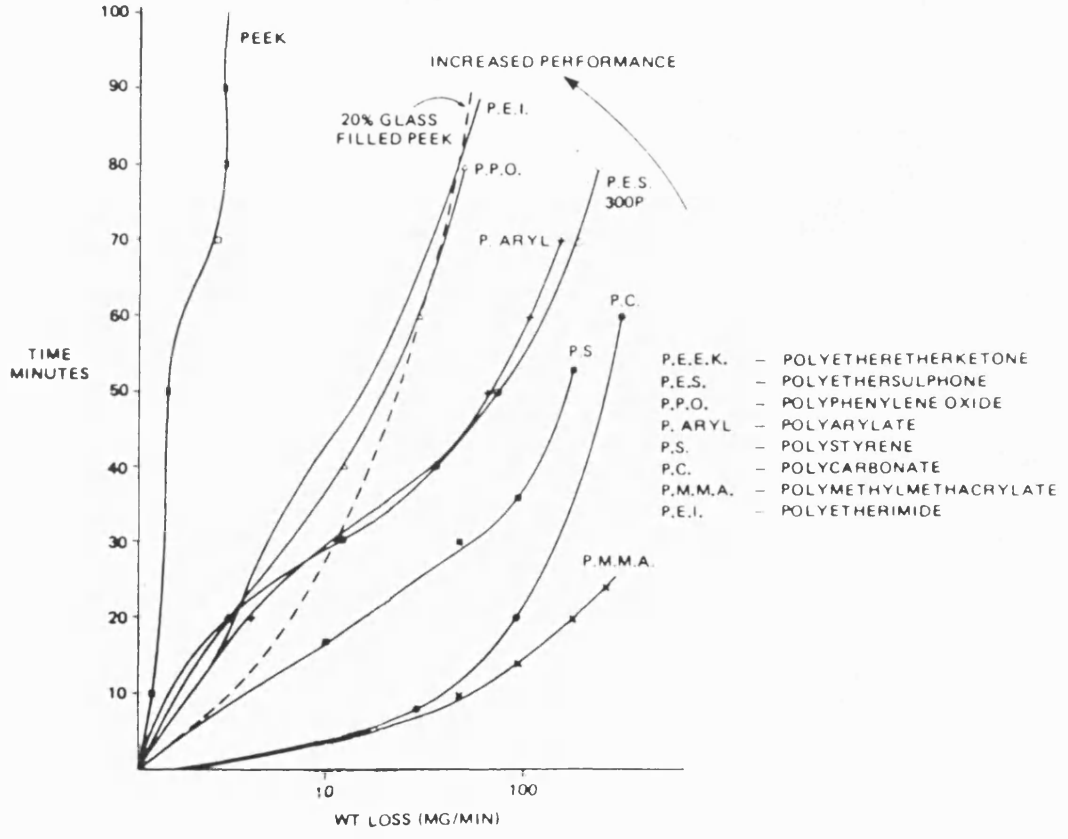

were provided for evaluation by Dr. J.Senior, then of Raychem Ltd, Swindon. The results obtained are presented in table 1.8. These unpublished results indicate that PEK is comparable with, if not superior to, PEEK. The mechanical properties of PEEK and PEK are very similar and the reason for this difference is the subject matter for further investigation within this dissertation.

Table 1.8. The rain erosion resistance of PEK carried out at a velocity of 225 m/s with a rainfall intensity of 25 mm/hour.
Sample dimensions: 25mm x 25mm x 3mm.

Sample	Weight Loss
PEK	13mg after 135 minutes
PEEK	44mg after 110 minutes
PES	364mg after 40 minutes

1.4.2. Concluding remarks.

In discussing the wide range of topics in this introductory chapter, an attempt has been made to place the theory and measurements of rain erosion in perspective, while outlining some of the engineering requirements that need to be met. The remainder of this dissertation will be concerned with a detailed description of the thermoplastics in question, followed by a study of their water drop impact erosion characteristics.

CHAPTER 2
MATERIALS

2.0.0. Engineering Thermoplastics.

The term 'engineering plastics', applies to those materials whose outlets are alternatives to, or replacement for, load-bearing applications traditionally met by metals or ceramics. Whilst a number of general purpose plastics such as polypropylene or high density polyethylene, with suitable modification by fillers or fibres, do find engineering applications, their usage is for less demanding conditions (33,34).

These materials are strong, stiff, tough, abrasion resistant and capable of withstanding elevated temperature fluctuations and exhibit a resilience to chemical and enviromental attack. These outstanding properties are a result of their crystalline nature and/or the strong inter- and intra-molecular forces.

The materials of importance in this dissertation are thermoplastic in nature, ie they are melt formable and on cooling achieve their optimum properties unlike, for example, polytetrafluoroethylene, which is not melt formable because of its very high melt viscosity above its melting point and would require processing conditions analogous to those used for ceramics, eg. sintering.

As has already been mentioned, a requirement for these polymers is to achieve performance at elevated temperatures and in this continuing search, the polyarylate or aromatic polyketone family of polymers have generated most attention. In particular polyetheretherketone (PEEK) and polyetherketone

(PEK), will be discussed as they are the materials under investigation in this thesis. Mention of polyethylene terephthalate (PET) will also be made as a comparator to these materials.

2.1.0. Synthetic routes to the production of aromatic polyketones.

The synthetic routes to the formation of these polymer groups may be considered as an extension to those routes used in the formation of polysulphones (35,65), which in principle involves polyetherification (the basis for current commercial polysulphone production) or polysulphonation.

(i) Polyetherification.

The condensation reaction proceeds by reactions of the following types;

a) $MO-Ar-OM + XAr'X \longrightarrow -(-O-Ar-O-Ar'-)- + 2MX$

b) $MO-Ar-X \longrightarrow -OAr- + MX$

where M is an alkali metal, X a halide and Ar/Ar' are groups which contain sulphone.

(ii) Polysulphonation.

a) $H-Ar-H + ClSO_2Ar'SO_2Cl \longrightarrow -(ArSO_2Ar'SO_2)- + 2HCl$
using a Friedel Crafts catalyst

b) $HArSO_2Cl \longrightarrow -ArSO_2- + HCl$

The polysulphonation reaction is extended to

form a carbonyl link by a polyaroylation reaction in the formation of polyaryletherketones.

a) H–Ar–H + ClCOAr'COCl ———> –ArCOAr'CO– + 2HCl

b) H–Ar–COCl ———> –Ar–CO– + HCl

Alternatively, a polyetherification reaction can be used where the ether link is formed by the displacement of activated halogen atoms by phenoxide anions.

a) XArX + MOAr'OM ———> –ArOAr'O– + 2MX

b) XAr'OM ———> –Ar'O– + MX
where X is a halogen.

In early preparations, difficulty was encountered in preparing the polymers with an adequately high molecular weight. This was found to be caused by the tendency of the polymer to crystallise, unlike polysulphones, and subsequently not remain in solution in the organic solvents used.

A more detailed account of their synthesis will now be described.

2.1.1 PEEK.

PEEK was first prepared in 1977 and then test marketed by ICI Advanced Materials under the tradename 'Victrex PEEK' (36). The reaction is based upon the polyetherification route. The problem of crystallization on the formation of the polymer was overcome by carrying out the reaction in a high boiling point solvent close to the melting point of

the polymer.

This polycondensation process was carried out in anhydrous conditions with the reagents being dipotassium quinone and 4,4-difluorobenzophenone in the presence of a solvent, diphenyl sulphone. The temperature of the reaction is maintained between 200 and 400°C to maintain the resultant polymer in solution. This reaction results in the elimination of KF, which then needs to be leached from the system. This is in contrast with typical condensation reactions in which the small molecule produced is volatile and can be removed directly from the polymerising system. The presence of KF in the PEEK polymerisation can lead to a reversal of the reaction, but as KF is relatively insoluble in diphenyl sulphone, it does not present a problem.

Reaction procedure:

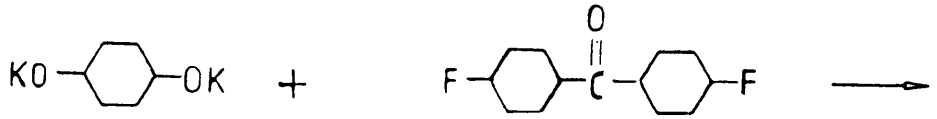

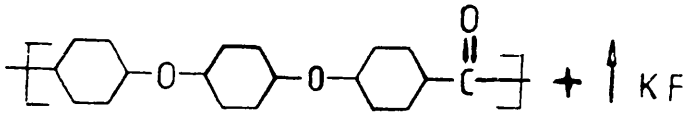

2.1.2. PEK.

Another solution to the problem of producing a high molecular weight from these crystallizable polymers is via a polyaroylation reaction in a good solvent to ensure that the polymer remains in solution. An effective solvent found to be capable of this is hydrogen fluoride (37). This process was further developed by Raychem Ltd (38), with the

reaction occurring in HF using BF_3 as a catalyst. PEK was produced and marketed under the tradename Stilan during 1972-1976. The manufacture of PEK can be briefly described as polymerising p-phenoxybenzoylfluoride using a Friedel Crafts type catalyst, namely boron trifluoride, in a suitable solvent, hydrogen fluoride. When the required molecular weight is achieved (the solution reaches a predetermined viscosity), the use of an aliphatic capping agent such as diphenyl ether, is used to terminate the reaction. The reaction proceeds through the formation of a highly reactive carboxonium ion intermediate as follows;

1. 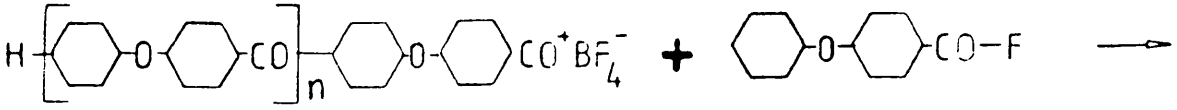

2. 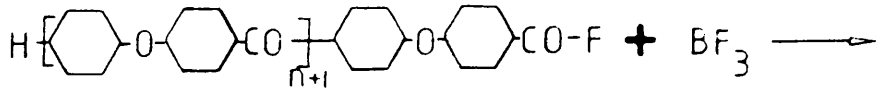

3. 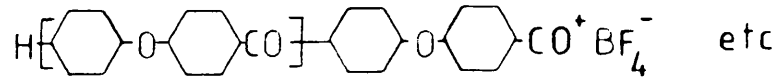

chain termination by the capping agent results in elimination of boron trifluoride.

4. 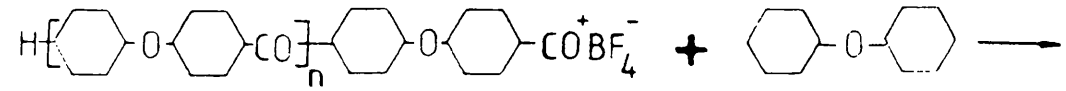

5. 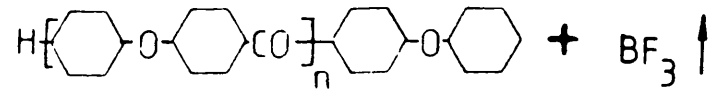

The PEK used for experimentation in this dissertation was not a virgin resin. Into the resin was compounded the following ingredients;

0.5% processing aid (PTFE in fine powder form)

1.0% Melt stabilizer (Al_2O_3)

3.0% White pigment (TiO_2)

The incorporation of a melt stabilizer results in a reduction in the melt viscosity, particularly at low shear rates. It is believed that this melt stabilizer neutralises potentially labile molecular branches, which could lead to crosslinking and gel formation. The processing aid further reduces the melt viscosity to yield very smooth extrudates (Stilan was introduced by Raychem for use as a wire covering), with the addition of a pigment being solely for aesthetic purposes.

2.1.3. PET.

As with the synthesis of PEEK and PEK, PET also involves a polycondensation reaction. The basic form of the reaction is between a diacid and a diol (di-alcohol), resulting in the formation of a polyester (39).

$$(HOOC{-}R{-}COOH)_n + (HO{-}R'{-}OH)_n \longrightarrow HO{-}[{-}OCRCOOR'{-}O]_n{-}H + (2n-1)H_2O$$

as the supply of monomer is used up, the likelihood of the growing polyester molecule reacting with other growing polyester molecules is increased.

$$HO{-}[{-}OCRCOOR'O{-}]_x{-}H + HO{-}[{-}OCRCOOR'O{-}]_y{-}H \longrightarrow HO{-}[{-}OCRCOOR'O{-}]_{x+y}{-}H + H_2O$$

and in so doing the formation of sufficiently high molecular weight of polymer is reached.

For PET, the reactants used are terephthalic acid and ethylene glycol

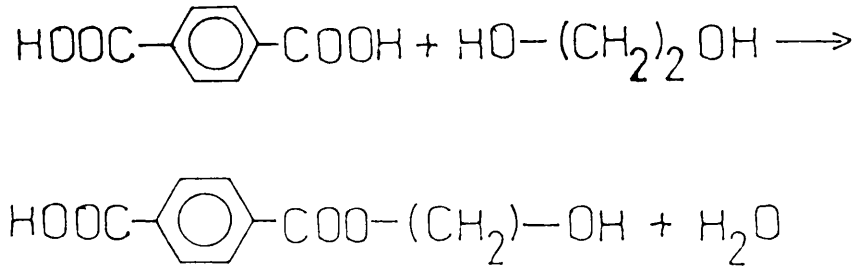

2.2.0. Crystalline characterisation

2.2.1. Introduction.

It has been considered important to discuss the crystalline structure of the polymers in more detail, as it is the effect of crystallinity which leads to the polymers having high mechanical performance and enviromental resistance. Literature has proved to be very sparse concerning PEK and, for obvious reasons, references concerning PEK manufactured by Raychem Ltd were non-existent. For this discussion, unless otherwise stated, it will be assumed that PEK will behave in a similar manner to PEEK as the chemical structures are so similar.

Before any detail concerning PEEK and PEK is written, a brief introductory passage is presented, to give the reader a basic understanding of the

crystalline process and polymer crystallinity.

Many polymers are crystalline and, for this to be so, the polymer chains must be able to align themselves into a regular configuration. The crystalline regions behave as reversible physical crosslinks which disappear on melting and re-appear on cooling. These crystalline regions contribute to the strength, stiffness, hardness and chemical resistance of the polymer and so an understanding of the structure is important. In table 2.1, some well known crystalline and amorphous polymers are listed.

A distinguising feature of crystalline polymers is that they exhibit both first and second order transitions and figure 2.2 illustrates this feature. The first order transition of a semi-crystalline polymer may occur over a range of temperatures ie. not exhibiting a sharp melting process because of the wide range of sizes of the crystalline units and also the variety of structure these units form. The effect of the glass transition temperature upon mechanical performance is diminished with semi-crystalline polymers, as there is little scope for segmental motion to occur, as most of the chain segments are involved in the formation of a crystal lattice, with a resulting restriction to motion. This results in small differences in properties immediately above and below the glass transition temperature, unlike the changes seen for a truly amorphous polymer.

The process of crystallization of a polymer can be described in two stages;

(i) Nucleation

Nucleation can best be described as the formation of sites of order in the molten mass, where the thermal energy is insufficient to outweigh all inter- and intra-molecular forces. Two types of nucleation occur, homogeneous nucleation, which involves the spontaneous aggregation of polymer chains below the melting point until a critical size is reached and crystal growth commences and secondly, heterogeneous nucleation, which arises from impurities either in the bulk or at its surface, where growth becomes instantaneous once the crystallization temperature has been reached.

(ii) Growth

During the growth stage, the enlargement of the nucleation sites gives rise to an increasing percentage of crystalline material. The growth of these sites of order can form differing structures which may be present at various levels and sizes within the polymer. These structures can be sub-divided into the following categories.

a) Crystallites.

As the material crystallises, nucleation sites are generated from which crystallites grow. After the growth of these has been completed, the crystalline regions are fringed by disordered, amorphous regions. This structure is known as a fringed micelle (figure 2.3). The sizes of these crystallites are much less than that of a polymer chain, so that an individual chain will pass through several crystalline and amorphous regions. The fringes themselves, represent transitional material between the crystalline and the amorphous.

b) Single crystals.

A single crystal can be formed from very dilute polymer solutions. The crystals are lamellae with the polymer chain molecules being orientated in the thickness of the lamella and not along the plane. The crystals are lozenge shaped as viewed from above and pyramidal when viewed from the side. The thickness of these lamellae can be increased by changing the crystallization temperature, or by annealing. This effect implies that the movement of the polymer chains is not greatly restricted within the lamellae. The lamellae are eventually stacked until a three-dimensional space has been filled.

c) Spherulites.

A spherulite will develop about a common centre from a single crystal into a birefringent entity, which is spherical in its symmetry. These can be observed in a polarising microscope, provided that they are large enough. They appear to show a characteristic Maltese cross pattern, (figure 2.4). The spherulite itself does not have any impurities and so is deemed polycrystalline. Any impurities will exist outside the spherulite and will be incorporated into the amorphous region. An important point to note is that the spherulite is not a single crystal but an aggregate of smaller crystal units. The size of the spherulite has ramifications for the final properties of the polymer. For example, large spherulites will in general lead to a strong, opaque and brittle polymer. Spherulites can be joined together by interleaving, where two or more spherulites meet during crystallization and lamellae from these extend across their boundaries into any uncrystallised material in the next forming

Table 2.1. Some common semi-crystalline and amorphous polymers.

Semi-crystalline	Amorphous
Polyethylene	Polyvinyl Chloride
Polyethylene Oxide	Polystyrene
PET	Polycarbonate
Nylon 6	Polysulphone
PTFE	

Figure 2.2. The volume/temperature relationship of a semi-crystalline polymer.

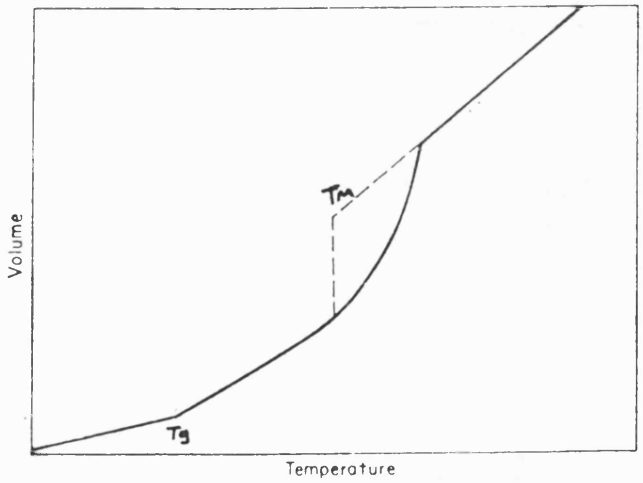

spherulite, or tie molecules can form across the boundaries of the spherulite, effectively knitting them together.

d) Fibrils.

Spherulitic development takes place by the outward expansion of fibrils from a central nucleus and therefore these fibrils must be considered as fundamental units of structure. In some polymers, for example cellulose (41), the fibrils are defined and show no tendency toward spherulitic development.

e) Hedrites.

These are polyhedral structures and because they have definite faces to them, they must be similar in feature to single crystals. They consist of several lamellar layers, growing towards a final thickness of 1μm (41), and have been observed on crystallizing polyethylene oxide from the melt.

A knowledge of the kinetics of crystallization is necessary so that one may be able to predict the types of nucleation and growth processes that occur within the polymer system. General treatments for the kinetics of phase change were developed by Avrami in 1940 (34). For his analysis to be valid, several assumptions need to be made;

(i) Nucleation/growth occurs at random

(ii) Crystallites grow at a rate which is proportional to the surface area and time

(iii) Their is no penetration of the growing surfaces. When penetration does occur the growth process will stop

(iv) The degree of crystal perfection is constant.

The crystallization process may be monitored by measuring the change in specific volume with time.

Figure 2.3. A fringed micelle model (34)

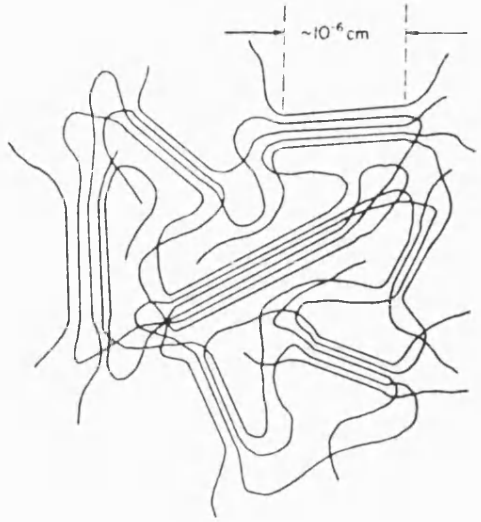

Figure 2.4. Spherulites in a silicone like polymer, observed between crossed polarizers. Large and small spherulites were grown at different temperatures.

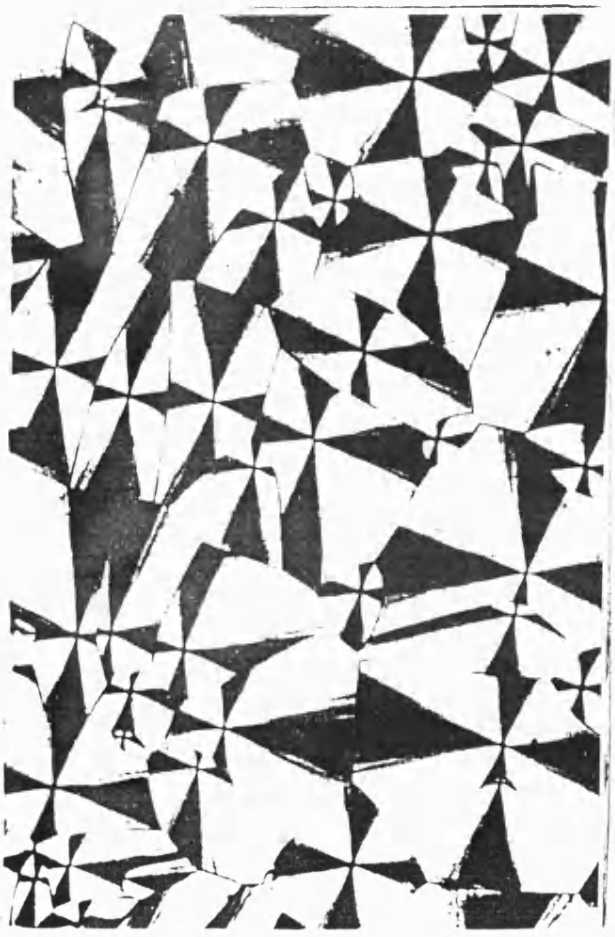

In practice this can be achieved by dilatometry, where the polymer sample is enclosed in a dilatometer and the change in volume can be measured by observing the change in height of a liquid which is proportional to the specimen volume. Time-dependent changes in a polymer mass during crystallization are given by the Avrami equation,

$$W_L/W_0 = \exp(-zt^n) \qquad (5)$$

where W_0 is the mass of a polymer melt, W_L is the mass of the non-crystallizable portion of the melt, z denotes the rate constant and n is known as the Avrami exponent.

From an experimental viewpoint, the change in volume is monitored , not the mass and this change in volume is determined from height measurements from a dilatometer, so equation 5, can be re-written as

$$(h_t - h_\infty) \div (h_0 - h_\infty) = \exp(-zt^n) \qquad (6)$$

where h_t is the height at a given time, t, h_0 and h_∞ are the initial and final volumes respectively.

The Avrami exponent, n, which characterizes the type of nucleation and growth processes, and the rate constant can now be found by constructing a plot of $\log \{\ln [(h_t - h_\infty)/(h_0 - h_\infty)]\}$ against log t, where the slope will produce n and the intercept will yield a value for the rate constant, z.

The importance of the Avrami exponent is shown in table 2.5, where the resultant value for n corresponds to a certain process.

Obviously severe limitations exist with the

above analysis, as crystal perfection, or secondary crystallization are not taken into account. More complicated treatments are available, but these go beyond the scope of this discussion.

Table 2.5. Nucleation and crystal growth predicted by certain n values (41).

n	
4	Spherulitic growth from sporadic nuclei
3	Spherulitic growth from instantaneous nuclei
3	Disc like growth from sporadic nuclei
2	Disc like growth from instantaneous nuclei
2	Rod like growth from sporadic nuclei
1	Rod like growth from instantaneous nuclei

Further crystallization of the amorphous regions can occur when the polymer is subjected to strain. This orientation induced crystallinity remains even after the force is removed. An exception to this rule is found with natural rubber, where the crystals formed are not stable and upon retraction of the sample the crystals disappear. For this to occur the polymer must still have a fairly regular structure. This effect is useful commercially in the manufacture of films and sheet products, where bi-axially orientated films of, for example, PET, polyvinylidene chloride or polypropylene, exhibit high clarity and mechanical strength.

Crystallization continues to occur after the theory suggests that it has reached a limit. This is

known as secondary crystallization and becomes increasingly more evident when the polymer samples are annealed. These secondary processes may be caused by;

(i) An increase in crystallinity caused by the slow crystallization of a component that is crystallizable only with difficulty.

(ii) Increasing the degree of perfection of the existing crystalline regions.

2.2.2. The crystallization processes of PEEK.

As has already been mentioned, literature concerning PEK is very sparse. This section will therefore concentrate on the behaviour of PEEK but, as will be revealed, comparisons between PEEK, PEK and PET can be made.

2.2.3. Unit cell dimensions.

The use of X-Ray diffraction, both wide and small angle (<5°) techniques, yields information relevant to the spacing of the component atoms within the crystalline phase. The scattering is characterised by diffraction rings in isotropic polymers and by a so-called fibre diagram, when analysing orientated polymers. From this information the size of the crystalline unit cell can be calculated, from which the density of the crystal can be determined which can further be used to calculate the crystallinity of a two-phase model of crystalline and amorphous regions. Since the difference between the crystalline and amorphous densities is small, slight variations in cell dimensions, lead to large variations in absolute crystallinity. It has been observed (59), that the unit cell dimensions of PEEK

will be altered on changing the conditions under which the crystallization process proceeds. Increasing the crystallization temperature, either from the melt or the glassy state, will result in a decrease in the unit cell dimensions. This can be explained by the increasing possibility for the crystalline regions to reach a more perfect state.

Some values for the unit cell dimensions can be seen in table 2.6. The structure of the unit cell of both PEEK and PEK is orthorhombic, with two molecules traversing the unit cell and the unit cell itself extending over two phenyl groups, see figure 2.7, in the chain direction, conventionally designated the c-axis. This unit cell is very similar to that of poly (p-phenylene oxide), (43,44). The a-dimension in PEK is significantly shorter than that of PEEK, which may be a result of its capacity for more regular packing of the oxygen and carbonyl groups, which is reflected in its higher crystalline density. Further confirmation of this is that PEK has been found to contain approximately 10% more crystalline material when crystallized from the melt (44). The cell dimensions quoted are dependent upon the crystallization conditions used and it has been reported that cooling extremely quickly from the melt will cause an increase in all dimensions because of the more disordered packing of the chains (45).

The crystallographic equivalence of the ether and carbonyl groups is the reason why most polyaryletherketones have almost identical unit cell dimensions. The ratio of ketone to ether linkages for PEEK and PEK are;

PEEK	0.50
PEK	1.00

The higher the amount of ketone linkage, the higher the rigidity of the chain, and this obviously has an effect upon the crystallization process. In general greater chain flexibility should give rise to a polymer which becomes easier to crystallise, as, for example, PBT is easier to crystallise than PET. A balance must be met, as increasing the ketone linkage will reduce the ability for the polymer to crystallise, but will increase its mechanical performance.

2.2.4. Morphology.

Both PEEK and PEK reveal a spherulitic crystalline structure similar to that of most polymers, for example PET(42). Within the spherulites are smaller lamellar crystals, the entities which are responsible for the growth process of the spherulite.

The spherulitic structure and lamellar detail has been revealed in studies involving solution grown crystals, where crystals and spherulites were grown from dilute solutions in hot α-chloronaphthalene and in hot benzophenone. In studies involving crystallization from the melt or from heating the polymer from the glassy state [amorphous] (42,47,48,49,50,51), a parallelism between solution grown and melt acquired crystals exists.

The basic underlying feature is that the solution-grown crystals follow a layer type morphology, with the layers being lath or spear

Table 2.6. Unit cell dimensions of PEEK and PEK.

Type	a/Å	b/Å	c/Å
Isotropic PEEK(38)	7.75	5.86	10.0
" " (40)	7.75	5.86	10.0
" PEK(40)	7.63	5.96	10.0
" " (41)	7.65	5.97	10.09
Oriented PEEK(42)	7.83	5.94	9.86

Figure 2.7. The unit cell of PEEK(63)

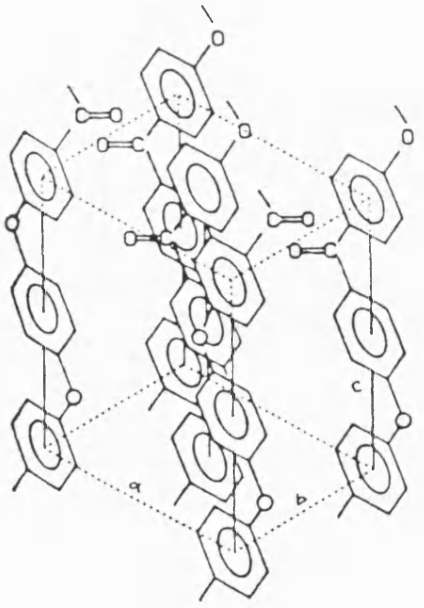

shaped with jagged edges. The `jaggedness' discloses a fibrosity which corresponds to the direction of growth of the crystals. These lath or spear shapes have also been observed in melt crystallized samples.

As in other semi-crystalline polymers, stacks of lamellae exist, consisting of alternate layers of crystalline and amorphous regions. These lamellae are approximately 5nm in thickness and they grow outwards from nucleating sites until they mutually impinge. These forming spherulites differ greatly in size, with the range falling between 1 and 10μm. The sizes of the spherulites greatly depend upon the nucleation density, the lower the density the greater being the spherulite size. The nucleation density is high where PEEK is concerned and so the resulting spherulites will be small, but again this spherulite size can be altered by increasing the temperature at which the crystallization procedure occurs. Both positive(40) and negative(42,48) birefringence have been observed, which may lead to a conclusion that different types of spherulite exist, as the measure of the birefringence, or change in the index of refraction, is made up of contributions from the crystal shape and any noticeable effect suggests that some differing crystal orientation is present. The b crystal axis is radial and the crystals appear to have {110} as the preferred growth plane in PEEK, see figure 2.8.

The interaction of the PEEK matrix with carbon or glass fibres is an important issue, as it will influence the behaviour of the matrix to fibre interface. This will now be discussed briefly. Two

differing effects have been seen when observing the morphology of a PEEK/carbon fibre composite named APC. It was found that nucleation of spherulites occurred within the matrix as well as the fibres, which was dependent upon the temperature at which the composite was allowed to crystallize (51). There was no evidence of transcrystalline growth (where nucleation proceeds preferentially from a substrate surface rather than from the bulk of the matrix). However, it has also been observed that substantial transcrystalline growth results in both PEEK and PEK (42), where the fibre spacing has accounted for differing spherulite size and structure, as can be seen in figure 2.9.

2.2.5. The process of crystallization.

The crystallization behaviour of PEEK and PEK is analogous to that of PET, where a differential scanning calorimetry (DSC) trace will reveal a glass transition temperature, followed by an exothermic crystallization peak and a melting process, see figure 2.10.

DSC scans on heating from the amorphous state for PEEK reveal a crystallization exotherm at 180°C (52) while the exotherm occurs at 255°C (40) when cooling down from the melt. The values quoted here depend upon the heating or cooling rates of the scan and in these quoted values the rate was 20°C/min. It was found under isothermal heating conditions that the maximum rate of crystallinity occurs at 230°C. Heating PEEK above its Tm for various periods of time will change its nucleation and crystal growth rate

upon re-cooling (53). Destruction of existing nuclei, formation of new nuclei, chain branching, crosslinking and chemical degradation can all take place. After holding the sample above its Tm, the resulting new Tm will shift to lower temperatures because of the formation of crystal imperfections. Isothermal DSC investigations have also revealed that the endotherm for the crystallization peak yields a heat of fusion, H_F=130 J/g, compared to a H_F=135 J/g for PET (40,54).

Analysis of the process by application of the Avrami equation has led to an Avrami exponent (n) value of 3, which gives rise to an instantaneous nucleation process followed by crystal growth, forming spherulites (54). An interesting investigation concerned with isothermal crystallization of PEEK with varying molecular weights (synthesised in laboratory conditions), revealed a two stage process with the first stage yielding a value for n of 3 and a secondary process yielding a value for n of 1, responsible for interlaminar growth (55). An explanation for this is that as the molecular weight increases, the melt viscosity increases, inhibiting molecular motion and in so doing retarding the crystallization process. It can be concluded that a two-stage process occurs with commercial PEEK where the secondary process is involved with crystal perfection.

The use of the Avrami analysis is limited and concern has been shown, as has been indicated, that it is only representative where conversion upto 30% crystalline content is present (56) and other kinetic

models have been proposed which fit this behaviour better.

Non-isothermal crystallization procedures, where the DSC was used to provide a constant rate of temperature change, have also been investigated. The Avrami analysis yielded n values much higher than those calculated by isothermal techniques and these were found to be a result of changes in the growth rate and higher resulting degrees of crystallinity (57). These studies were mainly concerned with the processing parameters of PEEK/carbon fibre composites, namely the crystal formation at different rates of heating and cooling.

In common with many other semi-crystalline polymers, PEEK shows multiple melting processes, with a minor melting peak just above the crystallization temperature, followed by the major melting peak at approximately 335°C. Again this behaviour is analogous to that of PET and probably to that of PEK. It was postulated that this lower melting peak indicated the presence of two differing crystalline morphologies, whilst others felt that it was a function of crystallites already present in the sample prior to the DSC scan (50,54).

The influence of stress or strain upon crystallization of a polymer is well known. The effect of flow rate (shear/strain rate) was investigated, where a micro-injection moulding machine was constructed to fit inside a Wide angle

Figure 2.8.Crystallographic orientation in PEEK lamellae.

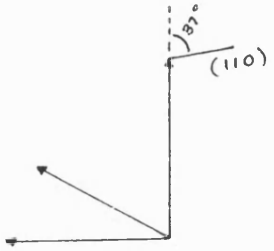

Figure 2.9.Schematic representation of two possible spherulite morphologies, resulting from constrained growth in composites (42).

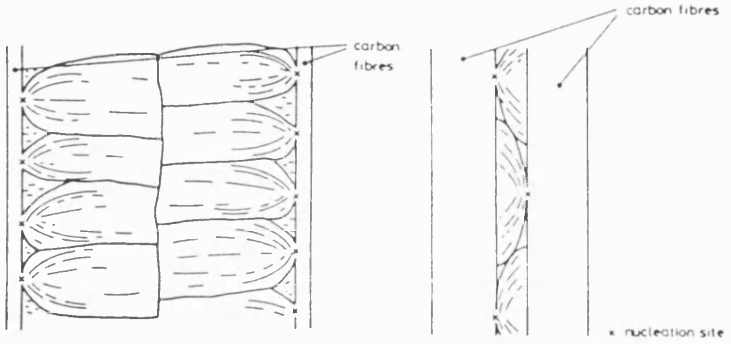

Figure 2.10.Typical DSC trace for PEEK illustrating an exothermic melting peak and a melting process, (52).

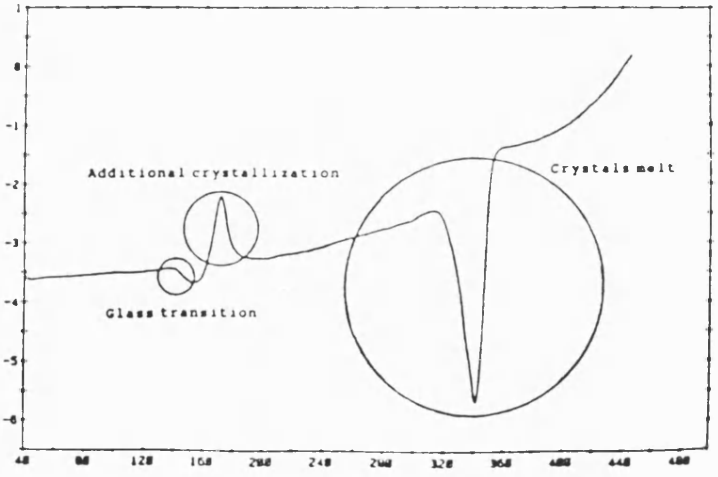

X-Ray scattering instrument (58). This has a direct relevance to this dissertation, as the polymer samples were moulded by an injection moulding route. Increasing the flow rate increases the molecular extension which, in turn, increases the ease and rate of crystallization, resulting in high values of crystal content. This occurs because the entropy of the melt is decreased with increased flow rate. It was also observed that an increase in the secondary process resulted, yielding higher cystallinity values, but no explanations were given.

2.2.6. Properties related to crystalline morphology.

The importance of polymer crystallization is its modifying effect upon a wide range of mechanical and chemical properties. The crystalline regions behave in a reinforcing manner, greatly increasing the modulus of the polymer whilst also increasing the polymer's chemical resistance. In general the following properties are influenced to some degree by the onset of, or increase in, crystallinity.

a)Mechanical properties.
Modulus increases.
Impact strength decreases.
Tensile strength increases.

b)Optical properties.
Transmission of light through the polymer decreases when crystallization occurs, because of the diffractive nature of the crystals and spherulites.

c)Permeability.
Since it is the amorphous regions that account for solubility, increasing the crystallinity decreases

the permeability of the polymer to gases and liquids.

d)Reactivity.
In general only the amorphous regions are likely to be susceptible to crosslinking, degradation and chemical attack.

An interesting measurement of the influence of crystallinity on PEEK was made by using a microindentation technique involving a pyramidal diamond indentor, primarily applied in characterising the surface structure of metals and ceramics (59). Here it was shown that the micro-hardness technique was very sensitive to the morphological characteristics of the PEEK samples. The hardness increased with increasing crystallinity as the deformation mode of the crystals predominate over the deformation within the amorphous regions, with values of 135 MPa for amorphous PEEK, rising to 256 MPa for crystalline PEEK.

2.3.0 Mechanical properties.

2.3.1 Introduction.

This section will provide a brief insight into the wide spectrum of mechanical properties achieved by PEEK. Little mention of PEK can be made here, as the literature review carried out has failed to produce any detailed information regarding its mechanical properties.

A great deal of attention has been given to fibre reinforced PEEK, especially those composites reinforced with carbon fibres and these are known commercially as Aromatic Polymer Composites (APC is

an ICI tradename), where the wide range of processing methods to produce engineering components leads to a broad property spectrum including a modulus in the range of 3-150 GNm^{-2} and strengths of 100-2000 MNm^{-2} at room temperature (60).

This dissertation is not concerned with the behaviour of the fibre reinforced structures, only with the matrix material itself. The information provided here will therefore be specific to the matrix, but it is recognised and understood that for most engineering applications, and in particular for aerospace end uses, the information regarding the composite is of greater interest.

2.3.2. Viscoelastic properties.

The general behaviour of thermoplastics can be defined as non-linear viscoelastic so that, for example, no value for modulus can be applied at any specific time under load or at a specific temperature. Consequently the modulus will be dependent upon the magnitude of the applied stress or strain. A simple pattern for PEEK follows, during a stress/strain plot at increasing temperatures from 20° to 180°C, where the stress falls and the strain increases on increasing the temperature. A large shift occurs when increasing the temperature above the polymer glass transition temperature of ≈ 143°C. It is also observed from creep data. There is only a small change in the time dependence of creep, even above the glass transition temperature (60), where the creep modulus remains fairly constant between 10^1 and 10^7 seconds.

Analysis by dynamic mechanical and thermal (DMTA) instruments were also used to investigate the viscoelastic behaviour of PEEK. Measurements carried out on amorphous and semi-crystalline (32% crystallinity) samples, produce a reduction in the flexural modulus at the glass transition temperature, but in the semi-crystalline sample the temperature at which this fall off occurred was increased by 10°C. This is attributed to the reduced mobility of the amorphous phase (62).

When observing the loss tangent (tan δ) change with increasing temperature, peaks occur at the glass transition and extra peaks become evident at the onset of crystallization when an amorphous sample is investigated. These changes in tan δ are closely followed by a decrease in modulus, as has already been mentioned. Plots of tan δ against temperature and frequency of testing (63), and subsequent Arrhenius calculations, yield some information upon the dependence of the observed glass transition on frequency. Activation energy values of 900 ± 100 $kJmol^{-1}$ for amorphous samples and 1200 ± 150 $kJmol^{-1}$ for the crystalline samples were determined at test frequencies of 5, 20 and 50 Hz. A low temperature peak at -80°C has also been identified and has been assumed to relate to the cessation, or onset, of local mode motions (64).

2.3.3. Toughness and strength properties.

The strength of a polymer is considered in terms of its magnitude and the mode of failure. The time under the applied load and the temperature at which this load is applied are also of importance. In

general PEEK exhibits a yielding or shear banding process which is governed by the ammount of crystallinity present. Exact values for tensile strength or elongation at break can be found in various tables supplied by material manufacturers and in figure 2.11 an indication of the increased yield strength of the polymer as a result of increased crystallinity can be seen. It is worthy of note that the stress in the formation of a neck decreases. This behaviour is a result of the crystallites acting as hard reinforcing domains embedded within the amorphous matrix.

Objective measurements of the toughness of a material are difficult to obtain because of the dependence on the geometry of the sample under the test conditions. Indications that PEEK is a very tough material are observed in its high stress/strain values, but some greater understanding, can be formed with regard to its impact performance.

The use of an instrumented falling weight technique (60), has shown that a ductile-brittle transition occurs at -15°C and the fracture energy values obtained at different temperatures can be seen in figure 2.12.

The component of energy required to initiate a crack is small compared to the total fracture energy. Consequently, the crack propogation process would be expected to be the dominant energy absorbing process. At temperatures below -20°C, crack propogation energy decreases relative to the energy required to initiate a crack, which is co-incident with PEEK becoming

brittle in its behaviour. Although this ductile-brittle transition is only of comparative value, it has been shown to be close to the extrapolated high frequency value of the secondary relaxation peak of -80°C found from DMTA measurements (64).

To eliminate the geometry dependence of the measurements, analysis was carried out by using linear elastic fracture mechanics. The thickness and depth criteria were only met at -40°C (ie where the transition from plane stress to plane strain fracture occurs) and the resulting fracture toughness results are plain strain, geometry independent values of (60) 3.3 $MNm^{-3/2}$ for K_{ic} (critical stress field intensity factor) and 4.8 kJm^{-2} for G_{ic} (critical strain energy release rate).

The influence of strain and temperature is an important one in the measurement of the fracture toughness. Moulded samples of PEEK were studied by using razor-sharpened, notched compact tension specimens (notched by a saw), of a crystalline content of ~ 24% (65). At low strain rates (1mm/min), the fracture toughness (Kc) does not alter to a great extent on changing the temperature of testing from +60 to -60°C. A reduction in Kc occurs when increasing the temperature from ~60 upto 180°C, where a ductile-viscous transition results. On increasing the strain rate to 10^3 mm/min a clear reduction in the Kc values is noticed, with embrittlement of the polymer upto 115°C. Above this temperature a brittle-ductile transition, followed by

Figure 2.11. The dependence of stress/strain behaviour to crystallinity at a strain rate of $2.1s^{-1}$, carried out at room temperature (52).

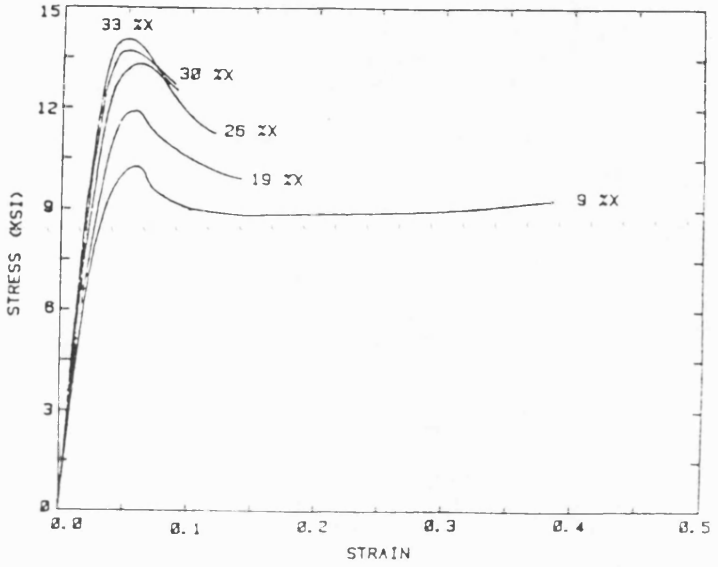

Table 2.12. Some fracture energy values determined for PEEK at increasing temperatures.

Temp °C	Fracture energy (J)
-70	5
23	80
140	55

a ductile-viscous transition, occurs. Annealing the samples to yield ~30% crystallinity caused another clear reduction in the measured fracture toughness, with a predominantly brittle type of failure.

2.3.4. Concluding remarks.

PEEK and PEK are considered to be tough polymers, suitable for engineering applications. Their thermal properties are analogous to those of PET, with the main difference being that the main transitions occur at substantially higher temperatures (40).

	PEEK	PEK	PET
Tg°C	144	165	80
Tm°C	345	365	290

These higher transition temperatures are a result of the restricted chain mobility imposed by the presence of the main chain phenyl groups. The higher glass transition temperature attributed to PEK, relates to a higher heat distortion temperature and the polymer can therefore be used for very demanding applications involving elevated temperatures where the properties of PEEK would become marginal.

PEEK, PEK and PET, are described as being linear semi-crystalline polymers. Compared to other regular polymers containing no aromatic groups, such as polyethylene or polyethylene oxide, they are slow to crystallise and this will result in a comparatively lower degree of crystallinity. The effect of

crystallinity is to give these polymers a high modulus, although increasing the crystallinity is also known to reduce the impact performance.

The importance of these polymers is enhanced by virtue of the fact that the high-temperature performance achieved is coupled with the ability to process the polymers by using conventional equipment such as extruders and injection moulding machines. It is important to note that for the polymer to be considered melt processable it is necessary for the viscosity at the processing temperature to remain constant for a sufficiently long period of time. The polymer should not be degraded to a lower molecular mass (reducing physical properties), be thermally crosslinked to such an extent as to render it intractible, nor have a melt viscosity too high for normal processing techniques.

Some typical properties of the above mentioned polymers can be viewed in table 2.13.

Table 7.13. Typical properties of PEEK, PEK and PET.

	PEEK		PEK		PET	
Property	Units	Value	Units	Value	Units	Value
Density: Crystal Amorphous	gcm^{-3}	1.32 1.265	gcm^{-3}	1.35 1.27	gcm^{-3}	1.45 1.33
Tensile strength @ break 23°C	MPa	70	MPa	100	MPa	53
Elongation @ break 23°C	%	150	%	120	%	130
Flexural modulus 23°C	GPa	3.9	GPa	3.7	GPa	2.8
Taber abrasion	g/1000	0.006	g/1000	0.0034	g/1000	0.0045
Izod impact str. Notched Un-notched	J/m	83 -	J/m	85 -	J/m	20 -
Poissons ratio		0.42		0.395		0.43
Rockwell hardness M scale		99		82		85
Critical oxygen index	%	35	%	36	%	25
Water absorption 23°C, 24hrs @ 40% RH	%	0.15	%	0.1	%	0.5
Dielectric str.	Kv/cm	190	Kv/cm	260	Kv/cm	45

CHAPTER 3
EXPERIMENTAL PROCEDURES

3.0.0.Introduction.

In this chapter the various experimental techniques employed will be discussed in detail. It will become apparent that a variety of methods of analysis were used. This was necessary because the use of a novel polymer, PEK, required a basic understanding of its mechanical characteristics so that more meaningful comparisons could be drawn between PEK, PEEK and PET.

It must be mentioned that because of the variety of experiments carried out, samples had to be closely controlled owing to the high cost of the base polymers. Unless otherwise stated data points were obtained by using ten samples per test.

3.1.0.Sample preparation.

The polymers were moulded in an Arburg injection moulding machine, which has a 25 ton clamping force and a 23 gramme maximum shot weight. The moulding parameters used can be seen in table 3.1.

The polymers were supplied in sealed cartons (except for the PET, which arrived sealed in a 25kg bag) and were labelled as being ready for moulding. Nevertheless, the materials were all dried prior to moulding in order to avoid the risks of voids and flaws due to moisture, and they were allowed to equilibrate to factory area conditions before opening to prevent any contamination because of condensation (see table 3.2).

Problems were encountered during moulding as a result of excessive shrinkage of the samples, with

PEEK exhibiting the most. The processing conditions mentioned in table 3.1 were found to be the best to keep shrinkage to a minimum (≈ 0.5%). The high injection speeds, short injection times and mould temperatures chosen were also important in keeping sample orientation down to a minimum (to ensure the melt is undergoing minimum shear during its cooling stage whilst in the mould) (66,67). The first ten mouldings of each run were discarded to ensure no cross-contamination was present.

Three types of sample were moulded;
(i) Discs: 64mm diameter x 3mm thickness
(ii) Dumbells: 75mm length x 4mm width x 2mm thickness
(iii) Impact bars: 75mm length x 6mm width x 4mm thickness

In order to obtain samples of differing structure, the following conditions were used;

(i) Samples were kept in their as moulded form
(ii) Samples were annealed under vacuum for 48 hours @ 250°C for PEEK and PEK and, 48 hours @ 170°C for PET. These temperatures were chosen because they were above, or at, the temperature at which the crystallization processes occur at their highest rates, viz.

PEEK 180°C (52)
PEK 190°C (42)
PET 170° (35)

3.2.0.Measurement of crystallinity.

Two methods of determining the percentage of crystallinity present in the samples were

Table 3.1. Arburg processing conditions.

Conditions	PET	PEEK	PEK
Cylinder temps:			
Nozzle	270°C	380°C	400°C
Front	270	380	390
Mid	270	380	400
Rear	270	380	400
Mould temps:			
Fixed	130°C	175°C	200°C
Moving	130	175	200
Pressures (psi):			
Injection	1000	1000	1250
Holding	500	500	500
Back	500	500	500
Timers (secs):			
Delay injection	5	1	1
Injection time	4	5	5
Holding time	2	2	2
Cooling time	10	20	20
Die open time	0.1	0.1	0.1
Speed (rpm)			
Screw	400	350	350

Table 3.2. Polymer drying conditions.

Polymer	temp	drying time
PEEK	120°C	4hrs under vacuum
PEK	120°C	4hrs under vacuum
PET	70°C	4hrs under vacuum

investigated, differential scanning calorimetry (DSC) and x-ray diffraction (XRD).

DSC was found to be unsuitable since it was not capable of distinguishing between the levels of crystallinity in as-moulded and annealed samples. The H_f values used for the determination of the crystalline content of the three samples were;

PEEK	130 J/g	(40)
PEK	Unknown	
PET	135 J/g	(54)

It was thought that the reason for this lack of sensitivity was that the slow rate of heating ie 10°C/min, caused further crystallinity to be induced. It is understood that many papers have been written on work in which this technique for the measurement of crystallinity was used, but as it was employed so as to observe a structural change for further experimental procedures, it was felt unnecessary to pursue this method further and to investigate the possibilities of using x-ray diffraction (XRD) instead.

XRD was carried out at the Analytical department of Raychem Ltd, by Mr B.Fox. Differing values of crystallinity were obtained by this method. It must be stressed that whatever method is used, the values obtained are comparative and are not to be taken as absolute. This statement obviousely applies to many experimental techniques.

The instrument used was a Phillips X-Ray Diffractometer with a PW 1130 generator and a PV 1050 goniometer. The experimental data were collected by

a BBC master computer and analysis carried out by means of software developed in-house at Raychem Ltd.

The procedure for determining the level of crystalline material involves the evolution of an x-ray pattern due to the amorphous regions of the polymer, which is calculated from the scatter of disordered regions. The amorphous halo produced is then compared with the scatter produced from the ordered region of the polymer (crystalline section), (68,69).

The percentage of crystallinity measured by means of x-ray diffraction refers to the weight percent of the polymer which is sufficiently ordered to give a diffraction pattern characteristic of crystalline materials (see figure 3.3).

3.3.0.Tensile testing.

Measurements were carried out following ASTM D638. Five moulded samples (dumbells), were tested in the annealed and as moulded states and the tensile strength and the elongation to break were recorded from the stress/strain curves. The values were determined at increasing temperature, ranging from room temperature to 160°C. The samples were conditioned at the test temperature for twenty minutes.

The following test conditions were used;
(i) An Instron 4301 tensile tester.
(ii) cross head speed = 100mm/min.
(iii) Elongation measured via a Wallace optical

Figure 3.3. Diffractometer trace from low density polyethylene. The dashed line shows the estimated position of the amorphous scattering intensity (70).

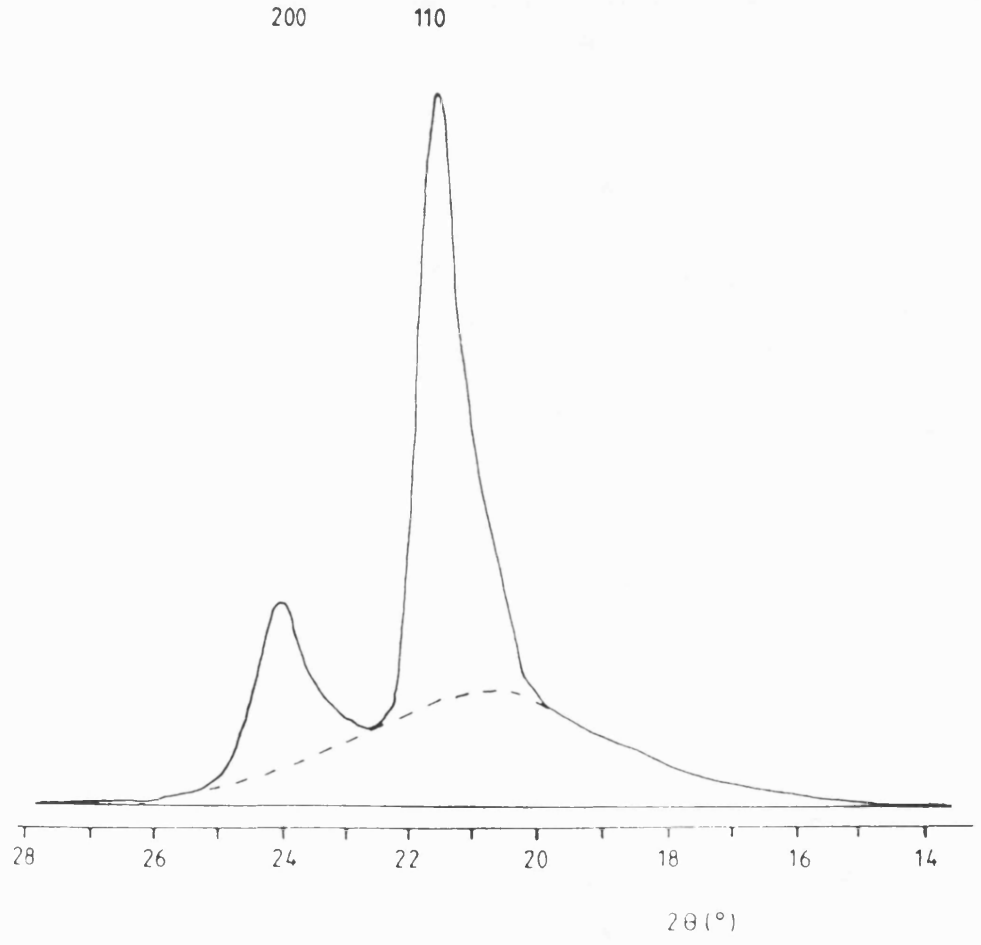

extensometer.
(iv) A 5kN load cell was used.

3.4.0.Dynamic Mechanical Thermal Analysis (DMTA).

Three samples of 20mm long x 10mm wide x 0.5mm thick, were machined from the annealed and as moulded discs. Their dynamic characteristics were analysed by means of a Polymer Laboratories, PL-DMTA machine as illustrated in figure 3.4.

The samples were clamped and oscillated at differing frequencies ranging from 0.1 up to 200 Hz (the full range of the instrument). The samples were heated at a rate of 10°C/minute from -125°C up to 250°C.

This technique was used to establish the loss modulus, the storage elastic modulus and the loss tangent at each frequency, as the measurements are particularly sensitive to molecular motions and transitions such as the glass transition, Tg (70).

Temperatures below the sample Tg were used to investigate any motion of molecular segments smaller than the main chain, for example local mode motions. Further analysis involved plotting the reciprocal of the temperature of the glass transition peak (K), or any other lower order transition, against the logarithm of the test frequency and, in so doing, the activation energy could be calculated by following the Arrhenius procedure. A more detailed account of these procedures can be found in chapter 4.

The dynamic mechanical parameters can be

Figure 3.4. Mechanical head of a PL-DMTA showing the essential features of sample mounting, vibrator system and transducer.

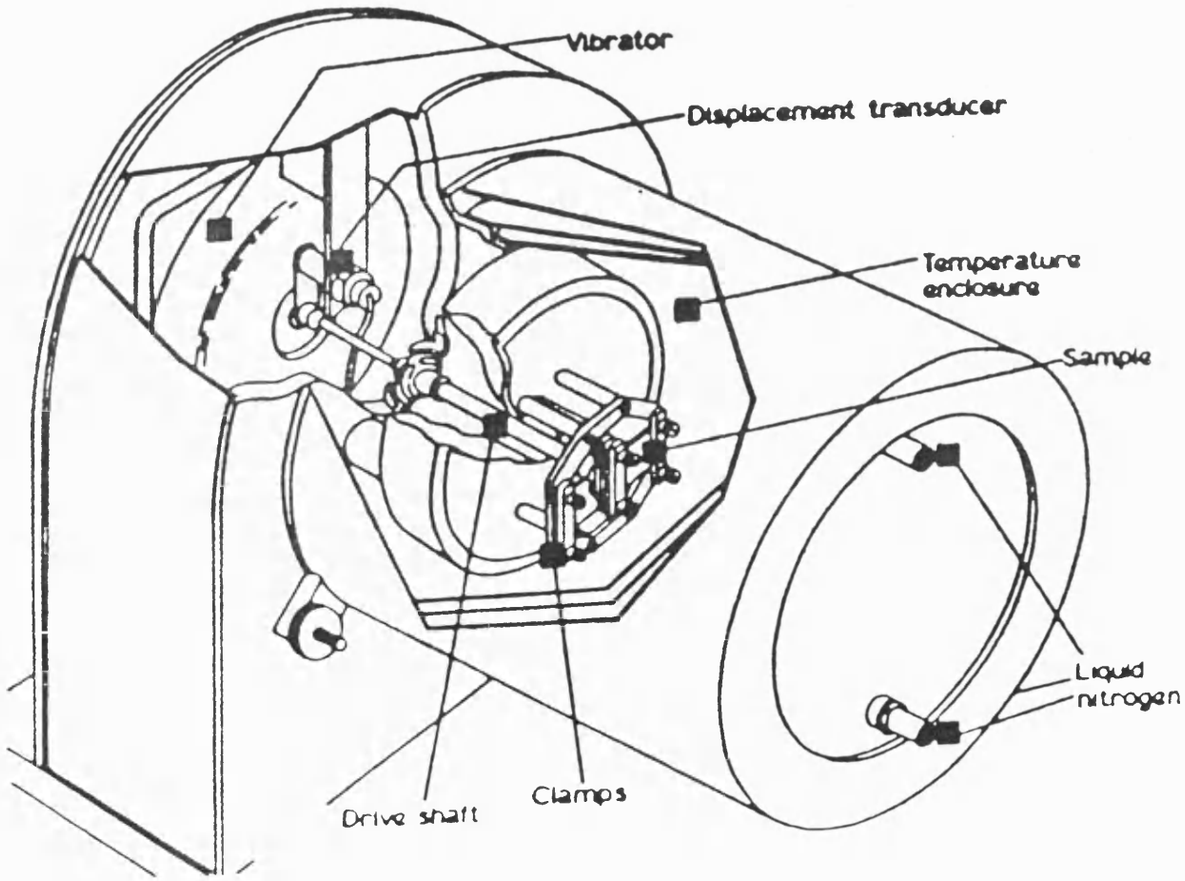

described as (70);
(i) E', represents the amount of energy stored elastically upon deformation and recovered per cycle. It is known as the storage modulus or simply as the elastic modulus.

$$E'(w) = \sigma_o/\epsilon_o . \cos \delta \qquad (7)$$

where (w) is the angular frequency, δ is the phase angle, σ_o is the stress component and ϵ_o being the strain component. In a cyclic test on a viscoelastic solid, σ_o and ϵ_o are the maximum values of the stress and strain per cycle, and they occur at different times because the strain is lagging the stress by phase angle δ. σ is applied cyclic stress, $\sigma = \sigma_o \sin wt$ (t=time) and ϵ is the resulting strain, $\epsilon = \epsilon_o \sin(wt-\delta)$. The ratio σ_o/ϵ_o is known as the complex dynamic modulus, $E^*(w)$.
(ii) E" represents the energy dissipated in various ways (for example, lost as heat) and is known as the loss modulus.

$$E''(w) = \sigma_o/\epsilon_o \sin \delta \qquad (8)$$

(iii) The ratio of energy lost to energy stored yields the loss tangent, or damping factor, tan δ and is defined by

$$\tan \delta = E''/E' \qquad (9)$$

3.5.0.Liquid jet impact.

Damage due to water drop impact was induced by means of a jet technique developed by Bowden and Brunton (12), but further modified so that impact

velocities as low as 100 m/s could be achieved by the use of a momentum exchanger (7). Work has also corroborated that the impact damage produced by the jets is very similar to that produced by a water droplet (71).

This technique has obvious operational advantages over the more realistic but very complicated technique of firing the sample under test at a stationary water droplet or spray (71,72).

A lead projectile is fired from a 0.22 calibre air rifle, into a stainless steel die containing water sealed with a neoprene disc. The resulting forward motion of the neoprene disc extrudes the water at high velocity through the die orifice and onto the sample face. It is important to keep the sample approximately 10mm away from the die face so as to ensure that a coherent jet with a rounded head will impact the sample surface. The resultant jet velocity is approximately five times the projectile velocity.

The gun is charged by means of pressurised nitrogen which is first held in a reservoir and then fired by opening a solenoid controlled valve (figure 3.5).

A wide range of jet velocities can be achieved by changing the pressure of the incoming nitrogen and the orifice diameter of the die. As has already been mentioned a momentum exchanger for velocities below about 300m/s is employed. This consists of a steel cylinder, 4.75mm in diameter and 4.8mm long, which is

placed into the die between the sealing neoprene disc and the impacting lead pellet.

The die chosen for experimentation in this thesis, had an orifice diameter of 1.6mm to obtain large equivalent drop sizes of about 10mm in diameter over the velocity range of concern (figure 3.6 and 3.7), as it is known that the larger the drop the greater the extent of damage that would occur (73). The velocities chosen for experimentation were in the region of 330 m/s up to 1000 m/s. Velocities lower than 330 m/s were not investigated as it was found that only superficial surface damage occurred when impacting PEEK and PEK at these levels. The velocities were measured with apparatus constructed by the Cavendish Laboratory, Cambridge (as was the gun itself). The time taken for a water jet to pass between two sets of optical fibre detectors was measured by;

$$\text{Velocity (m/s)} = (\text{fibre spacing (mm)} \div \text{time } (\mu s)) \times 1000$$

The fibre spacing was measured by means of vernier calipers and found to be approximately 8mm. The device was further modified by the Electronic department of Raychem Ltd and the Cavendish Laboratory so that a digital readout of the time in microseconds would be displayed. Care was taken so that no electromagnetic interference and/or shocks would produce unexpected triggering of the velocity measuring device.

A spread in velocities was observed at the set

Figure 3.5. Schematic diagram of the jet gun apparatus.

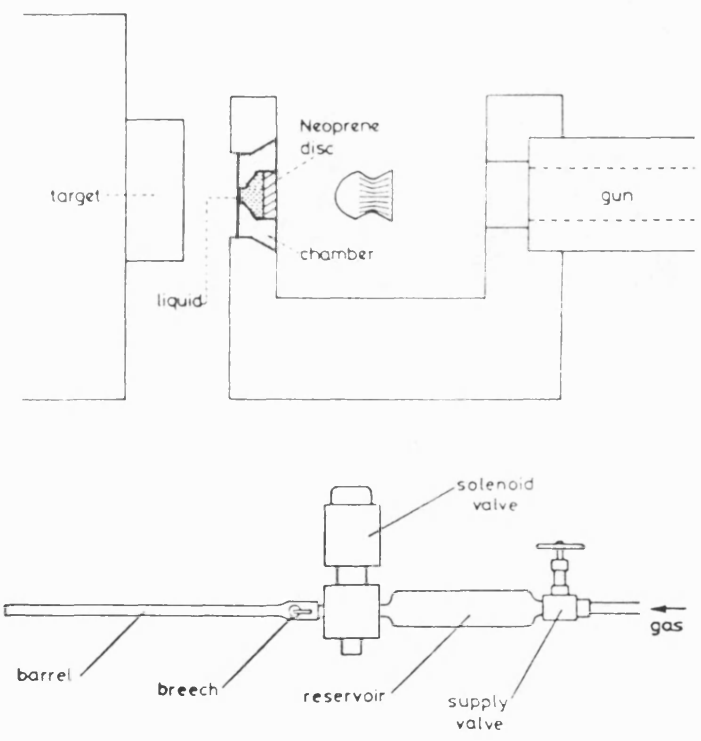

Figure 3.6. The relationship between the jet radius Rj, and the drop radius, R. The shaded area illustrates the compressed area which generates the high pressures.

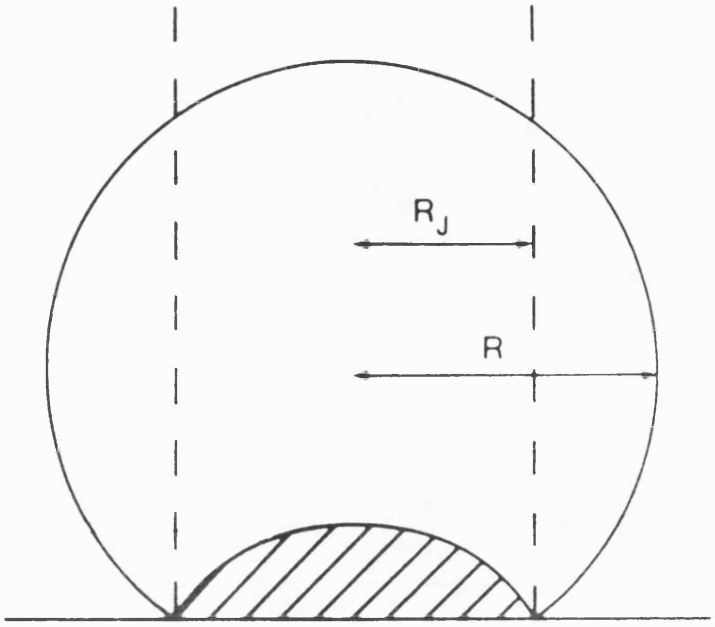

Figure 3.7. Equivalent drop size as a function of impact velocity for a 1.6mm jet.

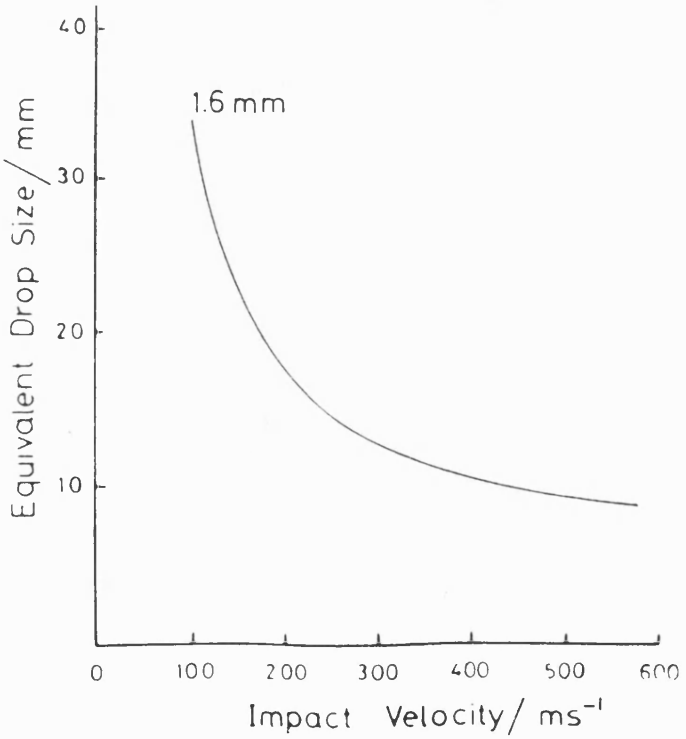

charging pressures (figure 3.8). It was found that this may be a result of the distribution in the weight of the lead pellets used, as can be seen in figure 3.9. The average of ten velocity measurements was taken at each set firing pressure and ten samples of the polymers were also impacted via the water drop procedure to minimise the effect of the velocity scatter.

Two modifications were made to the existing apparatus in order to improve its basic capability;
(i) A neoprene rubber backed sample holder was constructed to hold discs and impact bar specimens in order to prevent the occurrence of extra damage caused by stress waves being reflected from the back surface of a sample held against a rigid backplate. This construction also facilitated specimen insertion and removal (figure 3.10).
(ii) An oven was assembled to the side of the sample holder so that samples could be heated by means of a hot air blower away from the die and holder (figure 3.11). The purpose of this was to ensure that there was no direct heating of the jet apparatus which may have led to changes in the jet properties. When the sample reached the test temperature, as measured by thermocouples placed at the front and the back face of the sample, it was flipped across by means of a rotating arm attached to the holder and immediately impacted by a water drop so as to minimise cooling of the sample.

These modifications were carried out by the Engineering department at Raychem Ltd, from simple designs drawn up by the author.

Figure 3.8. Water drop velocity scatter observed on changing the charge pressures.

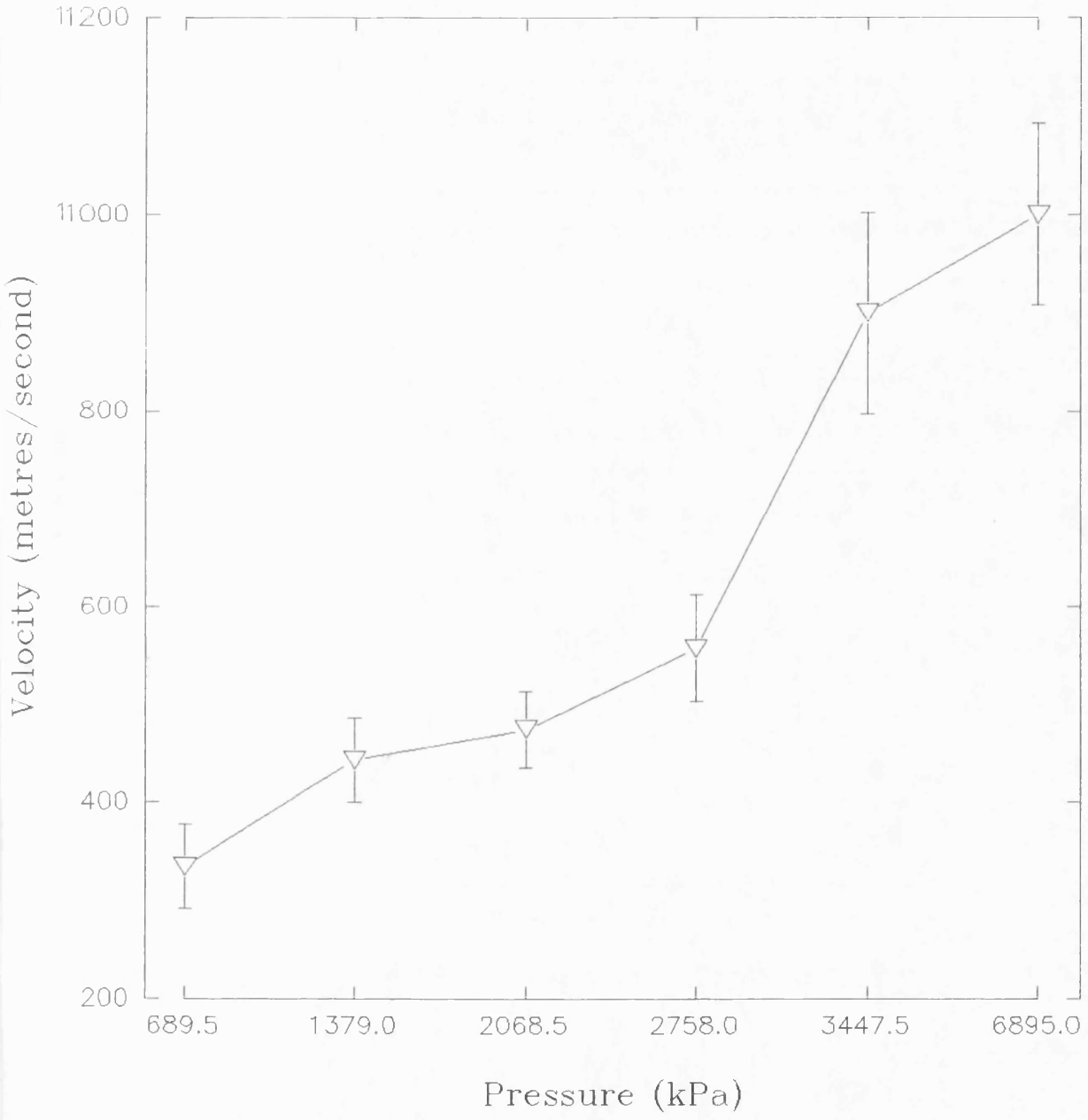

Figure 3.9. Weight distribution histogram, using 0.22 calibre lead air rifle pellets.

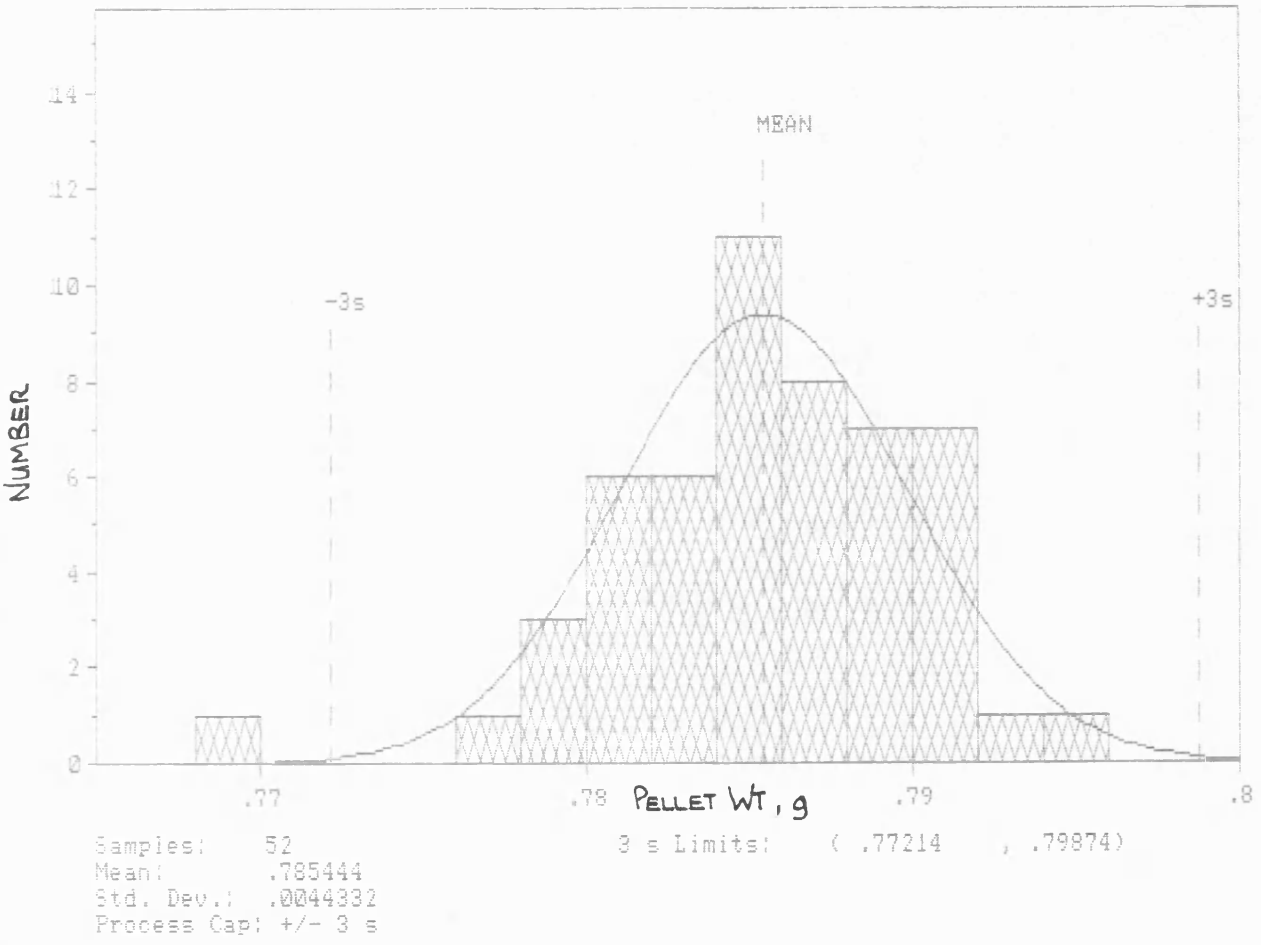

Impacted samples obtained in the above mentioned techniques were sealed in plastic bags, for subsequent residual strength testing and qualitative analysis.

3.6.0.Ceast Advanced Fractoscope.

The need for a qualitative measure of the damage caused by impact by a water droplet has arisen for single impact studies of polymers. Currently, multiple droplet impact studies are used to determine the weight lost by erosion during this process. Residual strength measurements using the hydraulic pressure technique (74,75) are not suitable for polymers because of the plastic nature of the materials and are only suitable when investigating damage to brittle materials.

A technique which has proved to be successful for quantifying the liquid jet impact damage to polymers has therefore been developed. Residual impact resistance or toughness measurements, have been determined with an instrumented Charpy pendulum impact tester manufactured by Ceast, based in Italy (figure 3.12). Here the introduction of a transducer onto the anvil of the machine allows the force to be monitored continuously throughout the impacting process. The transducer can give the following information (76);

(i) load vs time.
(ii) Energy vs time.
(iii) Displacement vs time.
(iv) Load vs displacement.
(v) Energy vs displacement.

Figure 3.10. Sample holder.

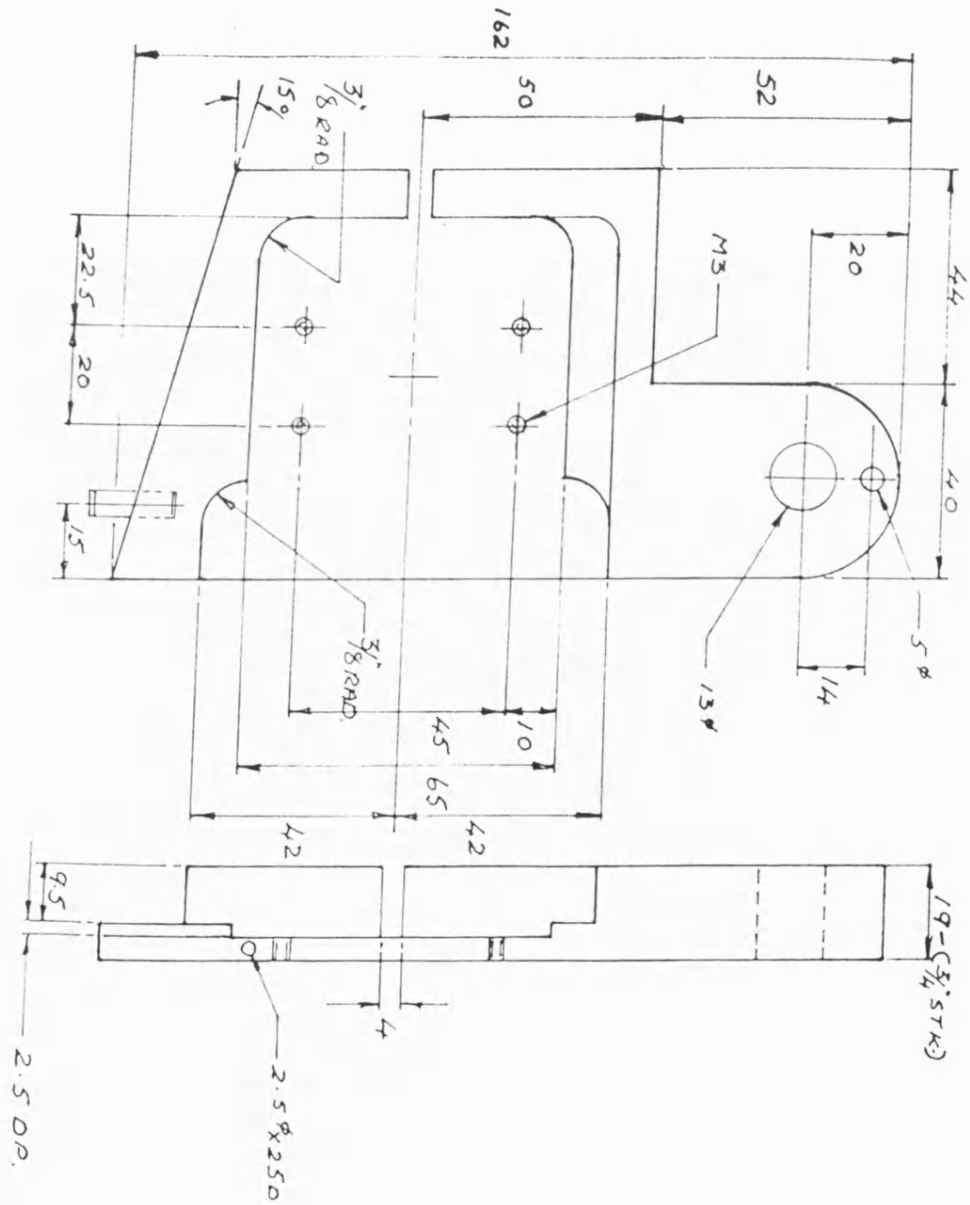

Figure 3.11. Schematic diagram of the oven.

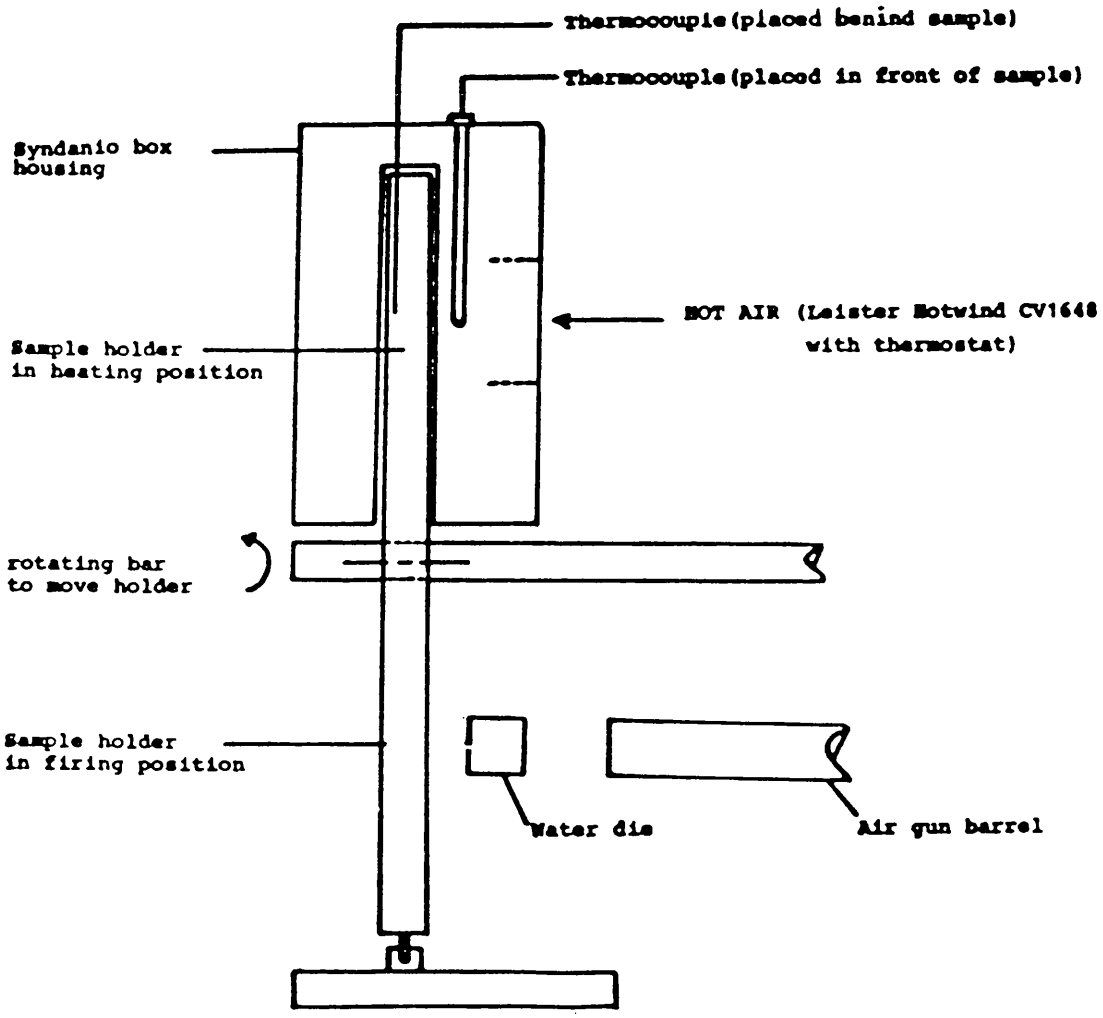

Although all of this extra information was available, for the purpose of this thesis it was felt that enough information could be obtained from observing the energy vs time and force vs time printouts. The advantages of using this technique have been the ease and rapidity of operation and of using a technique that has been well established in characterising the fracture properties of polymers.

Un-notched and therefore un-damaged specimens were first impacted to provide results due to shear failure or ductile behaviour which were then used as base-line values for the plotting of results for damaged samples. Notches were machined into some of the samples by means of a 46° cutting tool with a notch radius of 0.254 ± 0.025mm to increase the triaxial tension relative to the shear stress, and so accentuating the possibility of brittle fracture. These notched measurements were used as comparators for further analysis.

Specimens were impacted in the water jet apparatus at various velocities over the temperature range of 23°C to 160°C, with both single and multiple impacts. The residual toughness of the materials was then measured with the fractoscope. The following experimental conditions were employed for the fractoscope;

2.05 kg impacting weight.

3.546 m/s impacting speed.

3.7.0.Microscopy.

Qualitative analysis of damage caused by water droplet impact was assessed by means of scanning

Figure 3.12. A schematic description of the Ceast instrumented impact test.

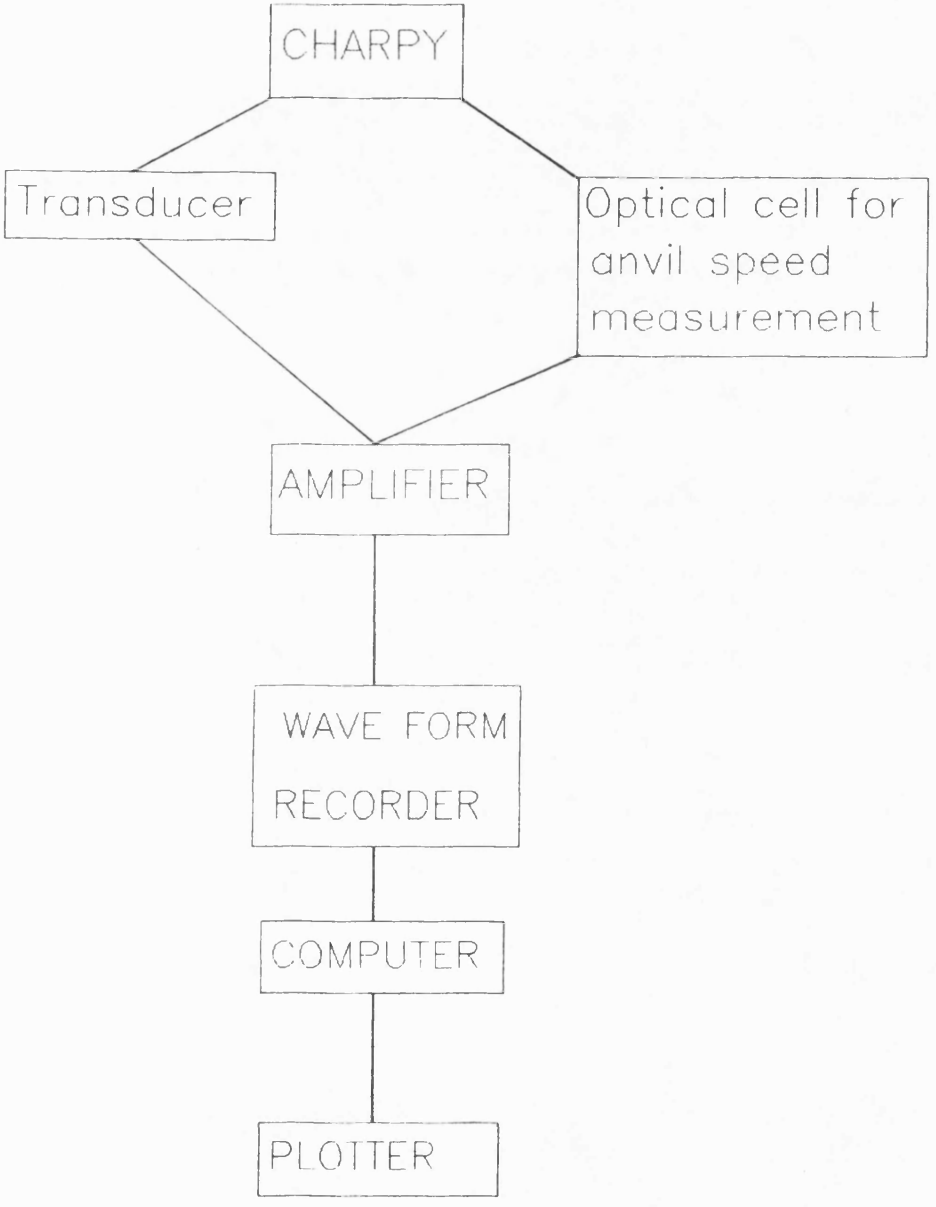

electron microscopy (SEM) and optical microscopy techniques. The SEM instrument was a JEOL JSM-T330. This was used to observe the surface and sub-surface damage after impact by a water droplet. An Edwards sputter coater was used to lay a conductive gold coating onto the specimen surface prior to observation in the SEM. The conditions chosen were to give a coating sufficient to avoid charging of the sample without detracting from the features of the surface under investigation.

Optical examination with a Sharp binocular microscope was employed to assess the amount of visible surface damage. The characteristic ring produced after water droplet impingement seen in figure 3.13 was measured and its size quoted as an area in square millimetres. The central, seemingly undamaged, region was ignored in these measurements: only the area associated with noticeable surface shearing and/or cracks was measured (ie the annulus).

Figure 3.13. Calculation of damaged area from optical examination.

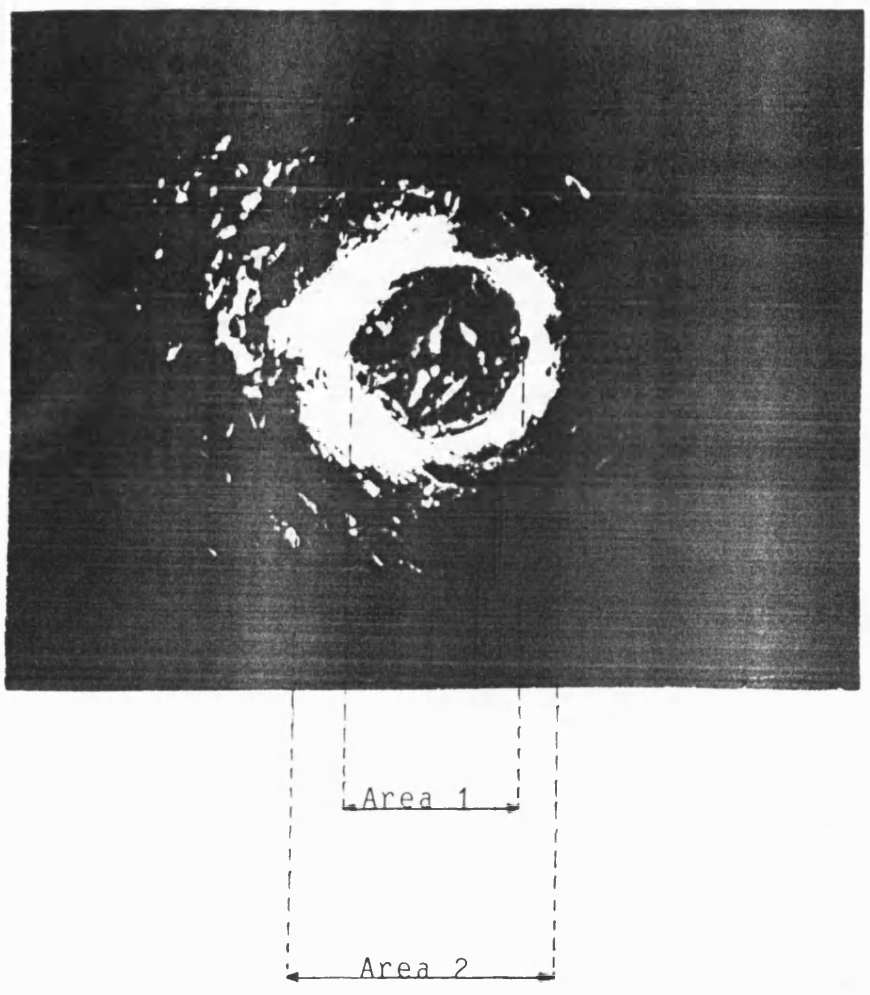

Damaged area = Area 2 - Area 1

CHAPTER 4
RESULTS

4.1.0. Measurement of crystallinity.

4.1.1. Introduction.

A detailed account of the crystallization processes and morphology of the polymers used in this dissertation can be found in chapter 2. In the following brief explanatory passage, we concentrate on an important factor which controls the final morphology of the polymers, namely the effect of thermal processing.

The use of screw injection moulding as a means of forming components is widespread. The process itself is a non-isothermal, semi-batch technique, able to produce a wide range of intricate shapes, from chairs to compact discs. The conditions and mould geometry used for moulding result in a complex thermomechanical history which will determine the polymer microstructure and resultant ultimate properties.

The structural features of the moulded part may be heterogeneous in nature, as semi-crystalline polymers with flexible chains which have the ability to crystallize rapidly, such as polyethylene, will usually produce a `3-zone structure' with:
(i) a highly orientated skin
(ii) a transcrystalline layer
(iii) a spherulitic core

Polymers with a rigid backbone, such as PEEK and PEK, are relatively slow to crystallize and the effect of any internal stresses produced by the anisotropic nature of the mouldings will become more detrimental to the final properties.

PEEK exhibits a largely amorphous structure when moulded below its glass transition temperature, with a highly localised shear crystallized zone at a depth below its surface dependent on the sample geometry and, in particular, on the sample thickness. As the mould temperature is increased, on passing through the glass transition a multilayer structure develops which gives way to a uniform structure at temperatures past the so called " cold crystallization point ", at about 170°C (77). Moreover, the influence of the time the moulding is kept at the mould temperature under clamping forces, known as the " holding time ", will alter the final structure.

The commercially available grades of PEEK have been shown to contain nucleating agents (compositions not disclosed) to increase the ability of the polymers to crystallize rapidly. It has also been observed that the molecular weight of the polymer produced an effect in which the more mobile and flexible low molecular weight species facilitated molecular packing and lamella formation, resulting in the polymer becoming easier to crystallize (ie PEEK 150 is easier to crystallize than PEEK 450) (78).

An interesting investigation into the above mentioned skin/core variations revealed that the annealing of moulded samples alters the skin/core morphology, the final crystalline content and the actual stress state of the moulding, as can be seen in figure 4.1 (79).

The skins of `as moulded samples' exhibited a glass transition, an onset of crystallization and a

melting transition, whereas, these distinctive features are diminished in the core of the sample. This behaviour is characteristic of semi-crystalline polymers with a high melting transition, such as polyphenylene sulphide, when the mould temperature is kept below the glass transition. In this work, the skin thickness was shown to be reduced on annealing until finally the skin and core became indistinguishable and the melting peak became more pronounced, indicative of a higher percentage of crystallinity.

It was important to discuss the injection moulding and annealing effects briefly as these were the techniques used for preparing the samples for further experimental investigation.

4.1.2. Measurement of the crystallinity of the samples.

The objective of this experiment was to observe the change in crystallinity produced after a predetermined (chapter 3) annealing procedure, in comparison to that of as-moulded samples. This change may be understood more fully at subsequent stages in this dissertation where the mechanical properties will be analysed.

As has already been mentioned, X-ray diffractometry was chosen to measure the degree of crystallinity because inconclusive results were obtained with DSC. A correlation between X-ray determined crystallinities and those found by DSC has been reported (80) and figure 4.2 illustrates the similarity of the resultant crystallinities measured

Figure 4.1. DSC thermogram obtained for PEEK at varying crystallinities, illustrating the differences between the skin and core of the samples and the effect of annealing (79).

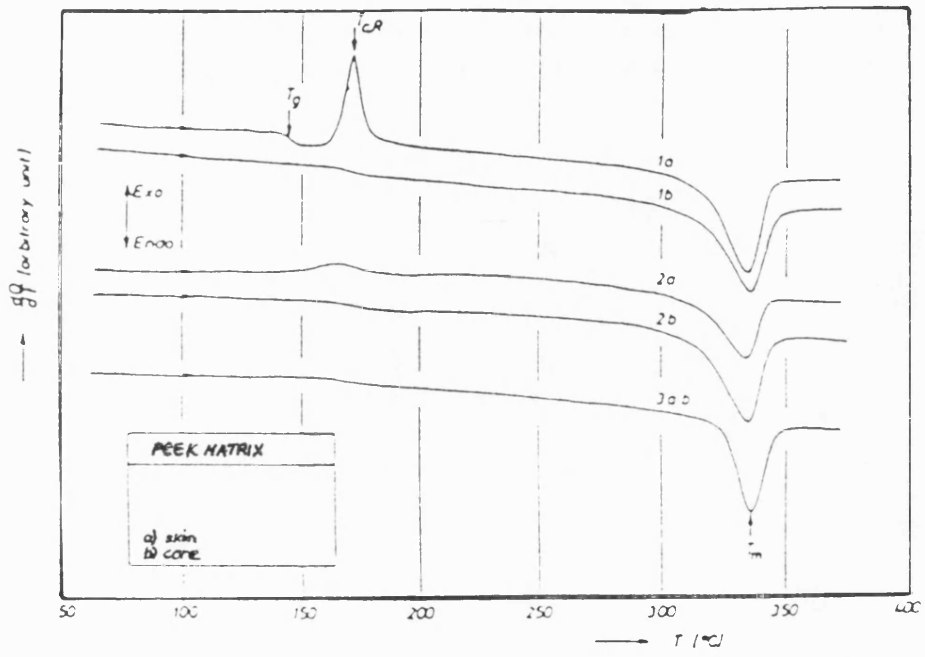

1. As moulded
2. Annealed 150°C for 120 hours (27% crystalline)
3. Annealed 325°C for 120 hours (34% crystalline)

by each technique.

Table 4.3 below, lists the values obtained from the diffraction data and figure 4.4 illustrates a typical diffractometer trace for the polymers used.

Table 4.3. Calculated values of crystallinity.

Sample	% crystallinity
As moulded PEEK	27
Annealed PEEK	35
As moulded PEK	35
Annealed PEK	37
As moulded PET	38

The diffractometer trace for PEK showed extra peaks relating to the additives present in the polymer. These peaks were smoothed out and corrected for during the analysis. In all cases the samples were prepared by slicing through the cross section, without regard for the skin or core regions. It was felt unnecessary to concentrate on these regions because the moulding conditions employed were chosen as a result of many experiments and were found to have little skin/core differences and no interference on the diffractometer trace because of excessive internal stresses.

The results suggest that PET crystallizes more easily and more rapidly than either PEEK or PEK since the as moulded sample exhibits such a high degree of crystallinity. It is understood that different moulding conditions were used in the preparation of the samples from each polymer and direct comparison

Figure 4.2. Relationship between crystallinities measured by DSC and those measured by x-ray, on PEEK 150 P (80).

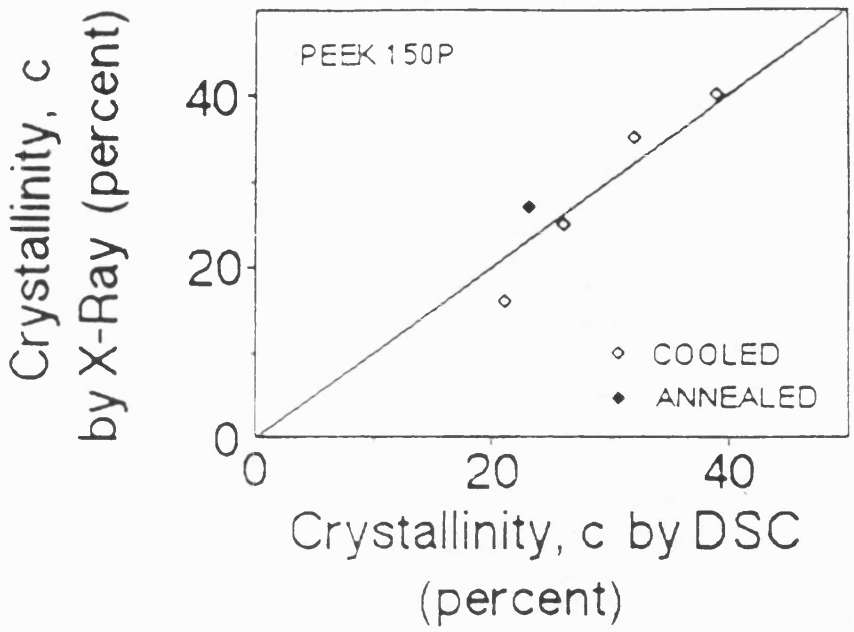

Figure 4.4. Typical trace obtained by x-ray diffractometry (PEEK 35% crystalline).

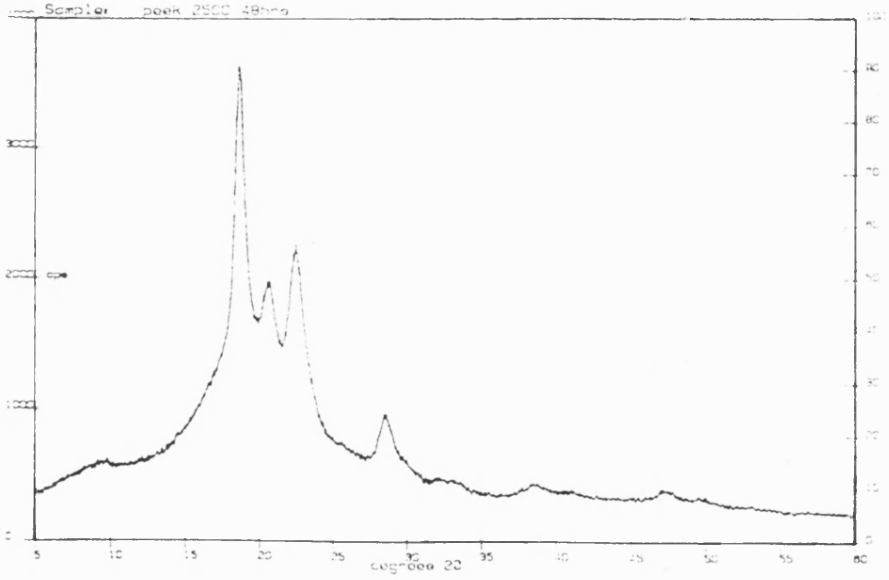

is difficult but it must be stressed that the need to change the moulding conditions for each polymer was necessary for the production of samples of the highest quality. The mould temperatures were kept well above the polymer glass transition temperature in order to keep the internal stresses to a minimum and to reduce the likelihood of obtaining samples exhibiting a noticeable skin/core morphology, although the annealing procedure will have considerably increased the uniformity.

The differences between PEEK and PEK need closer examination. Firstly, their molecular weights are different, as observed in measurements of intrinsic viscosity, calculated from dilute solutions of the polymer in concentrated sulphuric acid;

PEEK 380G IV = 0.84 dL/g
PEK IV = 1.14 dL/g

This illustrates that PEK is of a higher molecular weight, which would suggest that PEK should be more difficult to crystallize, resulting in a lower degree of crystallinity in the bulk than in PEEK under similar moulding conditions. In fact, this does not appear to be the case. The reason why PEK seems to crystallize more rapidly and form a higher level of crystallinity may be that the additives used for this particular grade of the polymer may act as nucleating agents (see chapter 2 for additive details). It is known that PEEK is relatively slow to crystallize and the need to use nucleating agents is apparent, but another possibility exists in that recent discussions concerning the polymerisation of PEK suggest that

parasubstitution occurs rather than orthosubstitution, which is the predominant growth scheme for PEEK. This would result in the formation of a more linear polymer and account for a polymer which will crystallize more readily. The orthosubstitution of PEEK also gives rise to a small percentage of branching which will also effect its ability to crystallize.

On annealing PEK only a 5% increase in crystallinity is observed compared to the 25% increase in PEEK. It is difficult to comment in any great detail on the points raised concerning the parasubstitution of PEK since no literature can be cited because of the restricted position of Raychem Ltd vis à vis its internally produced documents.

4.1.3. Concluding remarks.

The influence of the different values of crystallinity obtained here will be examined more carefully when analysing the performance of the polymers with respect to water droplet impact. An attempt was made to prepare samples of low crystallinity but this proved unsuccessful since a visible skin formed and it was felt that this structure would be unsuitable for further work.

4.2.0. The viscoelastic behaviour of PEEK, PEK and PET.

4.2.1. Introduction.

The results presented in this section are to be used as backround information in understanding how the experimental polymers behave under dynamic testing conditions.

In semi-crystalline polymers, the viscoelastic response is controlled by the mobility of the chains within the amorphous regions. As the polymer is cooled through its glass transition, it will behave as a supercooled liquid with an excess of free volume, which will decrease with time as the polymer reaches a state of equilibrium. The mobility of the polymer chains will be influenced by the available free volume but, conversely, the rate of reduction of the free volume will depend upon the mobility of the polymer chain. At temperatures in excess of the glass transition the mobility is sufficiently high to permit volume relaxation, while below the glass transition, and to a greater extent below any other lower temperature transitions, the mobility will be negligible and no volume relaxation will be observed.

An inhibiting effect of crystallinity towards molecular motion has been observed when dynamic mechanical testing was carried out on amorphous and crystalline samples of PEEK (81). A pronounced depression in the loss tangent peak height was seen in comparison to an amorphous sample, with an apparent increase of approximately 10°C in its measured glass transition temperature. This inhibiting effect of the crystalline regions also occurs for PET and polymers in general do not show a significant change in the loss factor peak with increasing crystallinity.

Before discussing the results obtained by dynamic mechanical and thermal analysis (DMTA), a brief description of the viscoelastic theory will be presented. This is a complicated and well documented

subject but to address it in any great detail would be beyond the scope of this dissertation.

4.2.2. Linear viscoelastic behaviour.

Most polymers can best be described as exhibiting characteristics between elastic solids, ie, ones that are governed by a Hookean response, where the stress is proportional to the strain and is independent of the loading rate, and liquids obeying Newtonian behaviour, where the stress is proportional to the strain rate and is independent of the actual strain. At low temperatures or high rates of strain they display elastic behaviour whilst at high temperatures or low rates of strain they act as viscous liquids and hence the term `viscoelastic' is employed. This behaviour is strictly only relevant at low rates of strain.

The viscoelastic response of polymers to small stresses can be simplified by the application of the following principles;

(i) Boltzman superposition.

During deformation in which the applied stress is varied, the overall deformation can be determined from the algebraic sum of strains during each loading step, since the strain is a linear function of the stress.

(ii) Time-temperature equivalence.

An increase in the temperature will result in accelerated molecular and segmental motion, bringing the polymer system more rapidly into equilibrium and so accelerating all viscoelastic responses. For example, a polymer which displays rubbery characteristics can be induced to behave in a glassy

manner simply by reducing the temperature: increasing the strain rate will give similar behaviour.

The temperature effect may be characterized by producing a series of curves showing the storage compliance, J_1, of an amorphous polymer as a function of temperature and frequency. To apply the time-temperature equivalence principle, a master compliance curve is produced by choosing a particular reference temperature and applying a horizontal shift on a logarithmic time scale which will result in a smooth curve, eliminating the effect of temperature and broadening the frequency range. The factor used to provide the horizontal shift is determined from the empirical Williams, Landel and Ferry (WLF) equation, where the shift factor, a_T, is given by:

$$\log a_T = [-C_1.(T-T_s)] \div [C_2+(T-T_s)] \qquad (10)$$

where C_1 and C_2 are constants, T_s is the reference temperature and T is the actual temperature at which the initial plot was obtained. If T_s is taken to be the glass transition temperature, then the constants become universal and will equal 17.4 and 51.6 K respectively ($T=T_s \pm 50°C$ for amorphous polymers).

4.2.3. Viscoelastic models.

It can be assumed, at least at low rates of strain, that the deformation of a polymer can be represented as the sum of an elastic component and a viscous component.

The linear elastic behaviour is given by Hooke's

law as

$$\sigma = Ee \qquad (11)$$

where E is the elastic modulus and e is the strain, and Newtons law will describe the linear viscous behaviour by

$$\sigma = \Pi (de/dt) \qquad (12)$$

where Π is the the viscosity and de/dt is the strain rate.

A useful way of formulating the combination of elastic and viscous behaviour is through the use of mechanical models. The two basic components used in the models are an elastic spring of modulus E, which represents Hookean behaviour, and a viscous dashpot of viscosity, Π, which behaves in a Newtonian manner.

(i) Maxwell model.

This consists of a spring and a dashpot in series and is used to explain the time-dependent mechanical behaviour of viscous materials. This will exhibit flow plus elasticity on application of stress, ie the spring elongates while the dashpot slowely yields. On removal of the stress, the spring recovers but the dashpot does not.

(ii) Voigt model.

This is also known as the Kelvin model and is useful for representing the response of a tangled mass of polymer chains to an applied stress, explaining the behaviour known as creep. Here the spring and dashpot are in parallel and the dashpot provides a damping resistance to the establishment of an equilibrium being reached by the spring. Figure 4.5 illustrates these relationships more clearly.

Figure 4.5. The strain-time relationships at a constant stress for simple models.

(a) Hookean elastic spring, (b) Newtonian fluid -dashpot, (c) Maxwell model, (d) Voigt model.

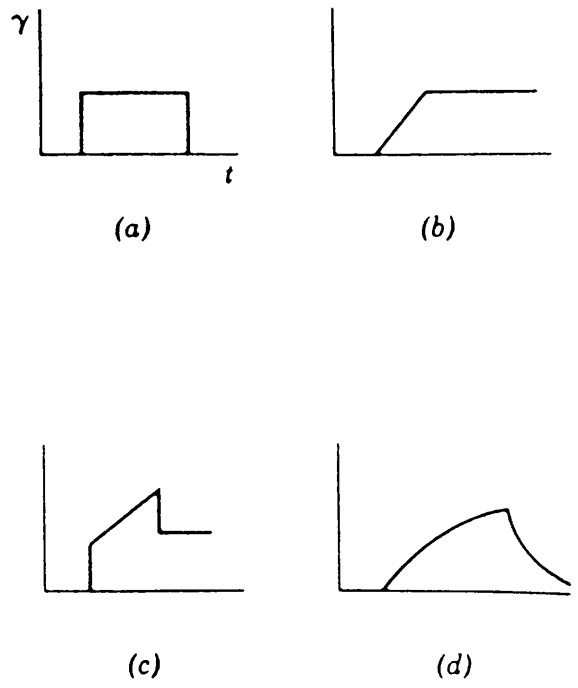

Various combinations of these systems can be formed to describe many different types of polymer responses which is useful in providing a theoretical tool for determining deformation parameters.

4.2.4. Non linear viscoelasticity.

For most polymers which are deformed in practical situations, the theory of linear viscoelasticity does not apply. For example, semi-crystalline polymers do not obey the Boltzmann superposition principle, even at very low strains and here it is found that the exact loading rate affects the final state of stress and strain. In these cases the best approach lies with empirical analysis.

4.2.5. Dynamic Mechanical Testing.

If a simple harmonic stress of angular frequency w , is applied to a sample, the strain lags behind the stress by a phase angle whose tangent measures the internal friction or damping. Measurements carried out in this section were by a forced vibration system, namely DMTA (see chapter 3.0 for more detail). The loss modulus (energy dissipated) and the loss tangent are particularly sensitive to molecular motions, various transitions such as the glass transition, relaxation processes, structural heterogeneities and upon the structure and morphology of multiphase systems (82). The dynamic mechanical spectrum of a material will fingerprint it, in terms of its 1st, 2nd and lower order transitions. In particular, at the glass transition damping is at its highest because of the onset of micro-Brownian motion within the molecular structure of the main chain.

Most chain segments are free to move and in semi-crystalline polymers this will occur within the amorphous phase. Energy is stored within the `frozen-in' segments and this energy will be dissipated as heat as soon as these segments become free to move (observed as a peak in the tan δ spectrum). Lower order transitions such as those arising from the cessation of movement of branches or side groups, which involve molecular segments which are smaller than those found within the main chain, can also be observed. These damping procedures are all sensitive to the frequency/temperature of the test. At high frequencies for example, there will be insufficient time for the molecular chain to uncoil and equilibriate and so the polymer will seem stiffer than if the test was carried out at a lower frequency.

4.2.6. Flexural modulus and tan δ measurements.

The variation caused by temperature and frequency in the flexural modulus and loss tangent can be seen in figures 4.6 to 4.9, which also include the change in behaviour at differing degrees of crystallinity in PEEK and PEK.

The tan δ curves show a primary dispersion peak which reflects the segmental motions of the molecular chains in the amorphous region; this is associated with the glass transition temperature.

The modulus of each material can be seen to fall (log scale) as it moves towards a rubbery plateau from its previous distinctive glassy behaviour.

By increasing the frequency of the test, both the point at which the modulus drops and the maximum loss tangent peak are shifted to a higher temperature, which is as one would expect because of the likelihood of the polymer exhibiting a more glassy and stiffer behaviour at the higher frequency. At these higher frequencies the polymer would require a larger input of heat to register as a reduction in modulus or a shifting of the tan δ peak.

Actual modulus values used for comparative purposes only do not seem to alter to a great extent between the three polymers tested, except that the values obtained for PEK beyond the glass transition are lower than those for PEEK and PET, as illustrated in table 4.10.

table 4.10. Flexural modulus values for PEEK, PEK and PET.

sample	Flexural modulus > Tg (E' MPa)	Flexural modulus < Tg (E' MPa)
PEEK 27%cryst	126	655
PEEK 35%cryst	178	609
PEK 35%cryst	79	611
PEK 37%cryst	126	682
PET 38%cryst	178	562

An interesting feature is that there is a shift in the glass transition temperatures occurring not only with increased frequency but also with the increased level of crystallinity. This shift has been mentioned and reported elsewhere (81), and it has been proposed that the shift arises from the inhibiting effect of the crystalline regions upon molecular motions within the amorphous phase (see table 4.11).

Figure 4.6. Loss tangent spectra for annealed PEEK and PEK.

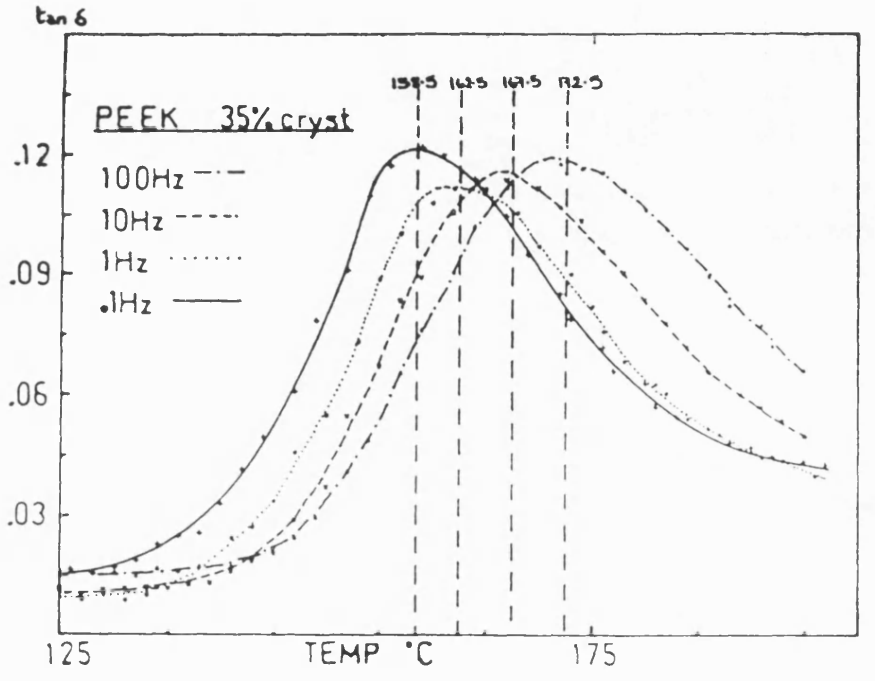

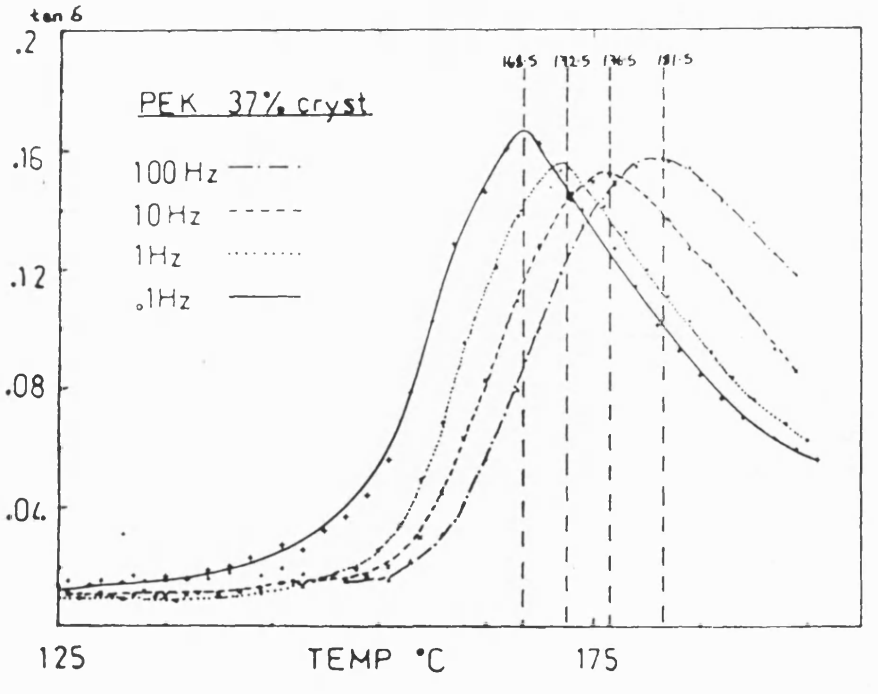

Figure 4.7. Loss tangent spectra for as moulded PEEK and PEK.

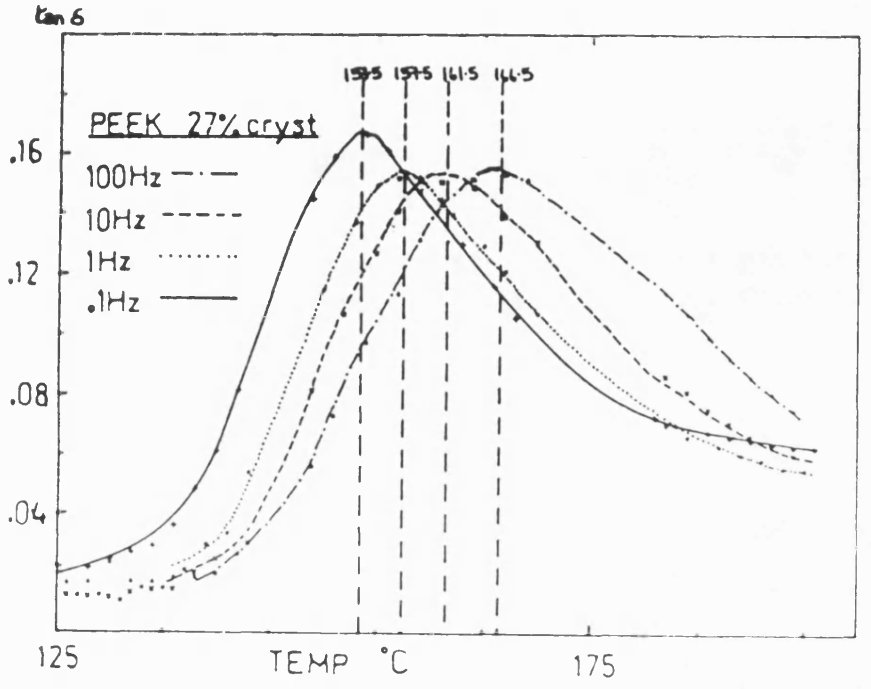

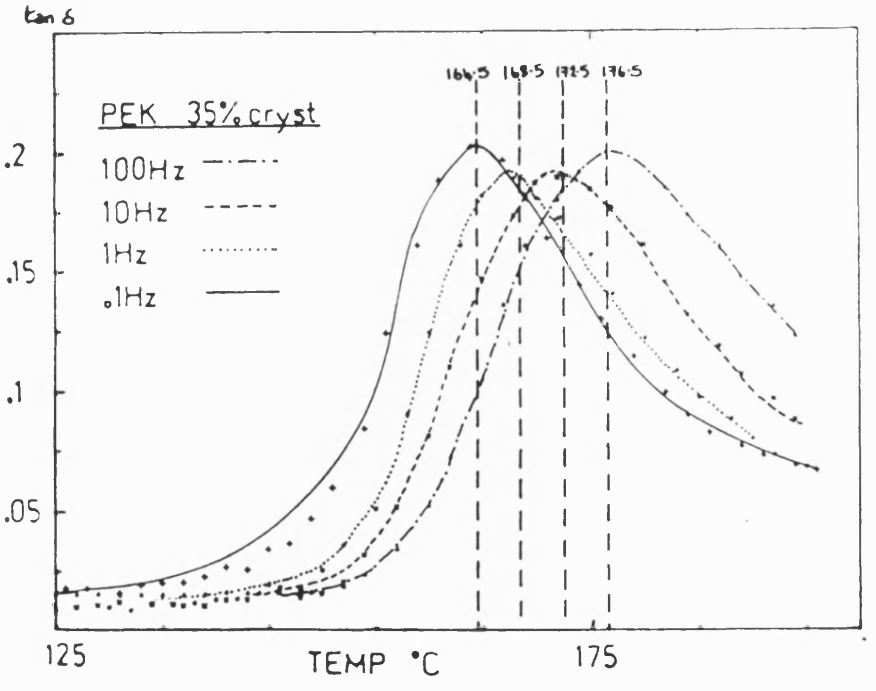

Figure 4.8. Flexural modulus curves for annealed PEEK and PEK.

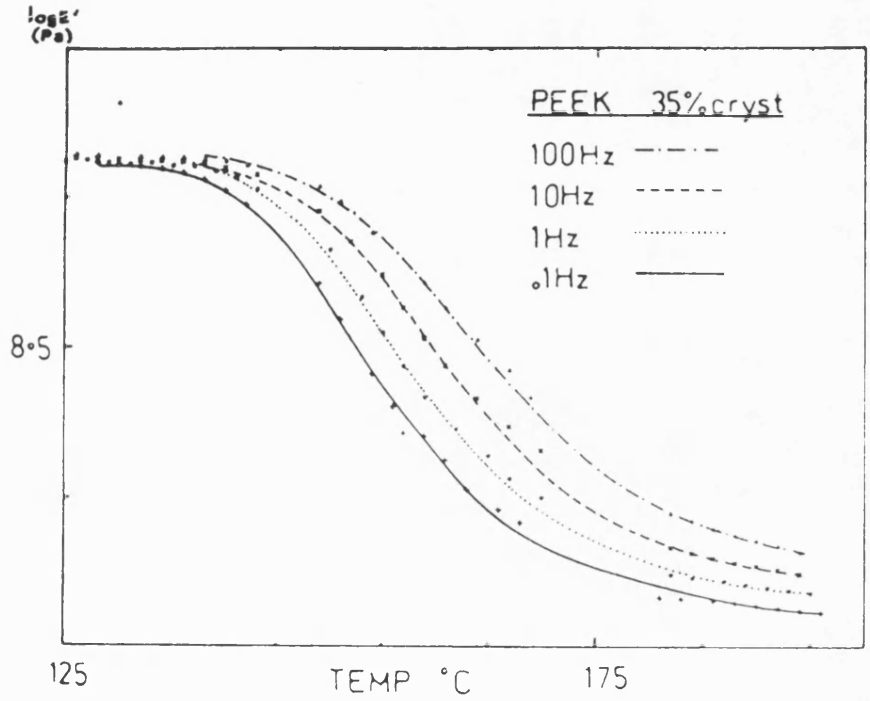

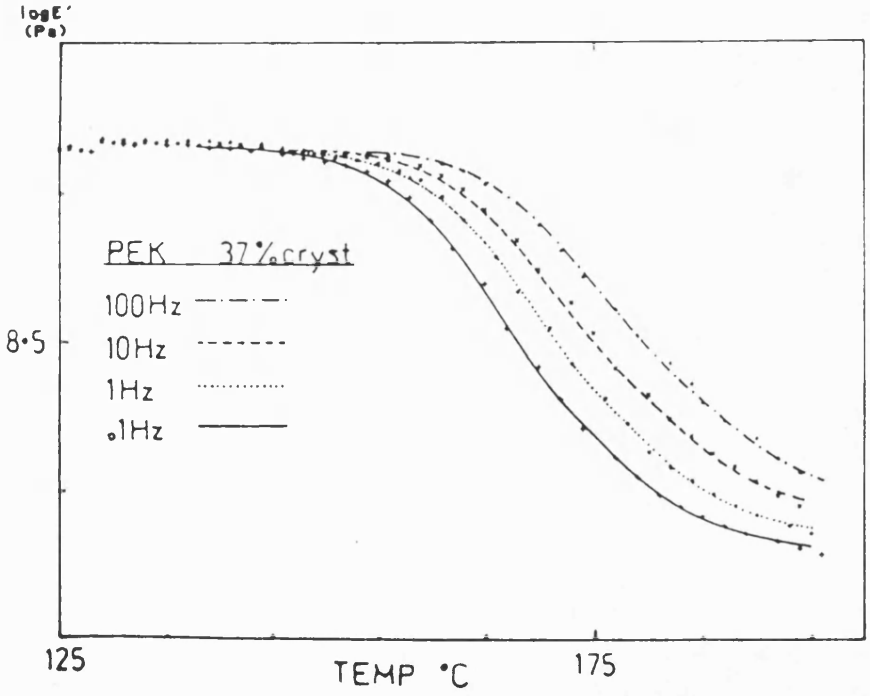

Figure 4.9. Flexural modulus and loss tangent measurements for PET (38% crystallinity).

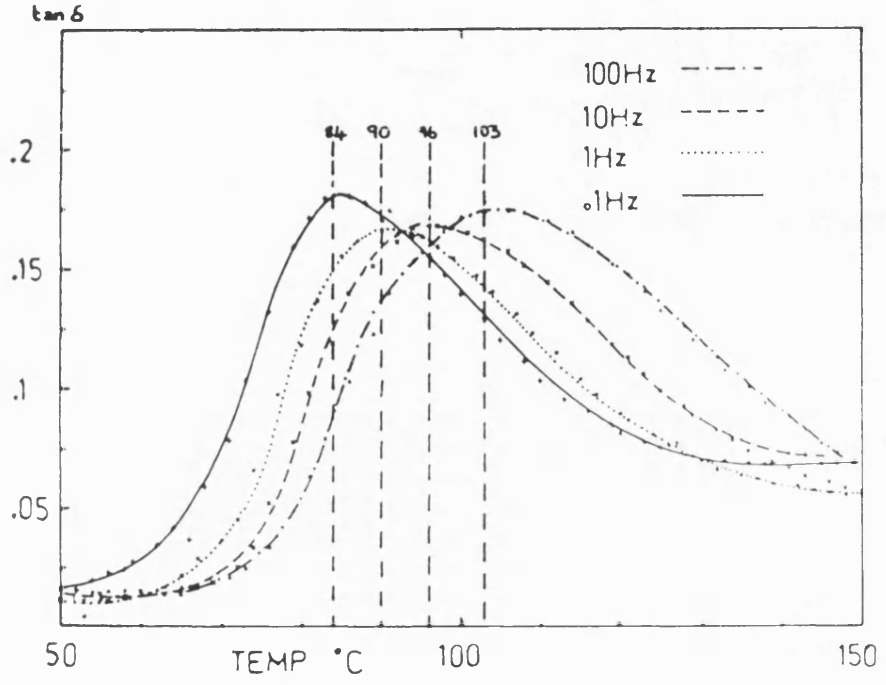

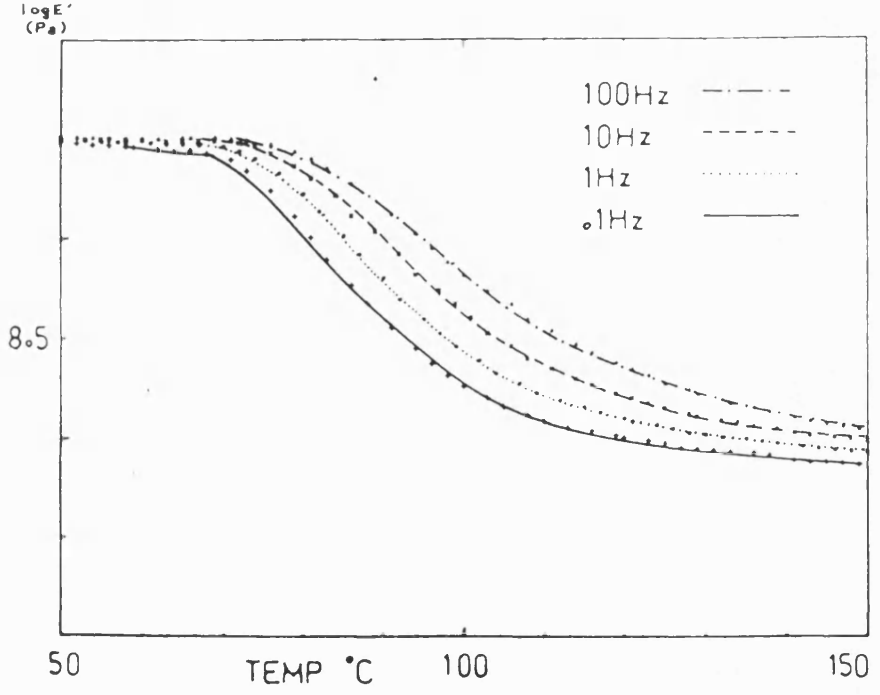

In the classical viscoelasticity theory it is the loss modulus peak (E") that defines the glass transition and not the loss tangent peak. In this case the loss tangent peaks were approximately 5°C higher in temperature and the information was much clearer, so it was used solely for the purposes of comparison. In any case there exists some doubt as to the acceptibility of defining the glass transition with either curve.

Table 4.11. The shift in tan δ peak temperatures as a function of crystallinity, taken from tan δ curves at 1Hz.

Sample	measured Tg (°C)
PEEK 27%cryst	157.5
PEEK 35%cryst	162.5
PEK 35%cryst	168.5
PEK 37%cryst	172.5

4.2.7. The dependence of the glass transition on frequency.

This was analysed by constructing an Arrhenius plot for each polymer and the activation energy of the glass transition process was measured. The activation energy was calculated by taking the log to the base 10 of the Arrhenius equation;

$$\log \text{freq} = \log A - (E/2.303RT) \qquad (13)$$

where E is the activation energy, A is the Arrhenius factor, R is the gas constant and T is the absolute temperature.

The plot can be seen in figure 4.12 and the

resultant measured activation energies appear in table 4.13. These values were seen as being a measure of the energy required to move a large segment of the molecular chain from a 'frozen-in' glassy state through to a rubbery plateau region. These chains are further restricted in their motion by the crystalline network and it is this hinderence that leads to such high values for the activation energy. Conventional measurements of the activation energy deal with the reactivity of a chemical process, the movement of individual groups or the motion of side groups and branches and so it becomes difficult to place these measured values into context, but some agreement has been found in comparison with some values calculated in literature.

Table 4.13. The activation energy for the glass transition process.

Sample	T_g	E_{act} kJmol^{-1}
PET 38%cryst	90.0	380
PEEK 27%cryst	157.5	731
PEEK 35%cryst	162.5	754
PEK 35%cryst	168.5	750
PEK 37%cryst	172.5	781
Polyethylene (84)	-80	46-75
Polypropylene(84)	-20	117-152
PEEK (61)		700-1400
PEEK (83)		depending on level of crystallinity

It can be seen that the activation energy values increase with increasing crystallinity but also change dramatically with increase in the glass transition temperature as can be seen by comparing polyethylene with PEEK. The hinderance to molecular motion is readily apparent from these data and PEK can be seen as exhibiting the greater restriction to motion.

Figure 4.12. The dependence of the glass transition temperature on frequency and crystallinity from loss tangent spectra.

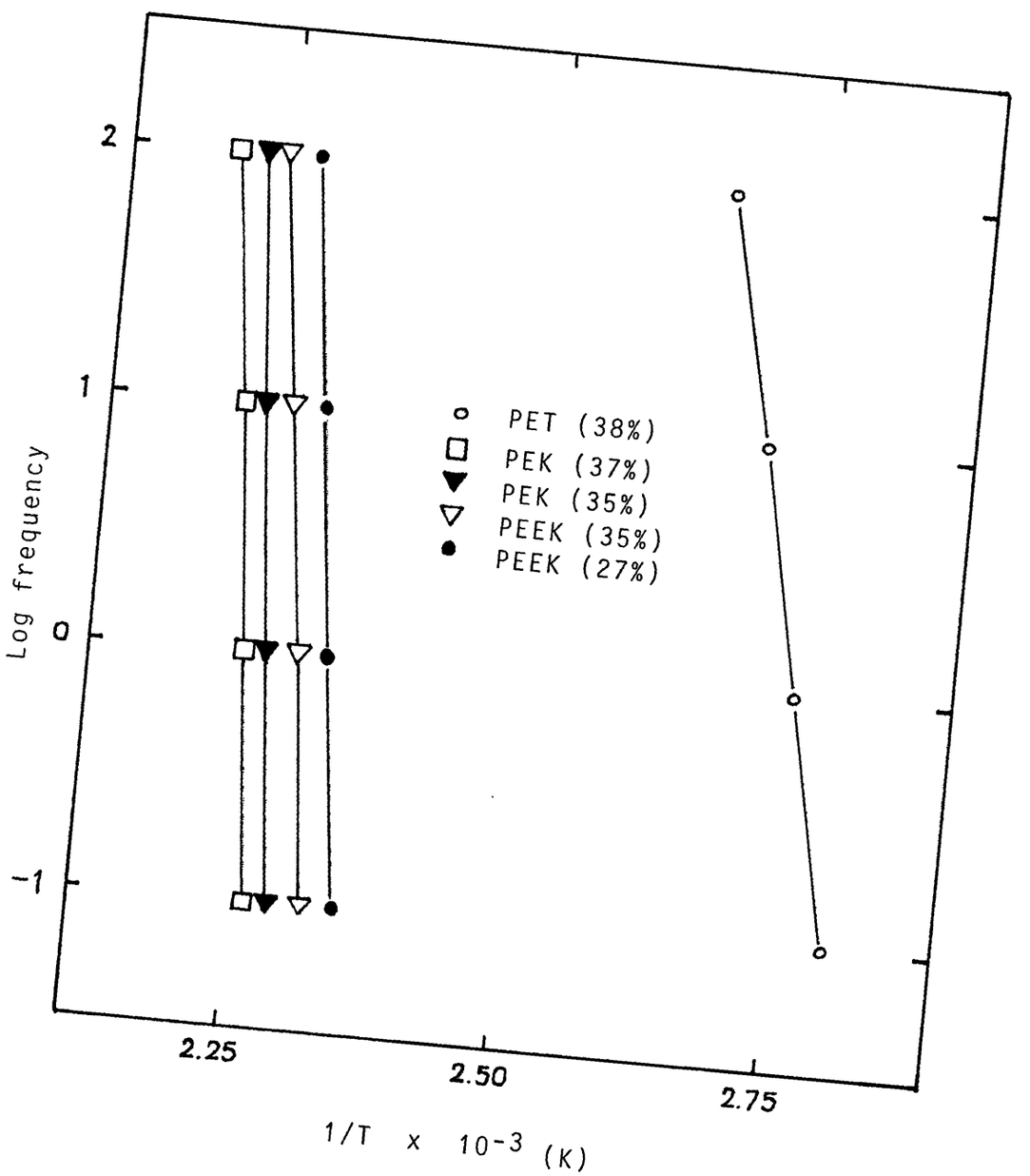

From this plot it is apparent that extrapolation of the lines to obtain the Arrhenius constant (the pre-exponential factor, A) would yield unreasonably large values of A. Over the frequency range measured it would be unjustifiable to do this, but it leads one to wonder whether or not the Arrhenius expression is valid for this type of process (ie a glass transition).

4.2.8. Time-temperature superposition.

The temperature and frequency dependence of dynamic mechanical properties in the region of the glass transition are well described by the WLF equation, which has been derived from the free volume theory of the glass transition, ie on the basis that for molecules or molecular segments to move freely there must be spaces available for them to occupy. Below the glass transition the free volume is too small for main chain movement but above it, where sufficient energy has been provided, the molecular movement is such as to create an increased free volume.

Figure 4.14 shows the plots obtained by redrawing the storage modulus curves (log E') at differing temperatures around the glass transition over various frequency ranges. A horizontal shift was applied by calculating log a_T to eliminate the differences in the glass transition temperatures, so that true comparisons of the flexural modulus could be made. The glass transition temperatures used for T_s, were the ones presented in table 4.11 and the values of C_1 and C_2 were taken as 17.4 and 51.6 respectively. Although these values for the

constants are for amorphous polymers exhibiting linear viscoelasticity, for the purposes of this investigation it was felt unnecessary to determine these constants which could be found at the intercept (C_1) and slope (C_2) of a linear plot of $(T-T_s)/\log a_T$ versus $T-T_s$, since this was again carried out for comparative purposes only.

A master curve of the dynamic flexural modulus versus the shifted log frequency, was constructed and is presented in figure 4.15. It can be seen that firstly there is an increase in modulus on increasing the crystallinity (more apparent in the case for PEEK) and, secondly, there is a similarity in the behaviour in all three polymers once the glass transition differences are removed. In fact the modulus of PEEK is the highest in the low frequency range and the curves for all three polymers converge at higher frequencies.

All the samples compare favourably and no significant differences can be seen. They have been analysed by using linear viscoelastic theory and it must be mentioned that the glass transition temperature cannot be ignored in this way as it does mean that the polymer with the highest glass transition temperature would be suitable for service at higher temperatures than the others.

4.2.9. Low temperature transitions.

The samples were also analysed at temperatures as low as -125°C in order to observe any low temperature transitions. There is some evidence to link these low temperature molecular motions with the

Figure 4.14. Dynamic mechanical characterization of PEEK, PEK and PET.

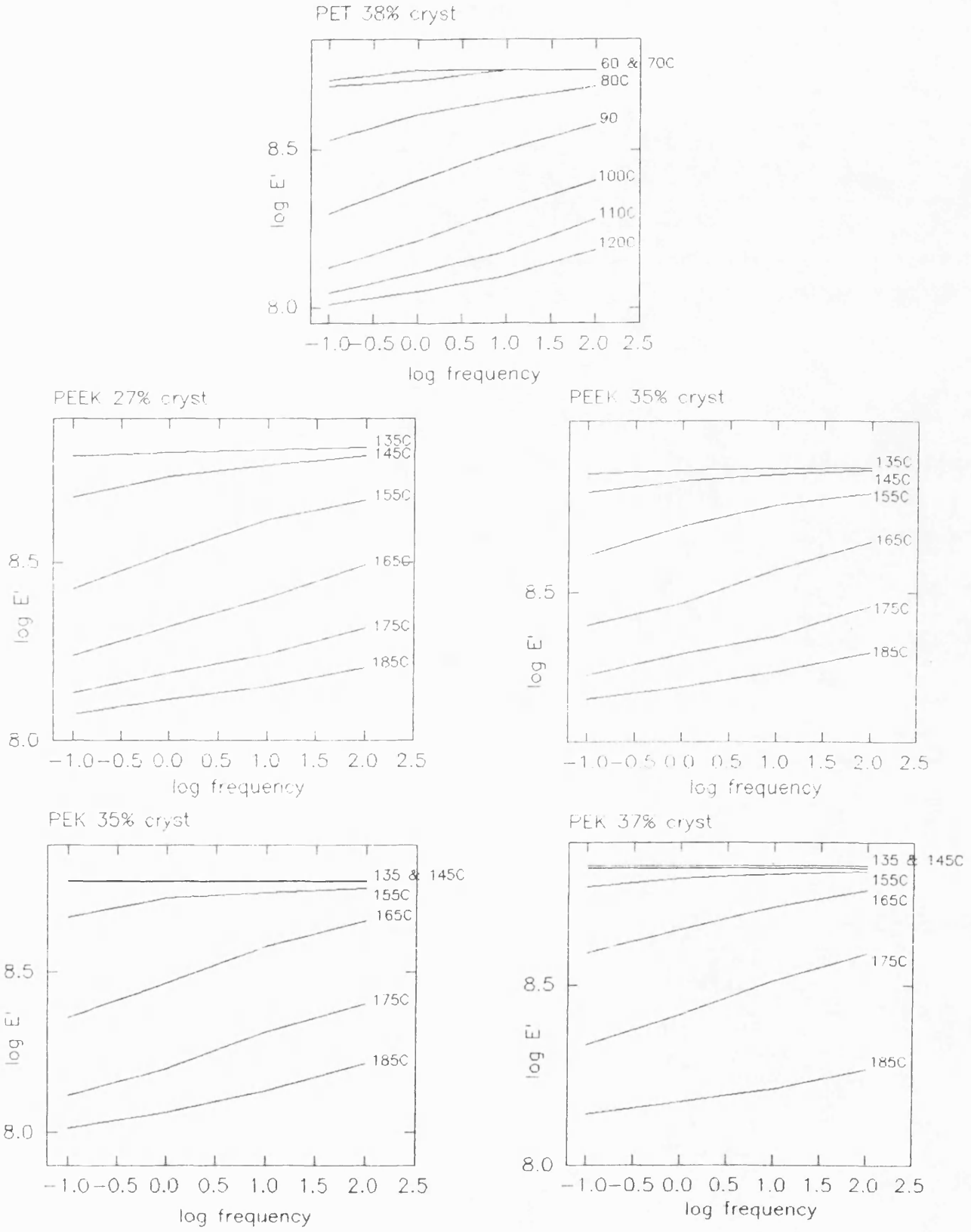

Figure 4.15. Flexural modulus master curves.

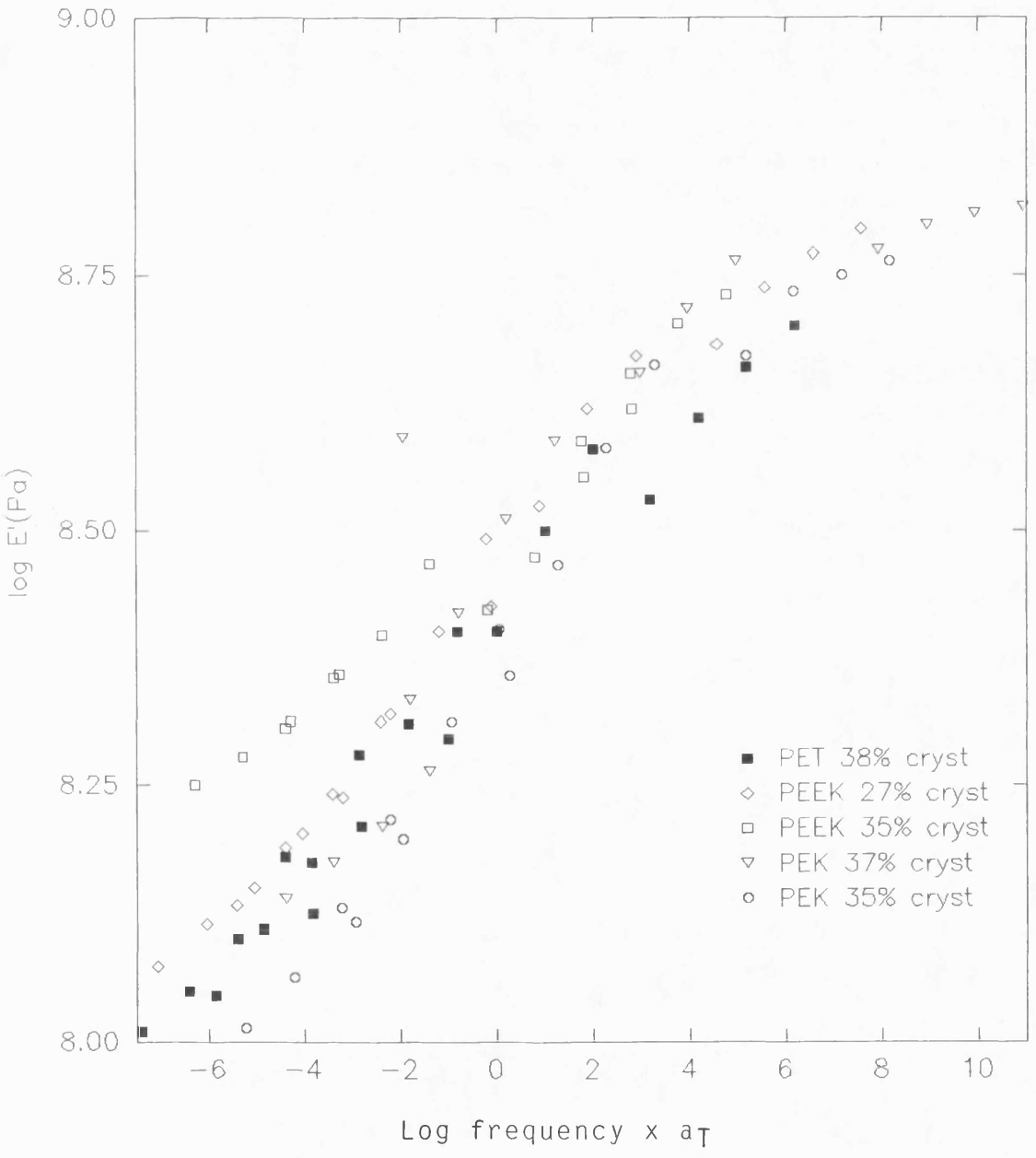

polymer impact strengths and to ductile/brittle transitions occurring below these temperatures (85).

Although the statement is inconclusive, one can propose that if damping occurs as a result of main chain motion then going through this maximum results in an increased impact strength whereas if it is caused by movement of side chains or groups, little difference between impact strengths will be observed. The experiments carried out here are limited and one may postulate that side chains in PEEK, PEK and PET will be virtually non-existent, although it is known that PEEK can exhibit some form of branching, so that any low temperature transitions will be as a result of main chain motions.

The modulus vs temperature curves for the polymers can be seen in figure 4.16, where a distinctive difference in behaviour can be seen between PET, PEEK and PEK. PET shows a sharp drop in modulus while for PEEK and PEK the drop is very shallow. This behaviour is also illustrated in figure 4.17, where the tan δ curves illustrate sharp peaks for PET whereas they are difficult to distinguish for PEEK and PEK. The values of tan δ are of a small order with little change when going through the transition for PET while an increase is observed for PEEK and PEK, values from 0.006 up to 0.015, on passing through this diffuse transition step. Activation energy values were also calculated for these low temperature transitions and these can be seen below.

Sample	Eact $kJmol^{-1}$
PEEK 35%cryst	47
PEK 35%cryst	47

Figure 4.16. Flexural modulus spectra for PEEK, PEK and PET, carried out at sub-zero temperatures.

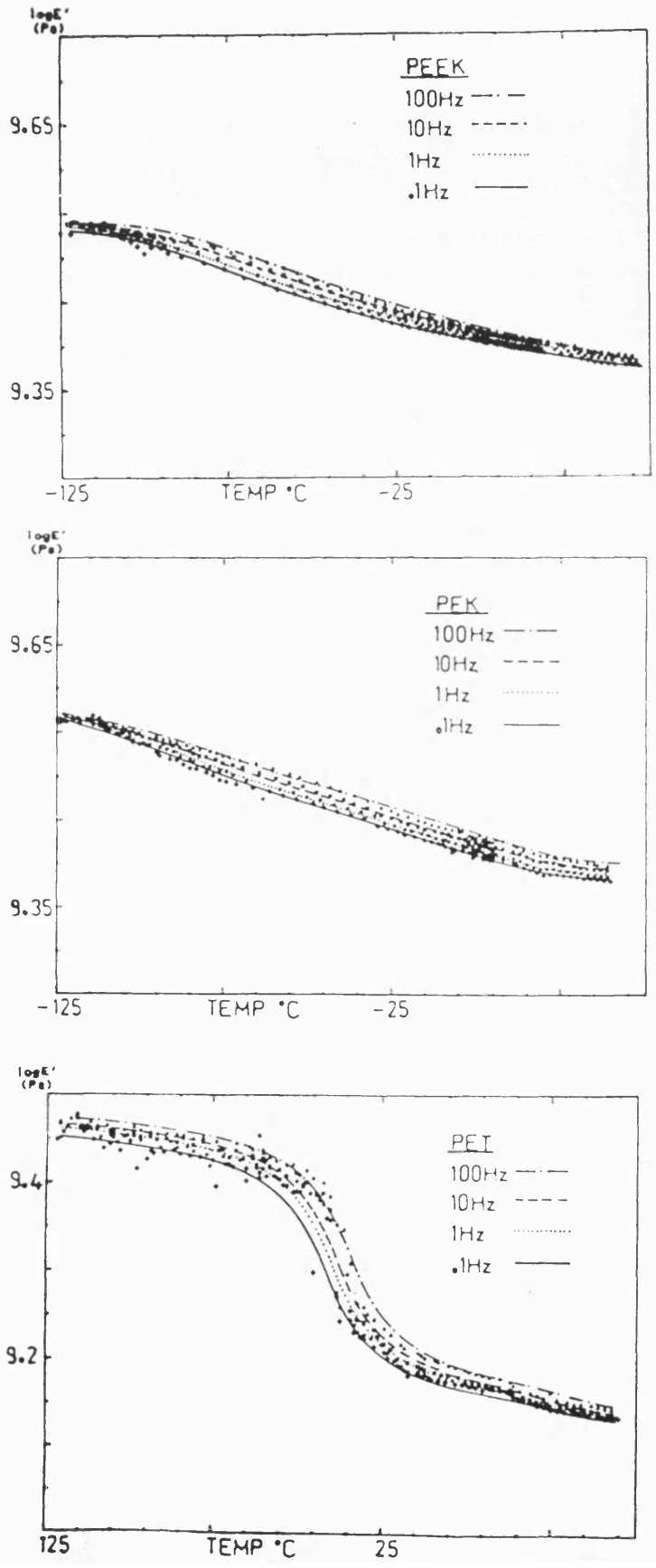

Figure 4.17. Loss tangent spectra for PEEK, PEK and PET, carried out at sub-zero temperatures.

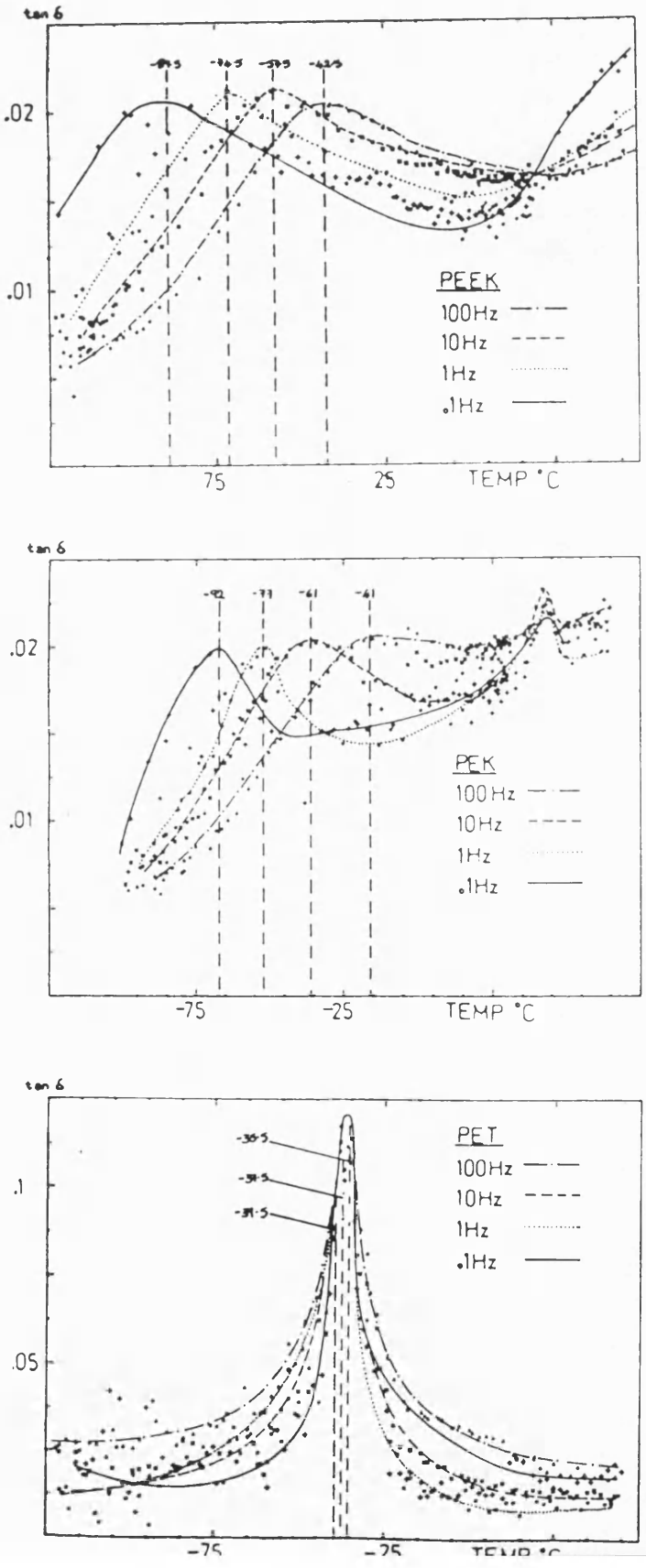

The values for PEEK and PEK seem reasonable as they are a measure of a small proportion of the chain in motion, whereas, the value obtained for PET (not disclosed) was completely unjustifiable and it could only be deduced that some error during testing was present, for example, clamp slippage (test carried out many times and always leads to the same result) or, that the Arrhenius expression does not fit the behaviour of PET.

The tan δ curves for PEK show a small sharp peak occurring at -30°C. This is thought to be a low temperature peak for PTFE, which is known to be present to a small degree. No indication of the PTFE additive was detected around the glass transition zone of PTFE (126°C)(84), but this may have been masked by the onset of the process occurring for PEK or that a certain compatibility exists between the two polymers at this level of addition.

4.3.0. Mechanical properties.

4.3.1. Introduction.

The polymers PEEK and PEK have obvious engineering applications and, as composites, they offer considorable advantages over thermosets in respect of damage tolerance, high temperature resistance, and reduced sensitivity to water absorption.

One of the main requirements for an engineering component is for it not to break in service. To obtain an indication of the relative toughness of these materials, some tensile and impact properties were investigated. It has already been remarked upon

that if the polymer exhibits high toughness then its resistance to water drop impact and erosion should also be high.

4.3.2. Tensile characterisation.

Waisted samples of PEEK and PEK were tensile tested at a constant rate to evaluate their ultimate tensile strength and elongation to break. The testing was carried out over the temperature range of 23°C to 160°C in order to observe the change in properties as they reached their glass transition temperatures. This was felt to be important as aircraft components may be subjected to aerodynamic heating and the actual temperatures reached, albeit for a short period of time, may exceed the advised service temperature for the given polymer system. Table 4.18, lists the results obtained from these tests.

4.3.3. The stress/strain relationship.

The general stress/strain response of these materials can be seen in figure 4.19: PEEK and PEK exhibit a similar response, albeit with different actual values of stress and strain. Although the illustration does not show it, for reasons of clarity, a shift of the curves to higher values occur with increasing crystallinity of the sample. The resultant increase in strength can be explained in terms of the extra reinforcement provided by the crystalline regions. There was only a slight shift observed for PEK which is as expected considering the small difference in the crystallinity of the samples.

The most interesting feature of the plot is the

Table 4.19. Tensile measurements on PEEK and PEK.

Material	Temp °C	No. of tests	Tensile strength MPa	S.D	Elongation %	S.D
PEEK	23	5	92	2.4	103	10.5
27% cryst	100	5	68	2.7	140	16.3
	140	5	55	2.2	170	16.6
	160	5	51	2.6	186	13.6
PEEK	23	5	96	1.0	48	11.2
35% cryst	100	5	68	1.2	69	5.4
	140	5	56	3.3	135	5.5
	160	5	56	2.3	183	11.8
PEK	23	5	97	2.1	75	10.0
35% cryst	100	5	70	2.5	104	14.1
	140	5	55	4.6	121	36.8
	160	5	52	1.2	155	10.8
PEK	23	5	100	2.3	58	15.9
37% cryst	100	5	75	3.7	93	32.1
	140	5	59	2.4	121	18.8
	160	5	56	1.1	156	6.1

ductile behaviour at room temperature, changing to a behaviour exhibiting cold drawing at elevated temperatures for both polymers. This transition in behaviour occurred when testing at 140°C and above, and is indicative of the increased mobility of the amorphous regions as the sample approaches its glass transition, ie glassy to rubbery behaviour. The behaviour of both polymers can be described as becoming `rubbery' which can be explained by the low modulus and high deformation over a smaller application of stress.

4.3.4. The effect of increasing temperature and crystallinity on strength and ductility.

The fall in ultimate tensile strength on increasing the temperature is demonstrated in figure 4.20. Some differences are evident between the differing crystallinities with an indication being that the higher the crystallinity the higher the resultant values, even at elevated temperatures. It must be pointed out that the standard deviations for most of these results overlap and that the effect of crystallinity is not statistically identifiable. It is interesting to observe that the curve for PEEK with 35% crystallinity seems to level off on going through its glass transition temperature, resulting in values similar to PEK with its highest level of crystallinity. This clearly demonstrates the extra reinforcement provided by the crystallites. Overall, the behaviour is as expected, the tensile strength falling as a result of the greater mobility of the amorphous regions as they come closer to changing from a rigid glassy solid to a solid with rubbery properties.

Figure 4.19. Load-elongation plot obtained for PEEK and PEK.

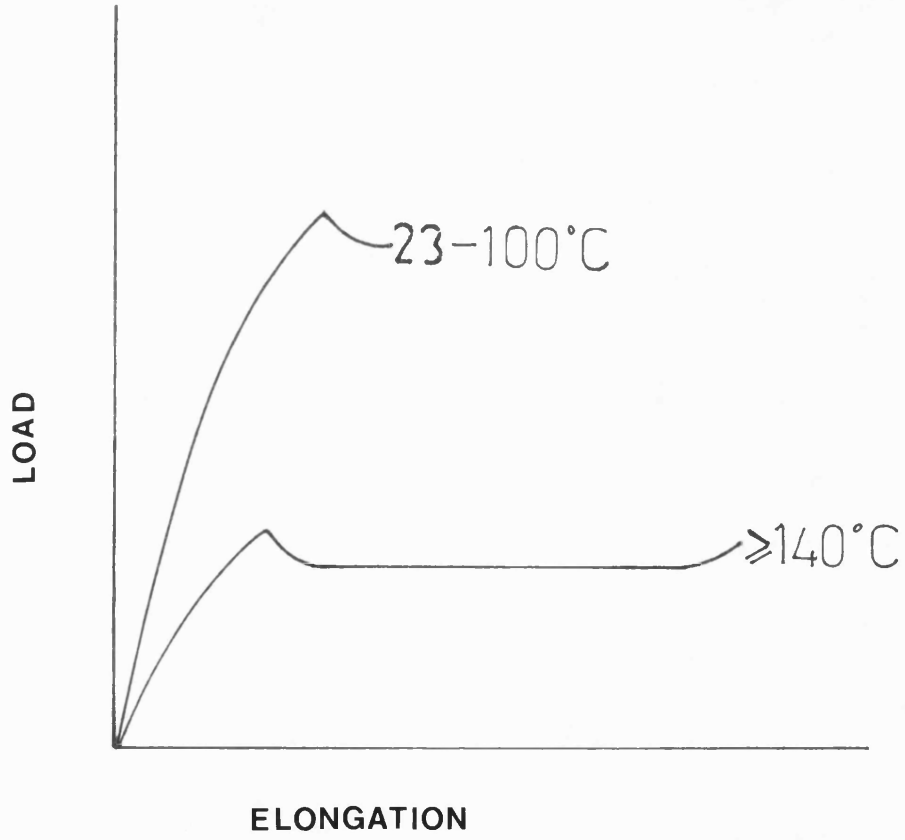

Surprisingly, the values obtained for PEK over a very small change in level of crystallinity differ to a much greater extent than those for PEEK, where the only noticeable difference occurs at 23°C and 160°C. More experimental work would be needed to see if these values are significant, as the error in the values may account for this difference as has already been mentioned. It could therefore be argued that both PEEK and PEK exhibit similar values over these temperature ranges for the crystallinity values studied.

An explanation of any differences between PEEK and PEK could be derived from an analysis of the more rigid chemical structure of PEK (having one less ether linkage), where even a small change in crystallinity could account for a large change in rigidity. This becomes more apparent when the elongation at break of the polymers is discussed and can be seen in figure 4.21. At room temperature an increase in crystallinity significantly alters the polymer behaviour, with the material exhibiting a more pronounced ductile response. As the temperature is increased the effect of the extra crystalline regions becomes more diminished, where again the increase can be accounted for by the increased mobility of the polymer chains within the amorphous region as the input of extra energy into the system by increasing the temperature takes effect.

One can make a direct comparison of PEEK with PEK for a degree of crystallinity of 35%. At room temperature, PEK behaves in a more ductile manner with a similar value of tensile strength but a higher

Figure 4.20. The effect of increasing temperature and crystallinity on tensile strength.

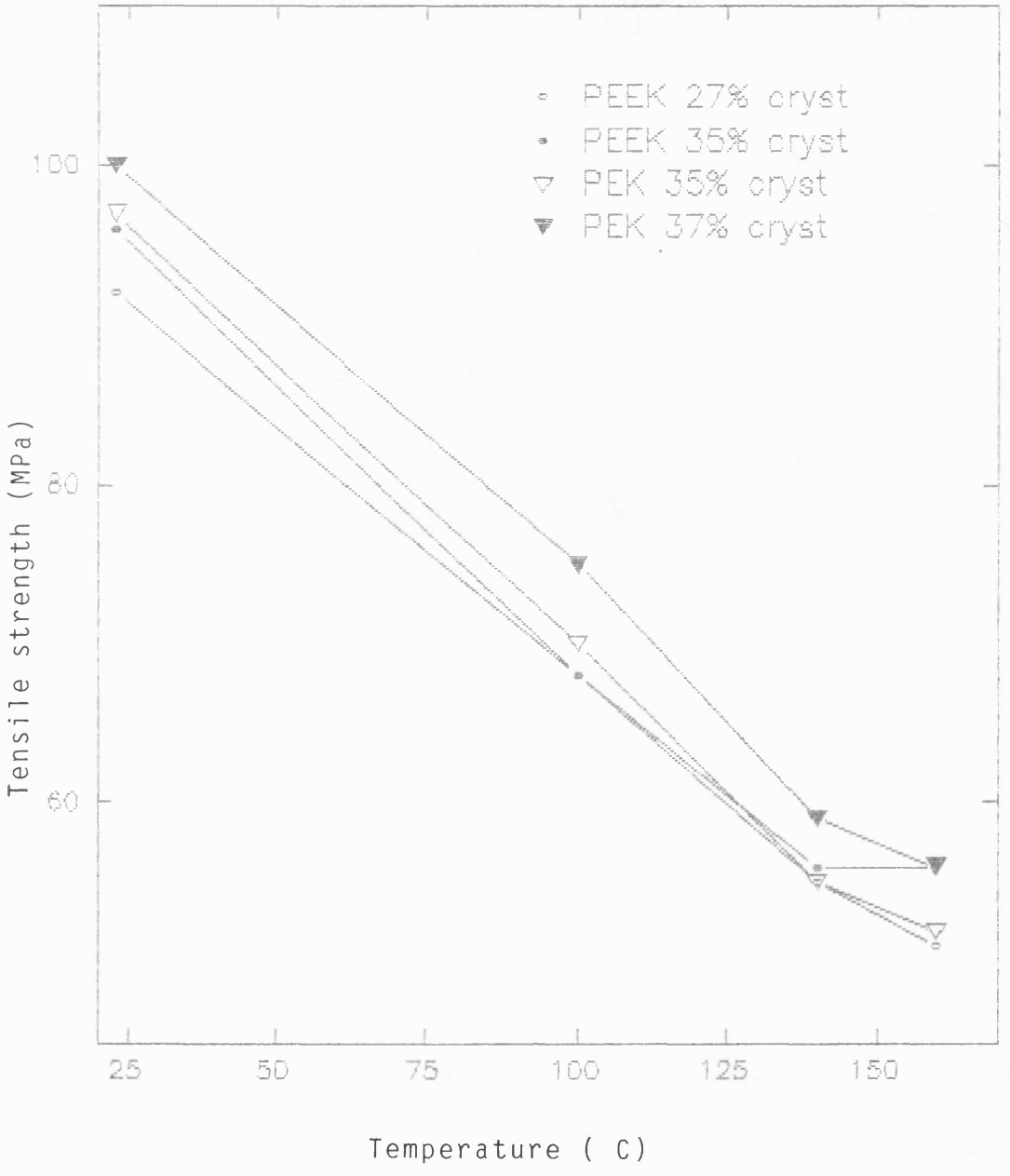

Figure 4.21. The effect of increasing temperature and crystallinity on ductility.

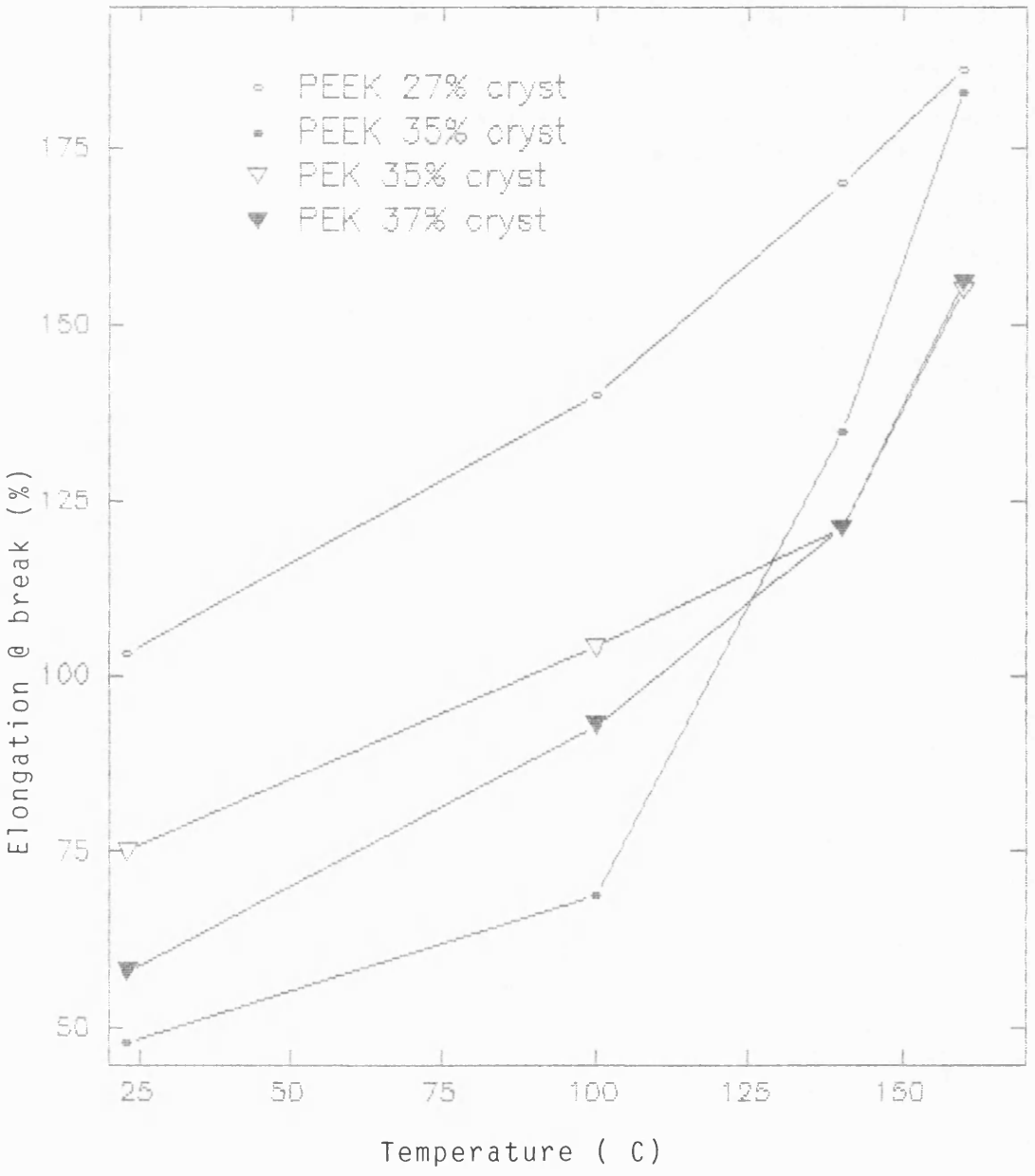

elongation at break. As the temperature of testing is increased, PEEK becomes tougher in nature although at 160°C it is close to or past its glass transition (NB. the glass transition is rate dependent) while PEK is just approaching Tg. This gives weight to the argument that PEK is a more rigid structure than PEEK, although one must be careful in making such statements because large variations in results do occur.

4.3.5. Impact performance.

The response to impact was determined with an instrumented Charpy type tester manufactured by Ceast, as described in chapter 3.0. The purpose of impact testing is again to obtain an understanding of the toughness of the polymers.

The first experiment that was performed was to investigate un-notched behaviour of the three polymers. The values obtained are to be used as base values in observing the effects of subsequent impact by water droplets. The samples did not break, so the values are in effect a lower bound to the fracture energy, and it can be concluded that this effect is a measure of the rigidity of the sample specimens, as the energy calculated was the energy required to bend the sample sufficiently so as to force it through the sample holder. The results can be seen in the following table.

The magnitudes of these values, even considering that the specimens have not broken, is very surprising and this illustrates just how tough these materials are.

These values can be compared to ones found for PET, where under the same impact conditions the specimens broke, leading to a calculation of a true fracture energy of 71 kJm^{-2}.

Sample	No. of tests	Impact energy (kJm^{-2})	S.D
PEEK 27% cryst	10	595	19
PEEK 35% cryst	10	612	37
PEK 35% cryst	10	625	27
PEK 37% cryst	10	667	31

An increase in the resultant energy with increasing sample crystallinity is observed, which is contrary to what is normally expected and to most published results, except that it must be stressed that the true fracture energy was not calculated, but what has been referred to as a lower bound fracture energy or sample rigidity, has. In view of this, one would expect a rise in the values on increasing the crystallinity, again because of the reinforcing effect that is provided. The values also suggest that PEK is a tougher material than PEEK.

Although these values are to be used at a later stage in this dissertation, a greater understanding of the polymers' response to impact is required. Values were also obtained on notched specimens, so

that the brittle transition could be induced and more information gained. Notches were machined at varying depths, with a root radius of 0.254mm and an angle of 46°. The tabulated mean results from three tests can be seen in the following table.

A/W	Fracture energy (energy/csa) kJm^{-2}									
	PEEK 27%	S.D	PEEK 35%	S.D	PEK 35%	S.D	PEK 37%	S.D	PET	S.D 38%
0.016	24	0.5	21	0.7	78	0.7	72	0.7	15	0.5
.0416	19	0.8	19	0.8	43	3.8	43	3.4	11	0.5
0.083	12	0.9	11	0.5	34	0.5	25	0.3	6	0.3
0.16	8	0.6	7	0.3	21	0.8	21	0.3	5	0.3
0.3	4	0	4	0	14	0.4	11	0.4	3	0.4

The differences in notch sensitivity are readily apparent in figure 4.24. First, increasing the crystallinity of the samples does not alter to a great extent the fracture energy as a function of notch depth, although it is well known that an increase in crystallinity will usually induce more brittle behaviour: this is only evident at small notch depths.

On increasing the depth of the notch the values obtained for PEEK tend towards those found for PET, whilst for PEK the values are significantly higher, by a factor of approximately three over the range of notch depths studied. This does indicate that PEK has a greater resistance to crack propogation than either PEEK or PET. The reasons for these differences are not clear, as the results referred to

Figure 4.24. The effect of the notch depth ratio, A/W, on the fracture energy.

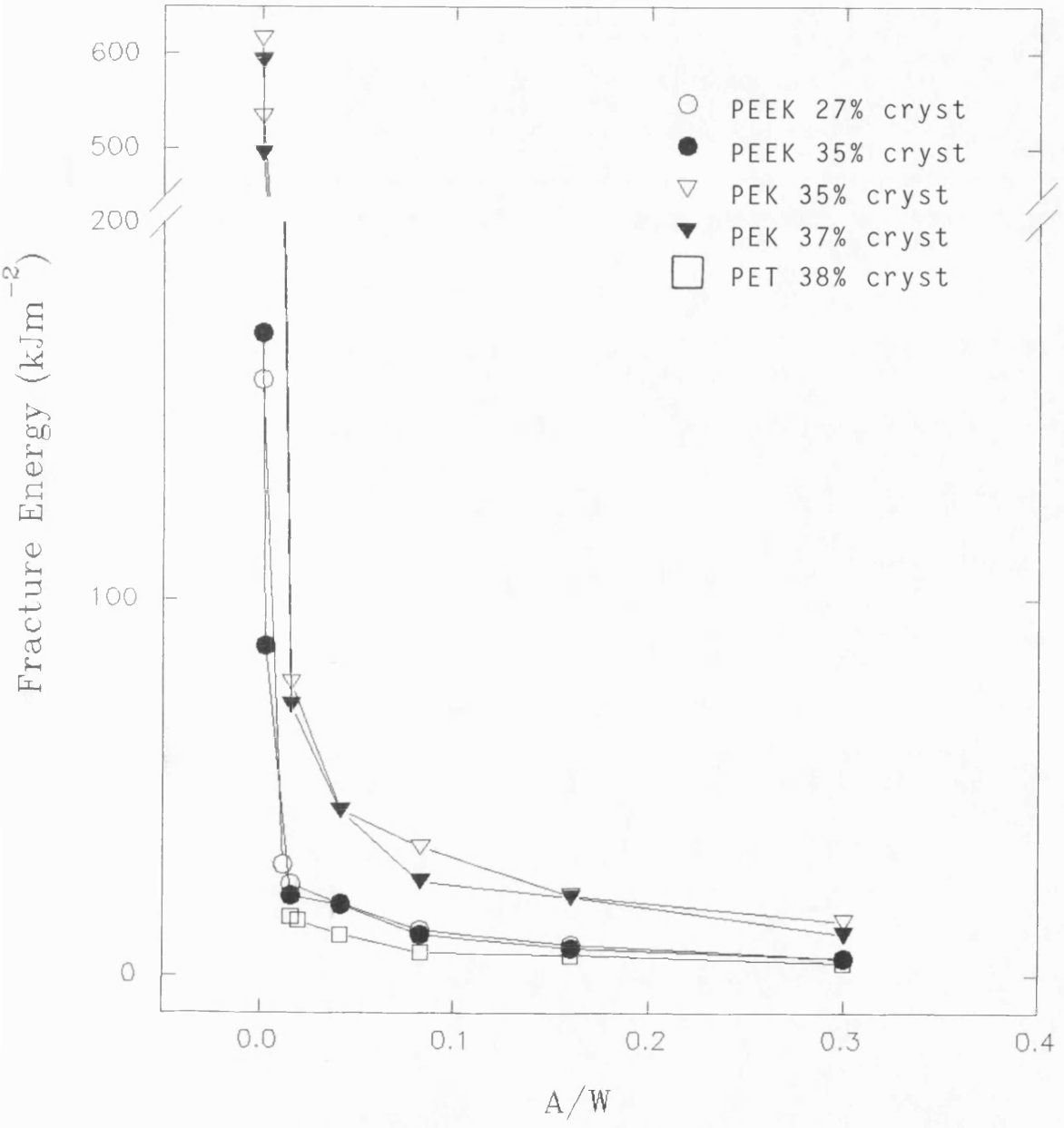

previously have indicated a very similar mechanical behaviour for PEEK and PEK. A possible explanation for the observed response is that the PEK contains a certain low percentage of processing additives, and in particular, PTFE. The addition of PTFE may have the effect of causing the PEK to behave as a rubber modified glassy plastic, like polystyrene modified with small particles of a rubber such as polybutadiene. It is important that the rubber-to-resin interface is well connected and one would assume that this would be the case for PTFE dispersed within PEK. The PTFE particles would have to act as areas where energy could be absorbed and dissipated in the form of very tiny cracks or crazes between the particles (the added filler would also assist in this process), and in so doing would impede the straightforward propagation of a crack under impact loading. From the data obtained so far and the known chemical similarity of the polymers, it is felt that this could be a reasonable assumption.

To reinforce these results, another technique was employed in order to understand more fully the fracture behaviour of the polymers. The technique used was a 3-point bend test, carried out on an Instron 1122, with a crosshead speed of 0.5mm/min. Un-notched and notched samples were tested and figure 4.25, illustrates the response of PEK. For both PEEK and PET a sharper fall off was observed after the peak load was reached, again showing a more brittle response than that found for PEK. The un-notched samples did not break so that the fracture toughness could not be calculated. Therefore the flexural strength was calculated from (75);

Figure 4.25. Force/displacement curves produced by 3-point bend testing of PEK (35% cryst)

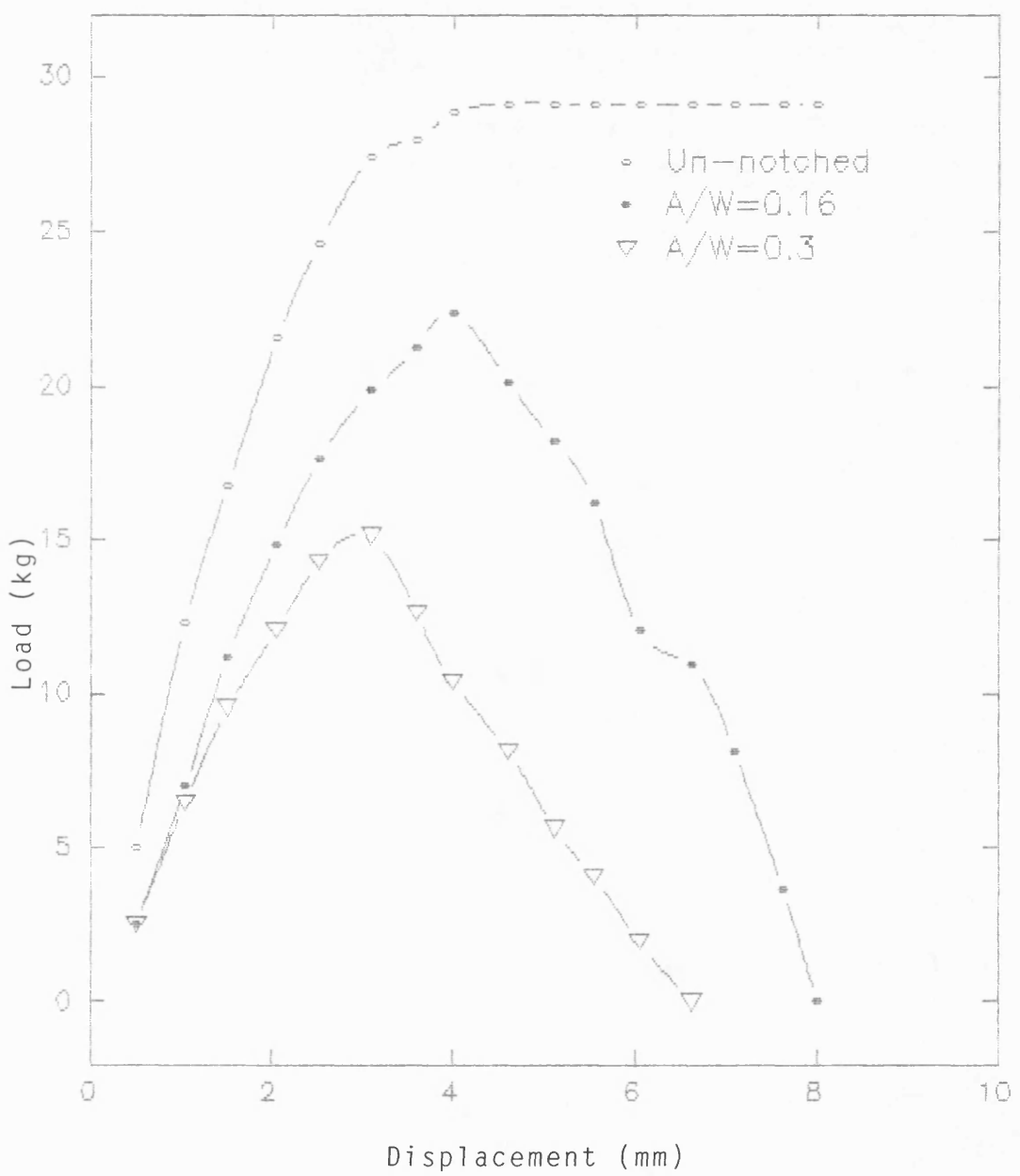

$$\sigma = 3FS/2BW^2 \qquad (14)$$

where F denotes the peak load, S the sample span, W the sample width and B is the sample thickness.

To understand what is happening at the tip of the notch, the plane strain fracture toughness (a measure of the stress intensity at the notch tip) was calculated for the notched specimens from the expression (86);

$$K_1 = 6.Y.P \,/\, B.W^{\frac{1}{2}} \qquad (15)$$

where P is the peak load, A is the notch depth and Y is a shape factor to give geometry independence and is calculated from;

$$Y = 1.93(A/W)^{\frac{1}{2}} - 3.07(A/W) + 14.53(A/W) - 25.11(A/W) + 25.8(A/W) \qquad (16)$$

The fracture energy from the notched specimens was simply calculated from the area under the force/displacement curve, divided by the cross sectional area. All the values obtained can be seen in table 4.26.

Again it can clearly be seen that the values for PEK fall off to a much lesser extent with increasing notch depth than for PEEK or PET. The effect of increasing the crystallinity is to reduce the fracture energy for all of the samples tested which is as expected. This fall off in fracture energy with increased notch depth is comparable to the data found in the preceeding table of results and these

Table 4.26. The fracture toughness and fracture energy values obtained from the 3-point bend analysis.

Sample	A/W	Flexural strength (MPa)	K_1 $MPa^{1/2}$	Fracture energy (kJm^{-2})
PET 38%	0	159	-	-
	0.16	-	1.5	8
	0.33	-	1.7	6
PEEK 27%	0	218	-	-
	0.16	-	2.3	34
	0.33	-	3.0	24
PEEK 35%	0	238	-	-
	0.16	-	2.5	19
	0.33	-	2.8	12
PEK 35%	0	218	-	-
	0.16	-	2.9	33
	0.33	-	3.1	31
PEK 37%	0	234	-	-
	0.16	-	2.9	23
	0.33	-	3.3	20

differences between the polymers are highlighted by the values determined for the fracture toughness, indicating the increased stress at the tip of the notch as the notch depth becomes more pronounced. The results do suggest that PEEK is more susceptible to crack initiation and propagation than PEK and an explanation for this has already been put forward.

4.3.6. Concluding remarks.

To summarise the information outlined so far, it can be said that PEEK and PEK undergo similar viscoelastic and tensile behaviour, with overall trends following the same patterns as those found for PET. A striking difference is observed under impact evaluation where PEK behaves in a very tough manner with PEEK being comparable to PET. Structurally, because of the difference in ether/ketone ratio, one would expect PEK to behave in a more brittle manner, but it is felt that the addition of PTFE may have a modifying effect resulting in improved performance and will be discussed in more detail at a later stage.

4.4.0. Response to impingement by a water droplet.

4.4.1. Introduction.

In determining the rain erosion characteristics of polymers, results have hitherto been limited to two approaches;

(i) Single impact studies, such as the liquid jet technique used in this thesis. It has been suggested as being unsuitable to use this technique to measure post water droplet impact (residual strength measurements) because of the plastic nature of polymers, and weight loss measurements are

impracticable because of the high number of impacts required to remove sufficient material for a significant reduction in weight as well as giving only limited information as to the erosion characteristics and not to the damage caused by the impact procedure.
(ii) Multiple impact studies, using, for example, a whirling arm technique, where the resultant loss of material is quantified, but as a result of the exotic nature of this equipment the technique is not readily available.

For the purpose of this investigation it was felt that if sufficient energy is transferred from the water droplet impact to produce a loss of material and/or the characteristic circumferential ring of cracks then it would be highly likely that the damage would extend into the sub-surface region of the sample and in so doing create damage zones measureable by conventional techniques ie in Charpy impact tests after water drop impact. Any crack present after an impact by a water droplet could then act as a stress concentrator, resulting in a reduction of its fracture strength, as in the case of machining notches into a sample.

In this section experiments have been concentrated on investigating whether this is a valid proposal, and on measurement of surface damage to assess the erosion characteristics of the three polymers.

4.4.2. The effect of a single water droplet impact on the fracture energy.

Samples of the three polymers were initially impacted by water droplets at increasing velocities and these impacted samples were then used for the determination of their post-impact fracture energies by means of the Ceast fractoscope. Table 4.27, lists the values obtained. Here it must be stressed that some of the samples did not break and the resultant fracture energies were taken to be lower bounds, as mentioned before. The undamaged values were obtained from the results in the table on page 126, in section 4.3.5, and the results can be seen more clearly in figure 4.28 as normalized impact energies measured as a percentage of the base line values plotted against the water drop velocity.

It is felt that a false representation of PET has been drawn as the plot indicates a linear fall off in impact energy with increasing water droplet velocity. Impacts at lower velocities would probably show this not to be true and it would be expected that a curve would be obtained, showing a similar trend as for PEEK ie a plateau region followed by a sharp drop. No impacts were carried out at lower velocities because the main area of interest was concerned with PEEK and PEK. PET impacted by a water drop at a velocity of 443 m/s underwent catastrophic failure, the samples shattering in the sample holder so that no post impact fracture properties could be determined.

A fall off in the impact energy was observed beyond an impact velocity of 558 m/s for PEEK with 27% crystallinity and 472 m/s for PEEK of 35% crystallinity. The resultant curves for PEEK are

Table 4.27. The effect of increasing velocity of water droplet impact upon the impact energy of PEEK, PEK and PET.

Sample	Velocity (m/s)	No. of tests	Mean impact energy (kJ/m^2)	S.D
PET 38%	0	5	71 *	32
	334	5	15 *	13
	443	5	-	-
PEEK 27%	0	10	595	19
	334	10	558	15
	443	10	558	72
	474	10	558	87
	558	10	578	44
	900	7	75 *	14
	1000	8	70 *	26
PEEK 35%	0	10	612	37
	334	10	646	12
	443	5	579	9
	474	10	325 *	18
	558	10	154 *	26
	900	5	71 *	23
	1000	5	48 *	2
PEK 35%	0	10	625	27
	334	7	625	23
	443	7	625	18
	474	8	625	17
	558	8	625	11
	900	5	603	48
	1000	5	584	66
PEK 37%	0	10	667	31
	334	8	667	22
	443	5	675	9
	474	7	678	29
	558	8	667	17
	900	5	625	0
	1000	5	625	15

'*' denotes that the samples broke during the Ceast impact.

Figure 4.28. Effect of water droplet impact on the impact energy of PEEK, PEK and PET.

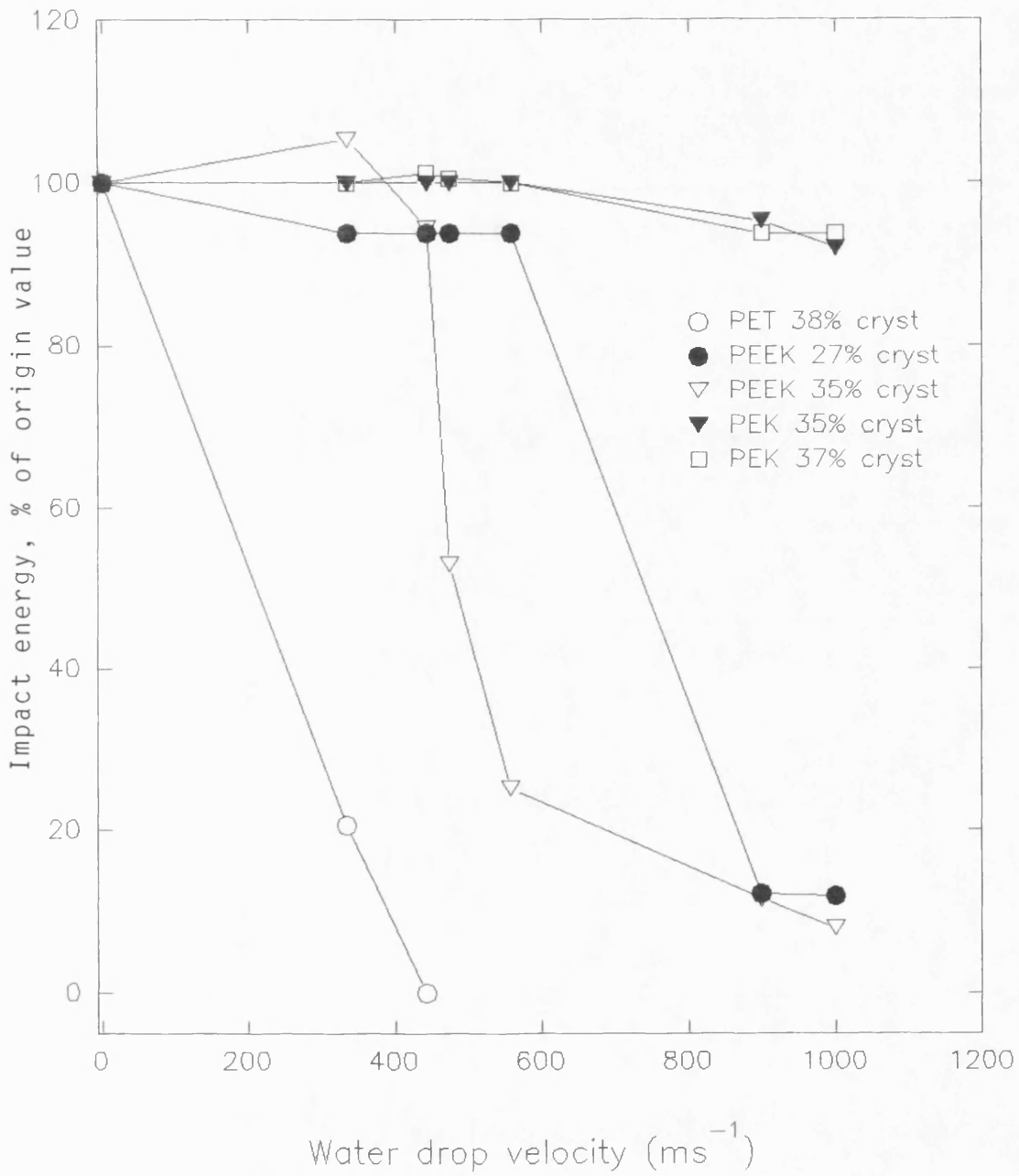

Figure 4.29. Force/time plot illustrating the ductile /brittle transition when a critical water impact velocity has been reached.

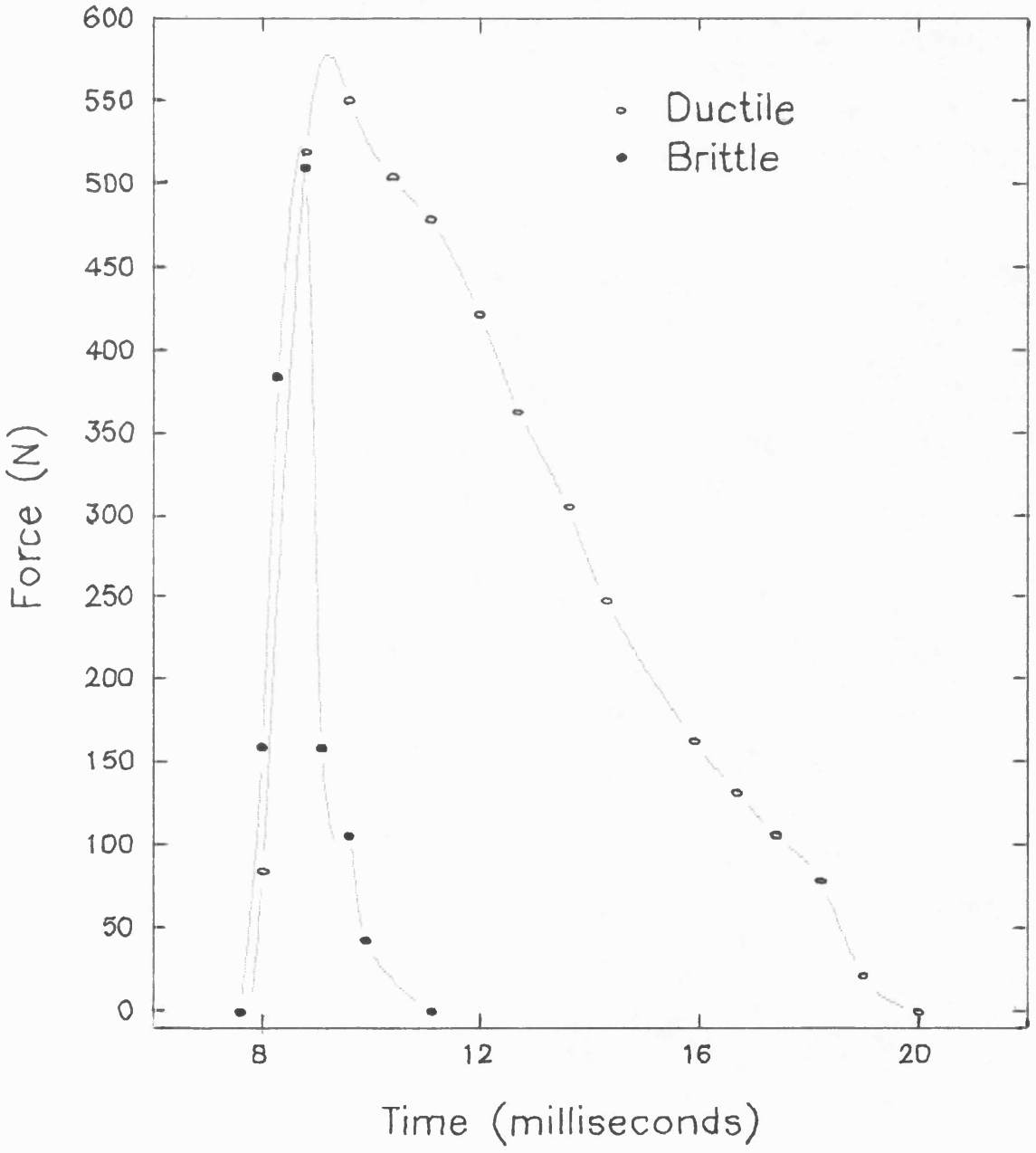

similar to curves produced when the fracture energy is plotted against increasing notch depth, ie stable values until a critical notch depth has been reached and then a transition to brittle failure. This transition can be seen in figure 4.29 where the force/time plot was recorded showing the ductile to brittle response when a critical water drop velocity had been reached. The plot was produced from impact data at 330 m/s and 900 m/s for PEEK with 27% crystallinity.

The main feature to be observed here is the apparent resistance of PEK to damage at increasing water droplet velocities, only a small drop occurring even after an impact at 1000 m/s. It was not possible to go to higher velocities because, with the water droplet cylinder used, further increases in the reservoir pressure did not alter the drop speed.

The fractured samples were examined by scanning electron microscopy. Plate 4.30 presents a cross-section of PEEK impacted at 900 m/s and PET impacted at 334 m/s. The top surfaces of the photographs are the points at which the water drop impacted and in the case of PEEK there is a clear indication of a central damage zone corresponding to the initial point of contact with the water droplet and a cone crack or possibly Palmqvist cracks, corresponding to the circumferential ring of damage produced presumably where `jetting' of the water droplet had occurred. The photograph for PET does not illustrate this very clearly but does present a very brittle fracture surface with an indication of a cone crack. We note that the photographs do not show

Plate 4.30.

Fractured PEEK (35% cryst) impacted @ 900m/s.

Central damage zone

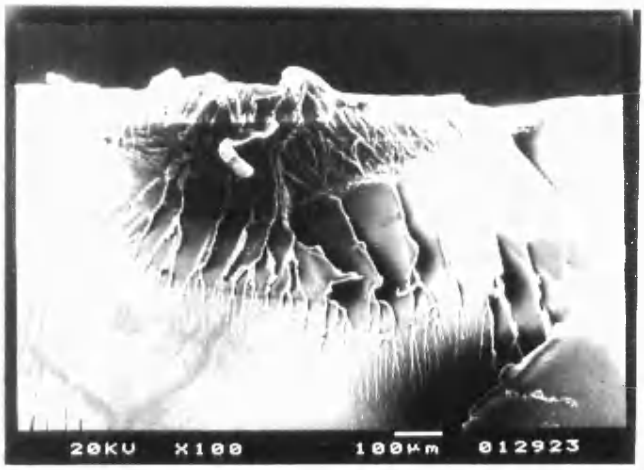

Fractured PET (38% cryst) impacted @ 334m/s.

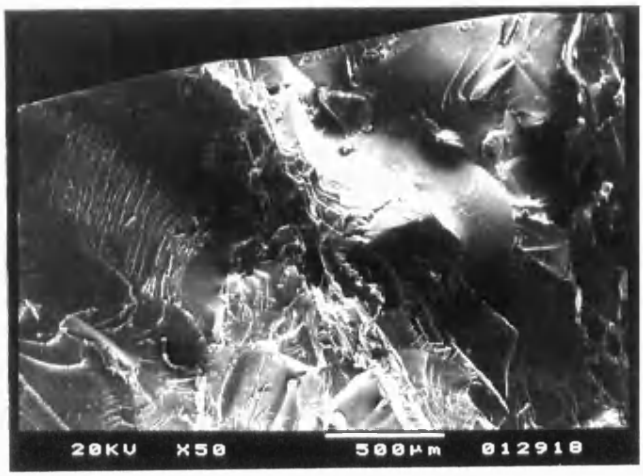

the point of impact provided by the Ceast anvil, but no damage could be seen there, just a sharp brittle plane.

On closer examination of the central damage zone for PEEK, one can see that the damage produced is similar to the deformational damage produced by a Vickers hardness indentor, namely a `half penny' crack, which is usual for the indentation of brittle materials. Cracks radiating outwards from the direct centre of the impact zone seem to predominate in the damage area. No indication of this extensive subsurface damage is evident from photographs of the surfaces after the water droplet impact.

Observations of the visual damage at the point of impact have been quantified by plotting the area of the circumferential ring, excluding the central undamaged region, against the droplet impact velocity, as shown in figure 4.31. It becomes readily apparent that the damage inflicted is much less than for PEK. The data for PET is again misleading because coupled with the circumferential damage zone were large surface cracks extending outwards at right angles to the circumferential ones, illustrating the extremely brittle response of PET to this type of deformation.

Increasing the crystallinity of PEEK and PEK causes a greater extent of visible (and subsurface) damage, as the polymer behaves in a more brittle manner in response to the interaction of the surface waves with the hydrostatic pressure produced by the impacting water drop. Plate 4.32 illustrates the

Figure 4.31. Effect of increasing water drop velocity upon the resultant visible surface damage.

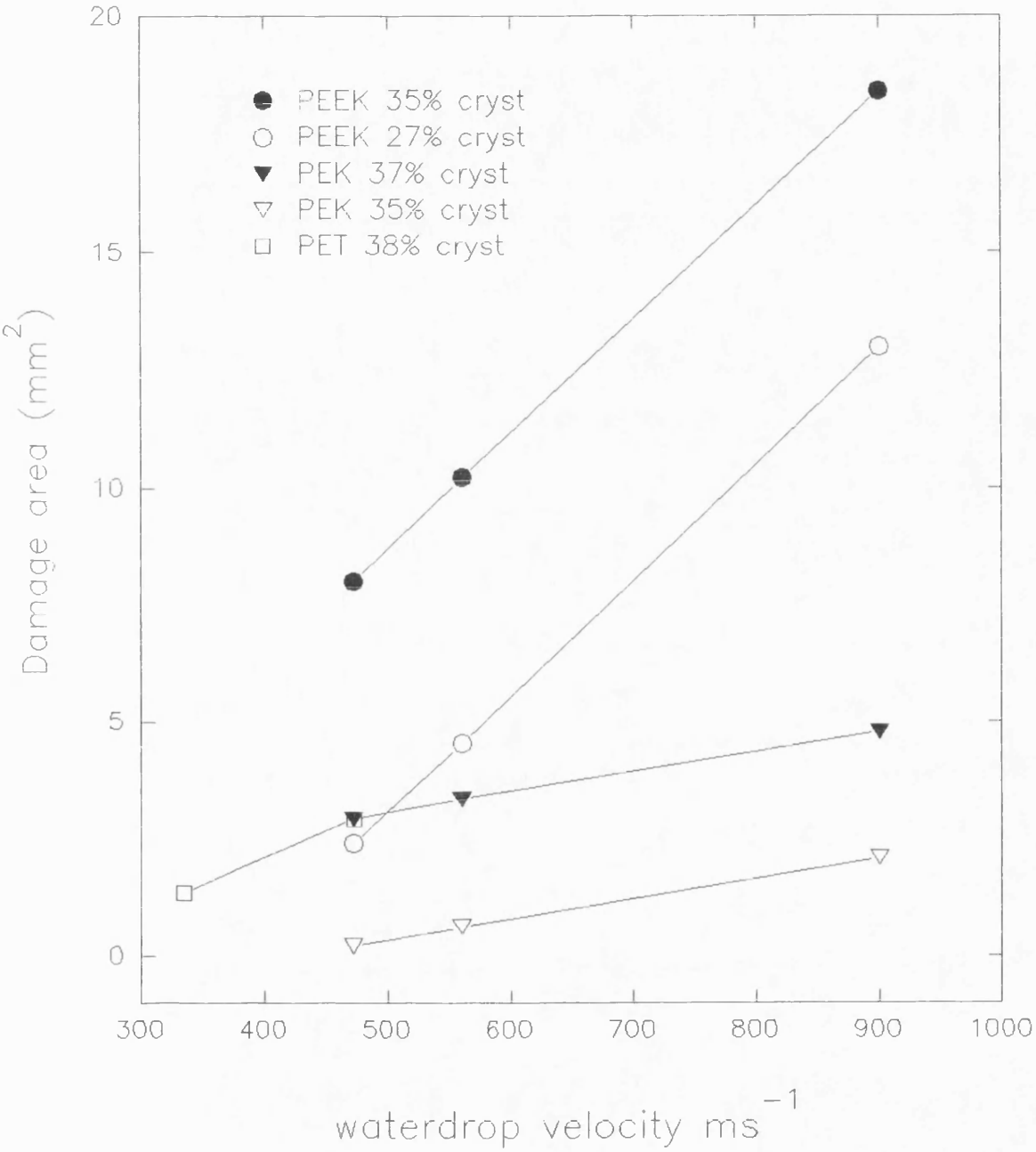

Plate 4.32.
Typical water droplet impact surface damage, carried out at 900 m/s.

PEEK 35% cryst.

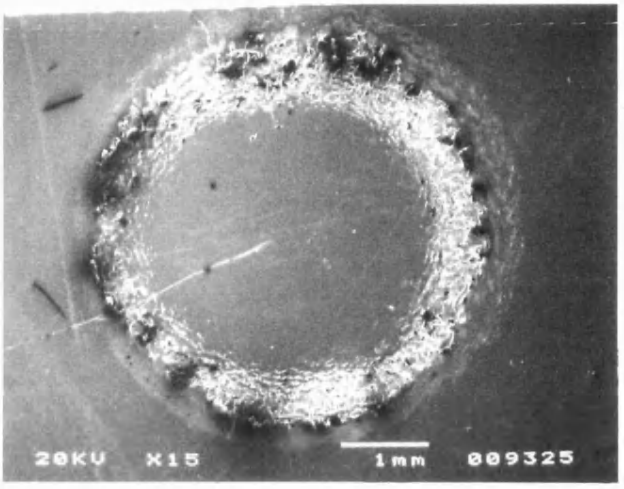

Enlargement, illustrating surface shearing.

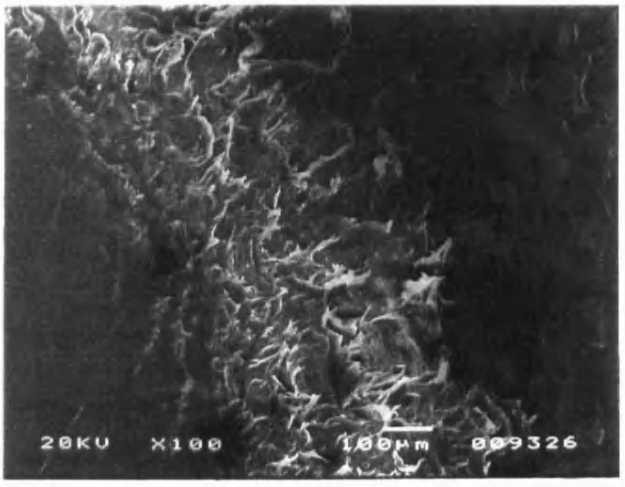

PEK 35% cryst.

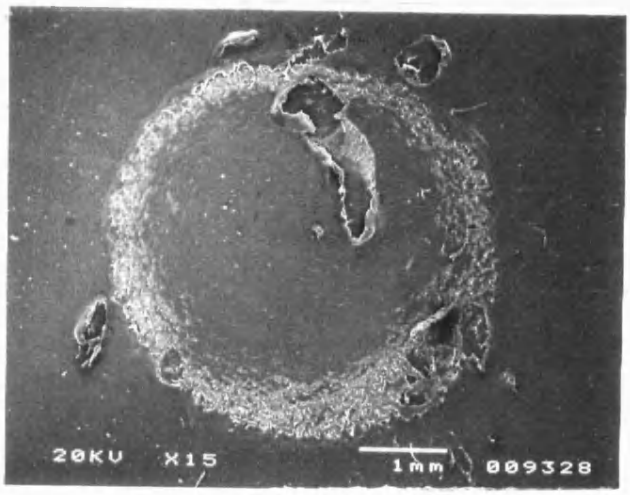

Enlargement, illustrating surface shearing.

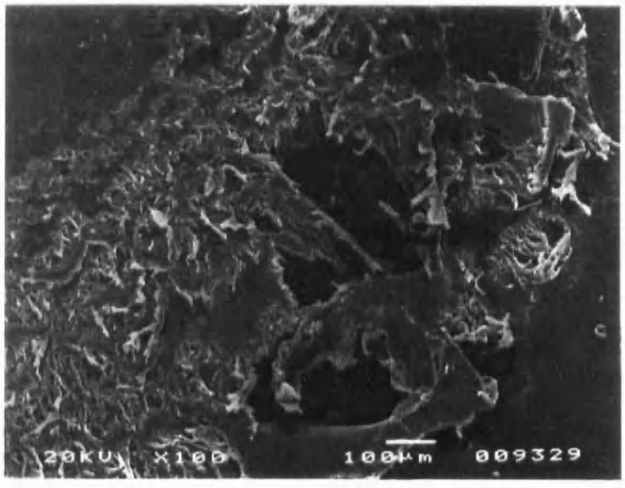

difference in damage observed between PEEK and PEK after impacting by a water droplet at a velocity of 900 m/s. The surface of PEK shows spallation (material removal) with the material shearing outwards along with the movement of the water droplet at the surface. PEEK also demonstrates this behaviour but, in addition to this material movement, cracks are also evident with a predominant radial crack clearly visible, corresponding to the failure caused mainly by the hydrostatic pressure. It would seem that PEEK is likely to erode to a greater extent than PEK whilst information on PET is limited since the damage produced was similar but comparable velocities resulted in extensive damage (shattering of sample), so that no direct comparison could be made.

4.4.3. The effect of multiple water droplet impacts on the impact energy.

It has been observed that PEEK shows extensive subsurface damage after certain critical water droplet velocities have been reached. No change in the post impact fracture strength over the range of velocities studied was observed for PEK. To permit a better understanding of the difference in the responses of PEEK and PEK, it was decided to carry out multiple droplet impacts and a velocity was chosen where no post-impact impact energy fall off was observed. The velocity used was 334 m/s. The values obtained can be seen in table 4.33, and the results are plotted in figure 4.34.

Here it can be seen that no differences occur between the crystallinities of 27% and 35% for PEEK

and a sharp fall off in post-impact impact energy occurs after three water droplet impacts. PEK impacted at 334 m/s showed no changes with increase in the number of impacts, so the impact velocity was increased and the results obtained by multiple impacting at 443 m/s and 900 m/s can be observed in table 4.35 and figure 4.36. No fall off in the post-impact impact energy occurs until five impacts have been reached at 900 m/s, and this behaviour is not affected by crystallinity. It is readily apparent that there is a dramatic difference in behaviour between PEEK and PEK, and it is obvious that a much larger amount of energy needs to be transferred by the water drop in order to cause a fall off in the impact energy of PEK.

To place all the results into perspective so that all the material responses could be viewed on the same plot, the energy of the droplet was calculated from the kinetic energy (KE):

$$\text{Total KE of drop impact} = \tfrac{1}{2}mv^2 \times \text{No. of impacts} \qquad (17)$$

This plot can be seen in figure 4.37 and the dramatic difference between all three polymers can be seen with PEK exhibiting by far the greater resistance.

The fractured samples were retained and their cross-sections examined by scanning electron microscopy. Plate 4.38 shows the different types of damage produced by a multiple impact. No evidence was visible of the type of cracking viewed from single impact studies. The samples here exhibited a

Table 4.33. Effect of multiple water drop impacts on the impact energy of PEEK, PEK and PET, (carried out at 334 m/s).

Sample	No. of impacts	No. of tests	Mean impact energy (kJ/m^2)	S.D
PET 38%	0	5	71 *	32
	1	5	15 *	13
	3	5	- *	-
PEEK 27%	0	10	595	19
	1	10	558	15
	3	5	539	45
	5	5	158 *	13
	10	5	29 *	0
PEEK 35%	0	10	612	37
	1	10	646	12
	3	5	629	26
	5	5	171 *	15
	10	5	87 *	4
PEK 35%	0	10	625	27
	1	7	625	23
	3	5	625	3
	5	5	613	14
	10	5	629	7
PEK 37%	0	10	667	31
	1	8	667	22
	3	5	646	15
	5	5	640	7
	10	5	625	11

`*' denotes that the samples broke during the Ceast impact.

Table 4.35. Effect of multiple water droplet impacts @ 474 m/s, upon the impact energy of PEK.

Sample	No. of impacts	No. of tests	Mean impact energy (kJ/m^2)	S.D
PEK 35%	0	10	625	27
	1	8	625	17
	3	3	614	34
	5	3	626	9
	10	3	613	18
PEK 37%	0	10	667	31
	1	7	678	29
	3	3	651	2
	5	3	651	2
	10	3	615	7

Water drop impact @ 900 m/s.

Sample	No. of impacts	No. of tests	Mean impact energy (kJ/m^2)	S.D
PEK 35%	0	10	625	27
	1	5	603	48
	3	3	622	13
	5	3	615 *	3
	10	3	533 *	3
PEK 37%	0	10	667	31
	1	5	625	0
	3	3	617	8
	5	3	593 *	14
	10	3	495 *	5

'*' denotes that the samples broke during the Ceast impact

Figure 4.34. Effect of multiple water drop impacts on the impact energy of PEEK, PEK and PET.

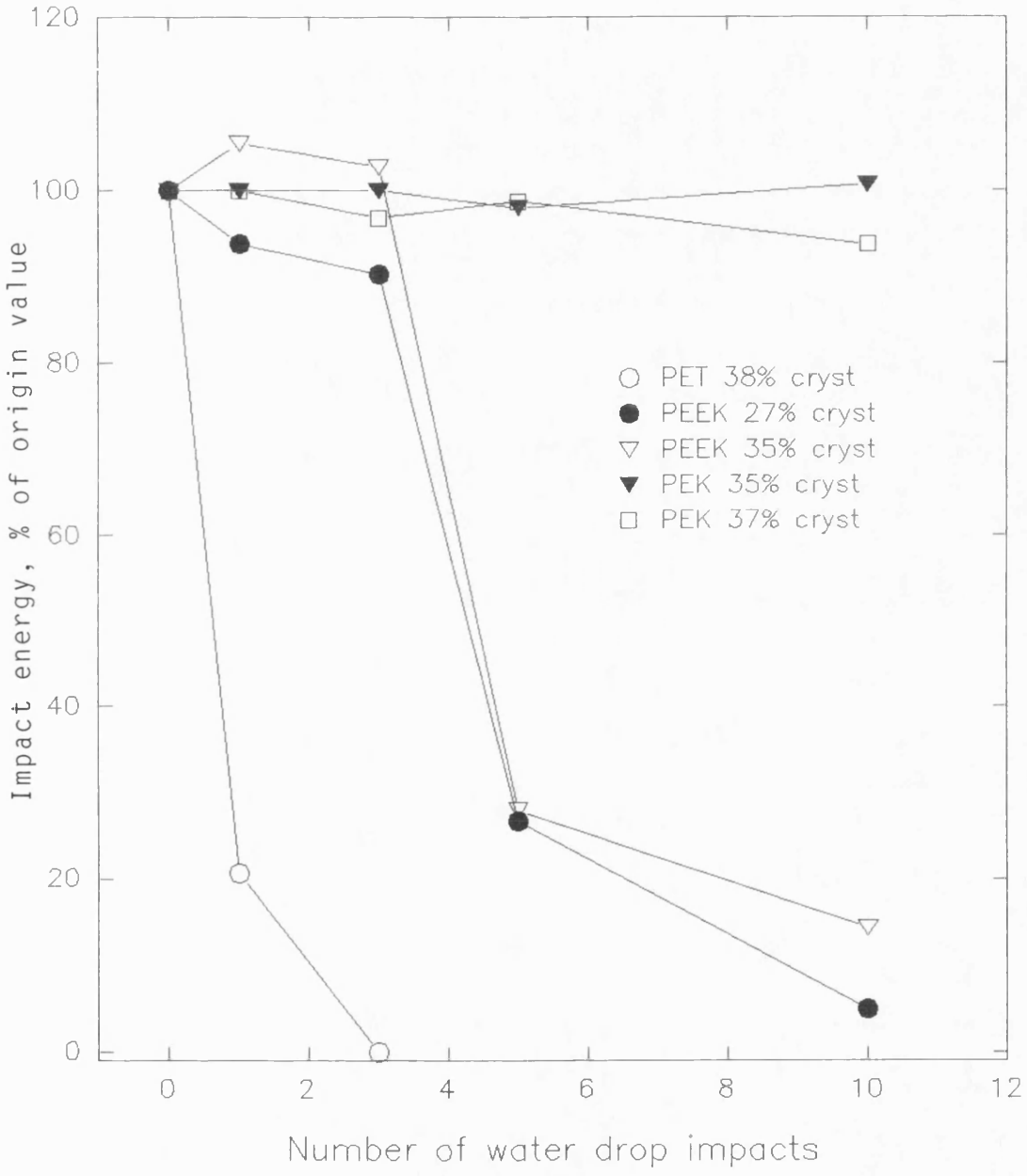

Figure 4.36. Effect of multiple water drop impacts on the impact energy of PEK at increased impacting velocities.

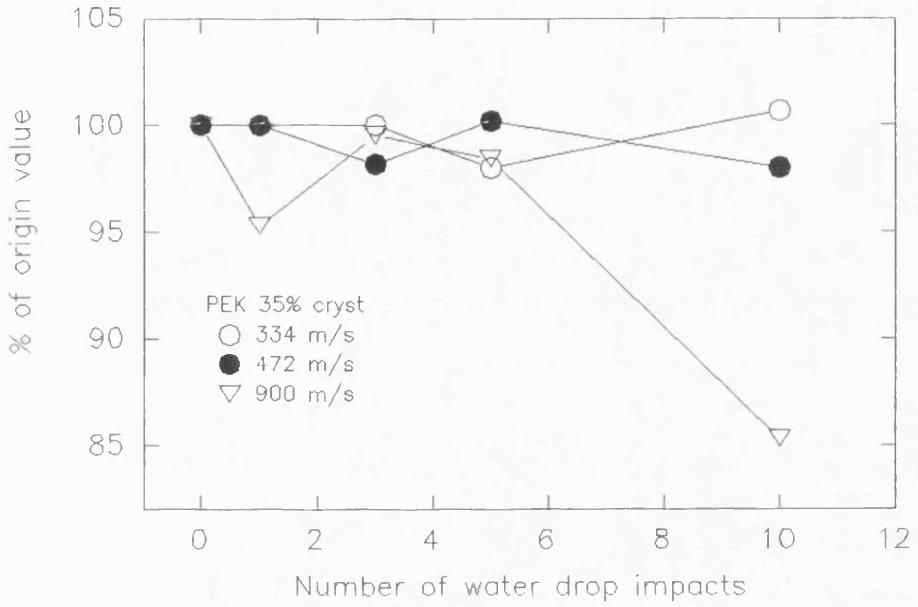

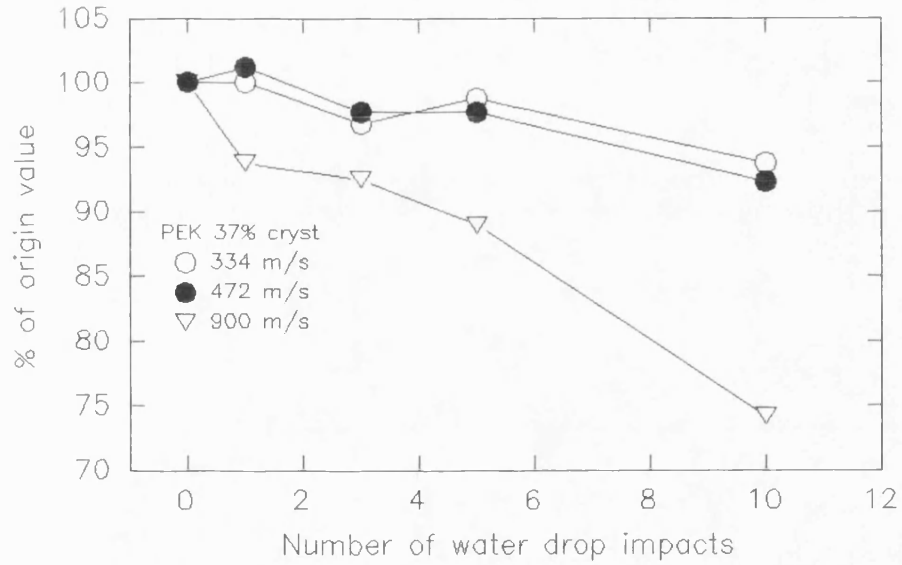

type of damage which could only be described as `crumbling' of the material, with a loss of material caused by the fracture by the Ceast anvil. It can be deduced that two processes are occurring;

(i) On single impact, the energy of interaction of shockwaves produced with the tensile waves is dissipated by means of creation and opening of cracks once a sufficient critical impact velocity has been reached.

(ii) Multiple impact damage results predominantly from the shockwave produced under the hydrostatic pressure of the drop where the compressive strength of the material has been exceeded, resulting in the sub-surface crumbling to depths which are dependent upon the number of impacts. This damage is sufficient to cause a reduction in the post-impact impact energy. Obviously the effect is cumulative and it must be remembered that the action of the water hammer pressure is likened to detonating a small explosive device at the surface of the material, so the resultant extent of the damage is hardly surprising.

This observed effect may be used to explain a certain behavioural pattern for PEEK when its erosion resistance was measured using the whirling arm technique (6). Figure 4.39 is a redrawn representation of the results of the weight loss during the experimental time period. Plateau regions can clearly be seen where no weight loss occurs. It can now be postulated that these plateau regions will occur during the so called `crumbling' process and when sufficient material modification is reached (making the area a weak point) easy removal of the

Figure 4.37. The effect of increased water drop energy on the impact energy.

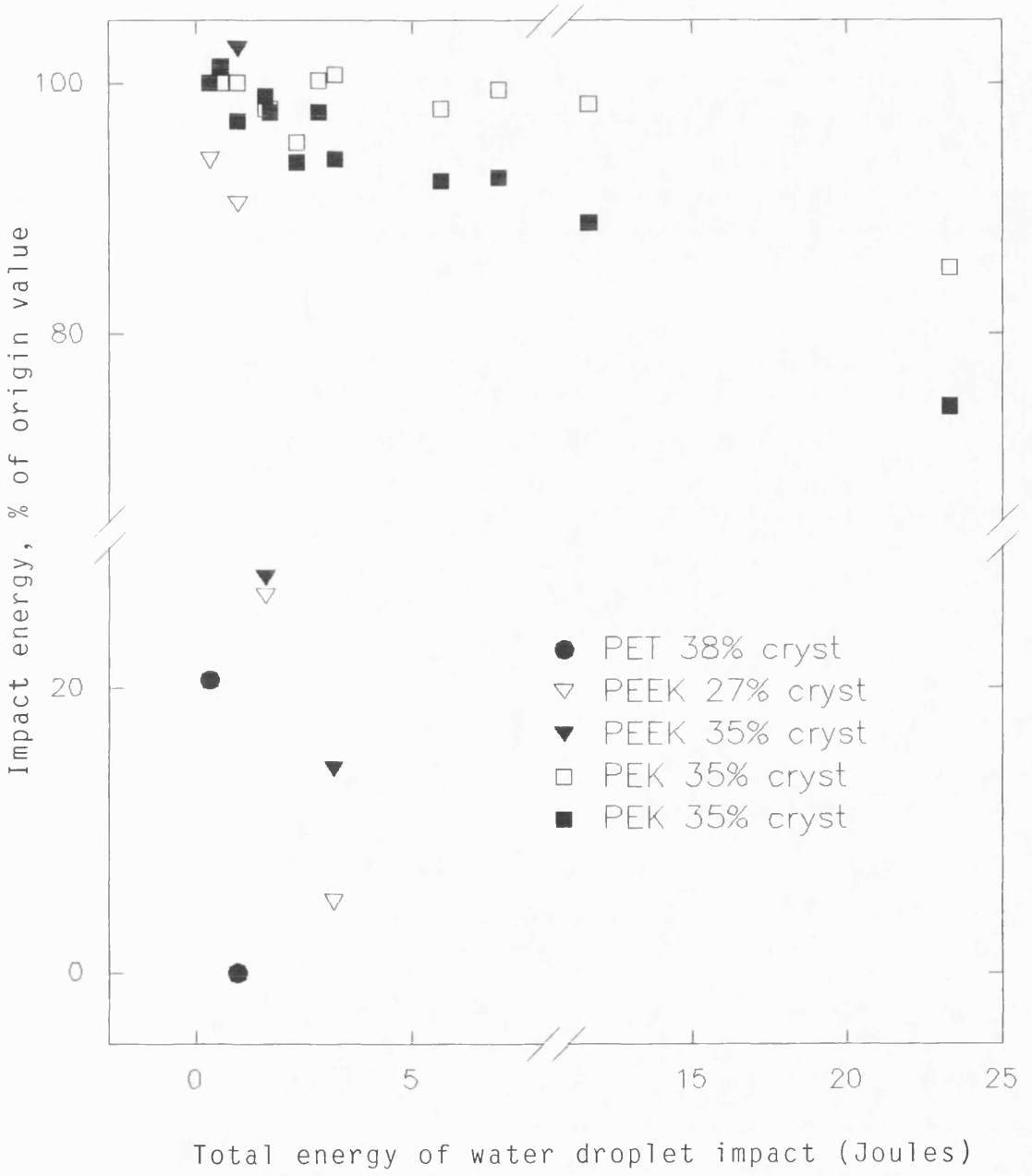

Plate 4.38.
PEEK, multiple water droplet impact (334 m/s x 10)

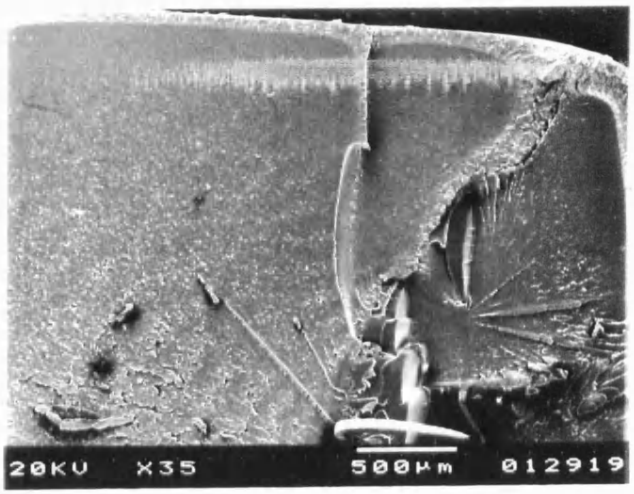

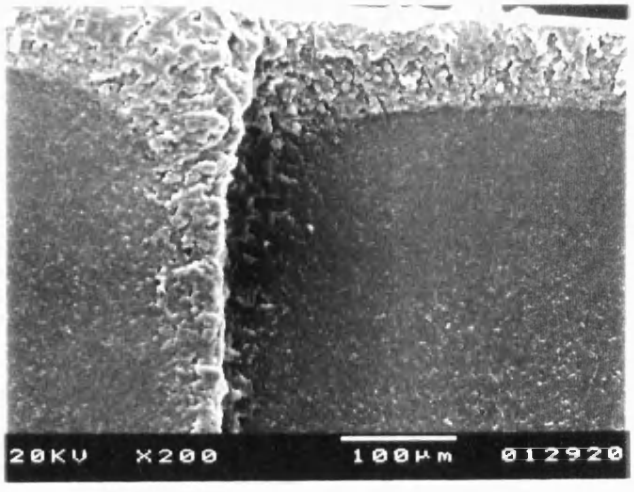

PEK, multiple water droplet impact (900 m/s x 10)

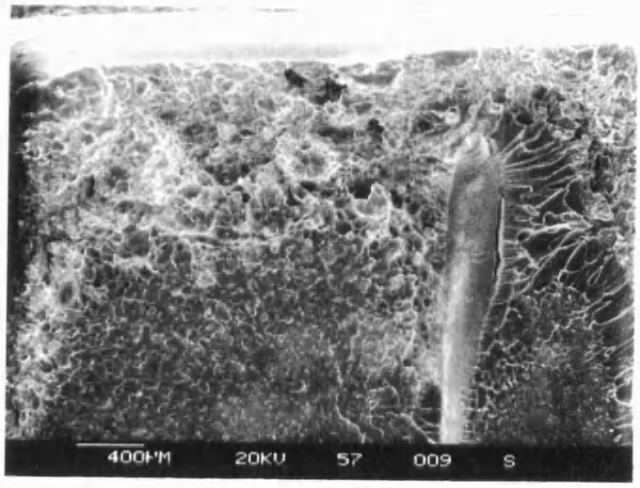

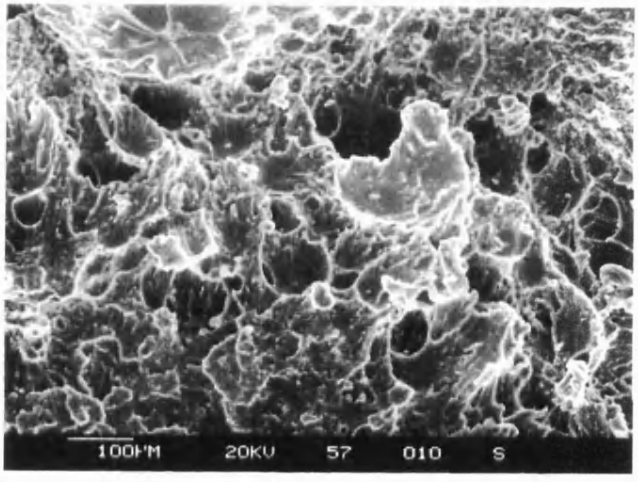

Figure 4.39. Water droplet erosion damage of PEEK carried out using the whirling arm technique.

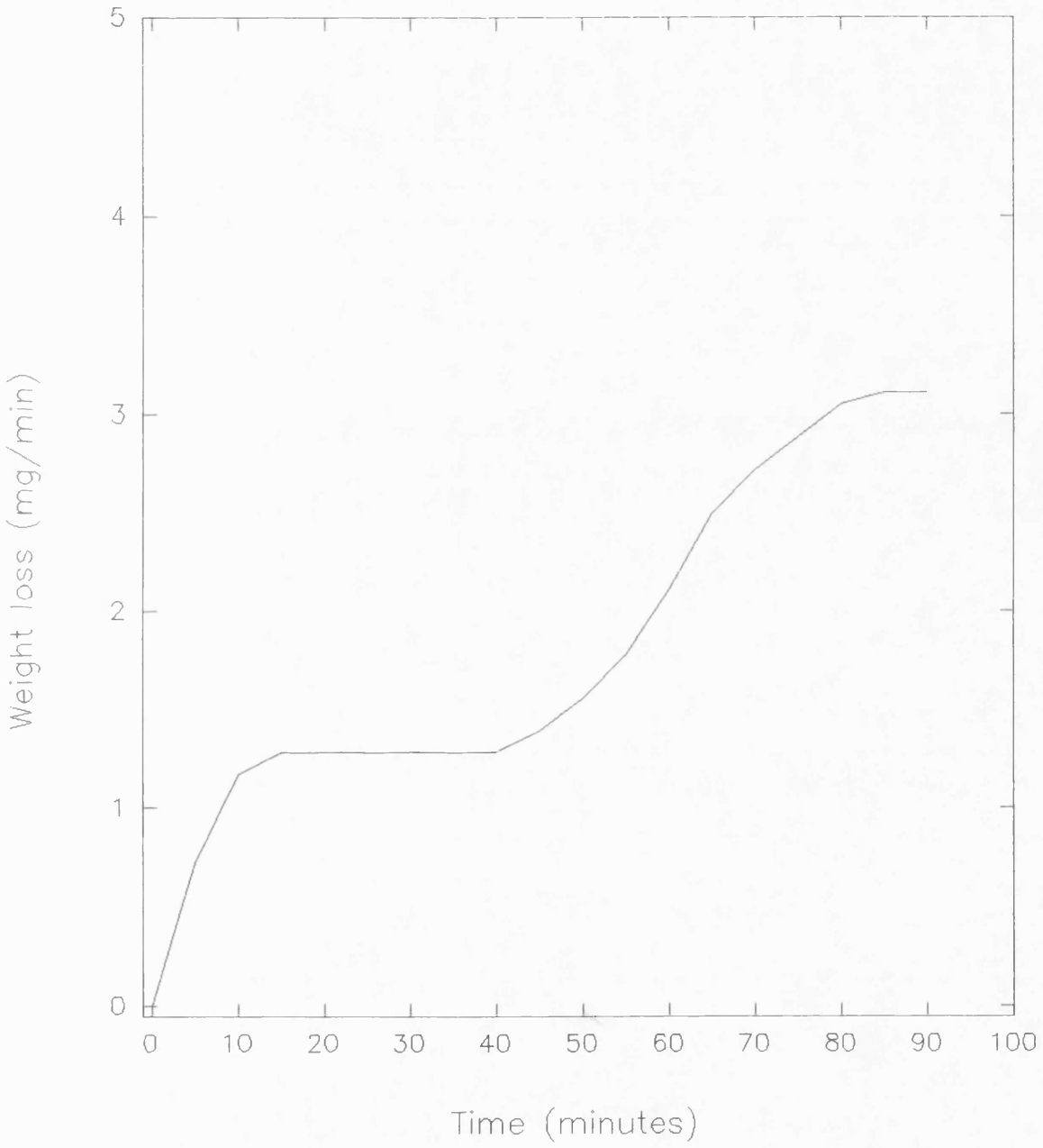

material is possible and so a sharp rise in weight loss is detected, until un-modified material is reached and then the whole process is repeated.

4.4.4. Water droplet impact at elevated temperatures.

Previous water drop impact experiments have concentrated upon the material characteristics at room temperature. An investigation with single drop impact techniques of the behaviour of PEEK, PES and soda lime glass (31) has yielded information on the observed reduction in the threshold velocity with increasing impact temperature. This is an important area of research as airborne components are subjected to aerodynamic heating in combination with impact erosion by liquids and solids, particularly at low altitudes. It was deduced that during the experimental procedure the nature of the jet was not affected by the heating of the material because the duration of the impact event was so short. High speed photography of jets impacting a surface at a temperature of 300°C has shown that the appearance of the jet is not modified.

The experiments carried out in this section used water drop velocities where it was known that a reduction in the post-impact impact energy would result,viz.

(i) 334 m/s for PET (38% cryst)
(ii) 474 m/s for PEEK (35% cryst)
(iii) 900 m/s for PEK (37% cryst)

The points of origin for the plotting of the results were taken as these post-impact impact energies. In figure 4.40 the results obtained for

Figure 4.40. Effect of single water drop impact at elevated temperatures on the impact energy of PEEK (35% cryst), carried out at 474 m/s.

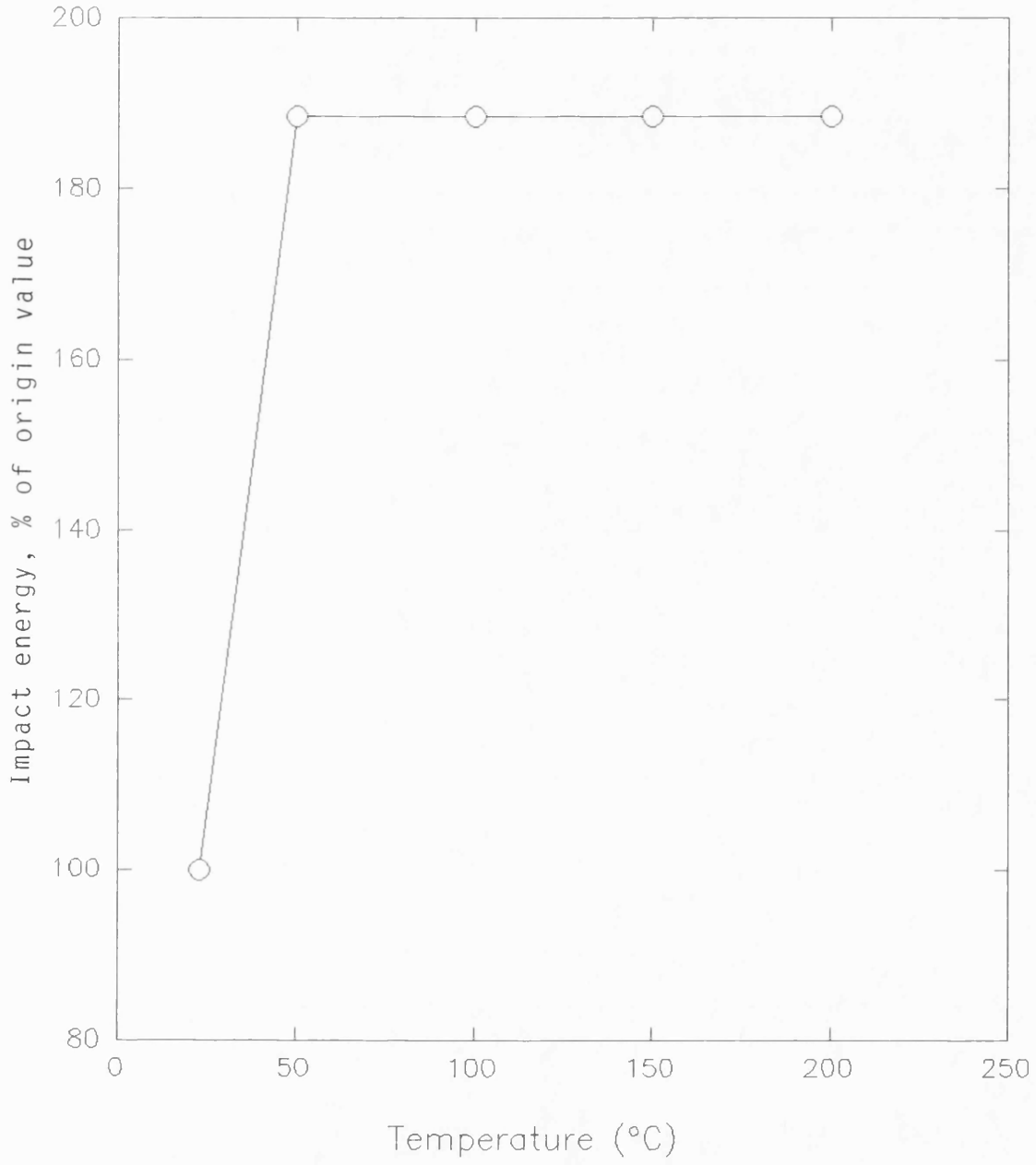

Figure 4.41. Effect of increased temperature of impact carried out at 560 m/s for PEEK and PEK, and 472 m/s for PET.

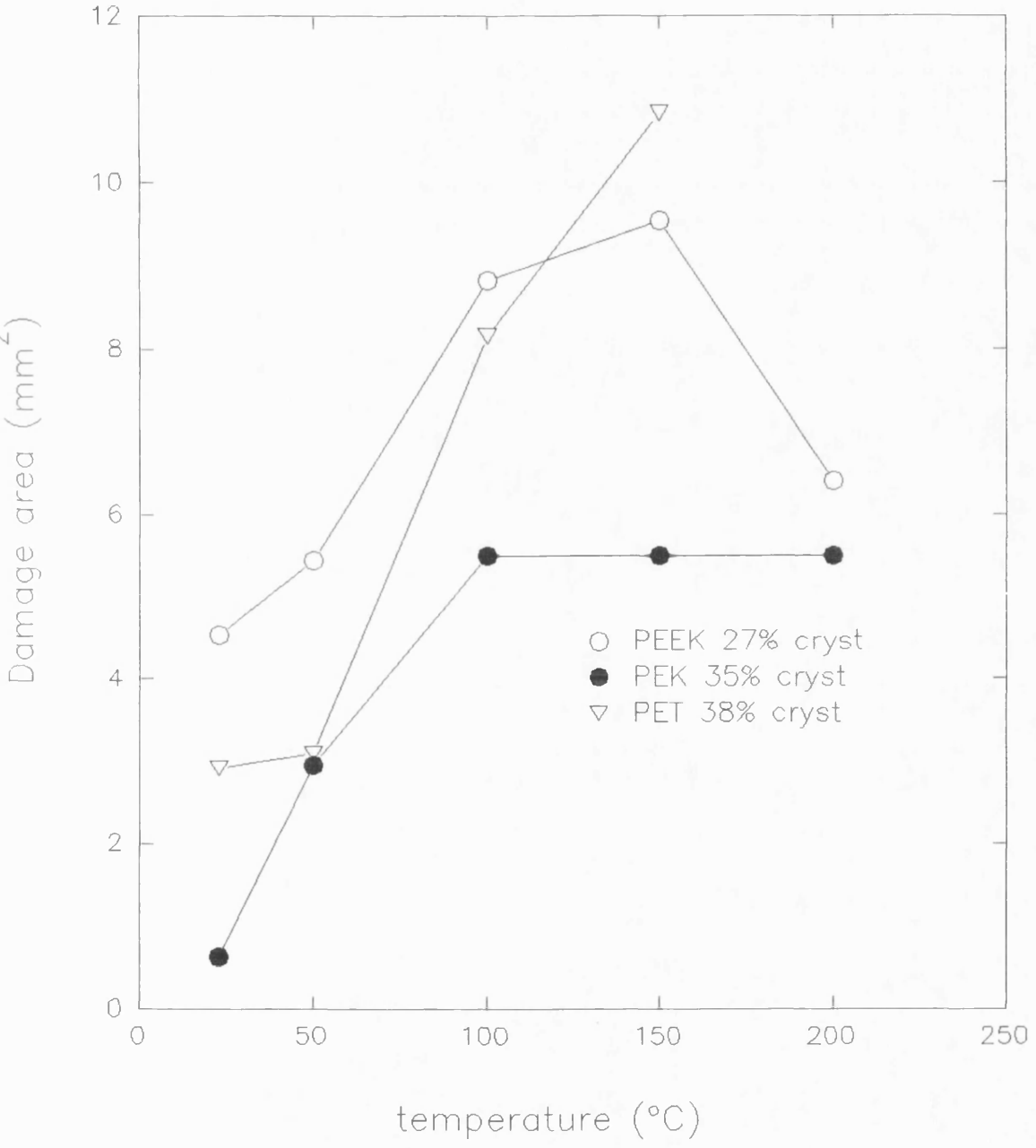

PEEK can be seen (PET and PEK underwent a similar response). Increasing the temperature of impact to 50°C was sufficient to modify the material behaviour in such a way as to return the impact energy value to its pre-damage level (sample did not break under the Ceast measurement). Further increases in temperature to 200°C did not alter the post-impact impact energy, so that it may be assumed that no sub-surface damage was occurring.

The surface damage, with the formation of the circumferential ring zone, can be seen in figure 4.41. The amount of surface damage increases to a greater extent with the increase in temperature. The central region or un-damaged zone becomes more pronounced and depressed, until the zone becomes similar in nature to the damage caused by pushing a ball bearing into the surface producing plastic deformation as the yield stress of the material is exceeded, and a raised lip is visible before the onset of the circumferential damage.

It can be seen that the damage area seems to diminish for PEEK up to 200°C, but this information is misleading as the central damage zone becomes so pronounced that it interferes with the circumferential ring zone making it difficult to calculate the damaged area (note that the damage is taken to be the area of the circumferential zone) . Concerning the damage to PET, it is noteworthy that the hydrostatic pressure was sufficient to cause large scale bulk plastic deformation of the sample when impacted above its glass transition temperature. This was observed as a raised dimple directly

opposite the impact zone on the rear of the sample. The type of damage can clearly be seen in plate 4.42, with the increased formation of a central pit on increasing the impact temperature.

The apparent improvement in the post-impact fracture performance is coupled with an increase in the surface material erosion and these are not altogether surprising. Mention has already been made in this chapter of the experimental investigation concerning the tensile properties at elevated temperatures. It is clear that the more rubber-like behaviour of the polymers at elevated temperature will permit absorption of energy without interacting with pre-present flaws to cause the formation of cracks, thus resulting in improved fracture resistance. It is well known that in the construction of a radome, for example, a coating of a rubberised paint over a GFRP dome will greatly assist the damage resistance of the component.

Plate 4.42.
Increased central annulus formation with increasing temperature. Carried out at 560 m/s on PEEK (27% cryst)

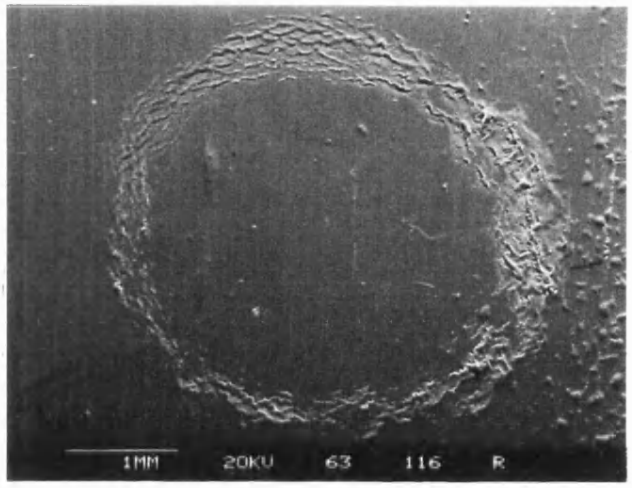

50°C

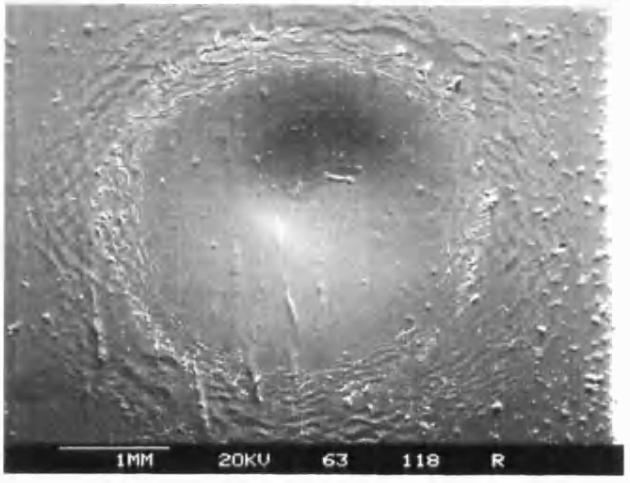

100°C

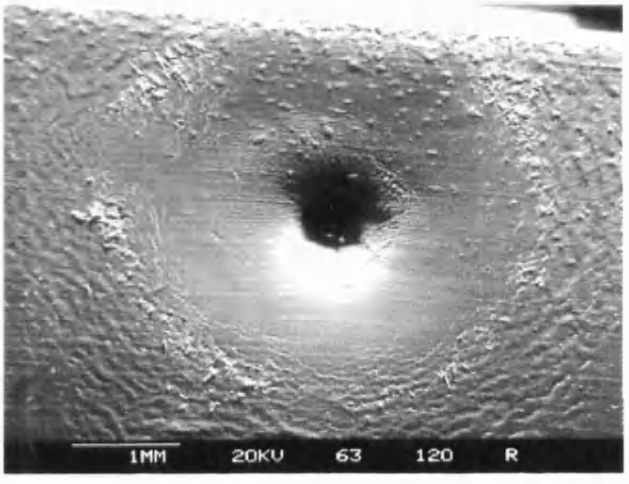

150°C

CHAPTER 5
DISCUSSION

5.1.0. Introduction.

In this chapter the results obtained so far will be discussed in greater detail. The chapter will be presented in two sections, namely, the response of the polymers to impact by water droplets and any correlation that may be determined from the mechanical properties.

5.1.1. Polymer response to impact by a single water droplet.

The results clearly show that a fall off in the toughness of the materials will occur when impacted by a water droplet (above a certain velocity). A critical velocity of impact may be determined, above which a fall off in toughness occurs, that has been found to differ for each of the materials tested. The single impact experiment did not result in a significant fall off in toughness for PEK up to impact velocities of 1000 m/s, and the critical velocities observed for PEEK and PET which were determined from figure 4.28 can be seen below in table 5.1.

Table 5.1. Critical water drop velocities, resulting in a reduction in polymer toughness.

Sample	Critical velocity m/s	Threshold velocity m/s
PEK 35 & 37% cryst	>1000	300-400
PET 38% cryst	118	108
PEEK 27% cryst	554	369
PEEK 35% cryst	445	300

These critical impact velocities do not correlate with the threshold velocities measured for the samples (the velocity below which no visual damage can be observed). This indicates that between the threshold velocity and the critical velocity, no subsurface damage is occurring and/or that the surface damage is not producing any cracks or flaws of a sufficient size to alter the polymer toughness.

In brittle materials such as glasses or ceramics the threshold velocity does correspond to a velocity at which the toughness of the material is reduced with the generation of flaws in the material (7). We note, however, when considering the behaviour of PET, that the threshold velocity is close to the value of velocity at which a reduction in toughness occurs. The threshold velocity of PEK was of the same order as that determined for PEEK, except that the extent of the observed damage was smaller as can be seen in figure 4.31. These initial results do compare favourably with results in the literature where PEEK and PEK are shown to behave in a very tough manner, and a value of the threshold velocity for PEEK was found to be 230 m/s (31), although the degree of crystallinity of the sample was not disclosed. One would assume that the sample studied in that work was of a higher level of crystallinity than those used in this analysis, leading to the lower threshold value, but this will be discussed later as the geometry of the sample was also found to have an effect on results.

A reduction in both the velocity to cause a loss in toughness and the threshold velocity has been

observed with increasing crystallinity of the sample. Increasing the crystallinity leads to more brittle behaviour of the polymer (in general), which would facilitate the formation of flaws and subsurface damage as a result of the interaction of the material with the stresses set up during the impact event.

The reduction in toughness of other materials has been seen in single impact studies and figure 5.2 illustrates the response of a truly brittle material (soda lime glass) to an increasing water drop velocity (7). The results were obtained by the hydrostatic burst technique and one can see the similarity between this figure and the results presented in this thesis.

Analysis of the fractured specimens by SEM has revealed subsurface damage when the critical water drop velocity has been reached. There exists a central damage zone, similar in nature to the half-penny cracks produced by a Vickers diamond indentor, and a cone type crack extending into the sample corresponding to the circumferential damage zone produced at the sample surface.

It must be assumed that this type of extensive damage only appears when the critical velocity has been reached, as the specimens did not fracture when impacted below this critical velocity. This was not observed in the samples of PEK because none of the post-impact specimens fractured, so that the cross sections could not be viewed. It was decided not to cut the samples that did not fracture in order to look for subsurface damage because it was felt that

the cutting of these ductile materials would obliterate any pre-present damage below the surface.

The occurrence of this sub-surface damage is not surprising as the water hammer pressure from a 1.6mm jet orifice (corresponding to a 10mm diameter water drop) impacting at 700 m/s is of the order of 1.5GPa, depending on the substrate properties, and would last for approximately 1μs (87). This value of 1.5GPa is by far in excess of the yield strengths of all of the polymers tested here and of course it would also be beyond any likely brittle fracture stress too, so that damage would be likely. But in the case for PEK the surprising fact is that there is no evidence of sub-surface damage resulting from single impacts to cause a drop in toughness, found. Mechanisms other than the effect of the water hammer pressure coupled to the interaction of the stress waves must therefore be present, and it is assumed that the properties of the material must make a significant contribution. For the moment, the behaviour of PEK in response to the single water drop impacts will not be discussed as no information can be gathered except that PEK exhibits no fall off in toughness over the velocity range studied and that the amount of surface damage produced is less than that found for PEEK and PET.

PET behaved in a very brittle manner, similar in behaviour to glasses and ceramics. At velocities greater than 334 m/s, catastrophic failure occurred, and the specimens (both disc and impact bars) shattered, indicative of a truly brittle response to the water drop impact event.

Sub-surface cracking has been observed after single impacts in PMMA, PS, PVC, (26,13) and for materials such as polycarbonate (PC) and PES (27), but no information has been found in the literature on the post-impact toughness of polymers in general.

The extent of damage observed is considered to be no cause for surprise because of the excessive pressure placed on the material during the impact event and it is assumed that the gross plastic deformation seen in the contact zone is a result of this. The jetting process of the water drop would cause a shearing action across the surface of the sample, initiating and interacting with any pre-present flaws. The surface erosion or shearing action becomes more evident on increasing the velocity of the impact and this is because of the increased velocities of the surface and shock waves produced, as can be seen in table 5.3 below.

Table 5.3. Wave velocities for impact of a 2mm diameter water drop impacting PMMA. The values obtained have been converted to SI units (88,89).

Velocity of Impact, m/s	Velocity of longitudinal wave, m/s	Velocity of transverse wave, m/s	Velocity of Rayleigh surface wave m/s
283	2345	1714	1555
284	2352	1716	1556
298	2365	1724	1564

The values from this table show that high velocity stress waves exist and that the effect of

Figure 5.2. Impact of soda lime glass, single impact with a water jet of 0.8mm ø (7).

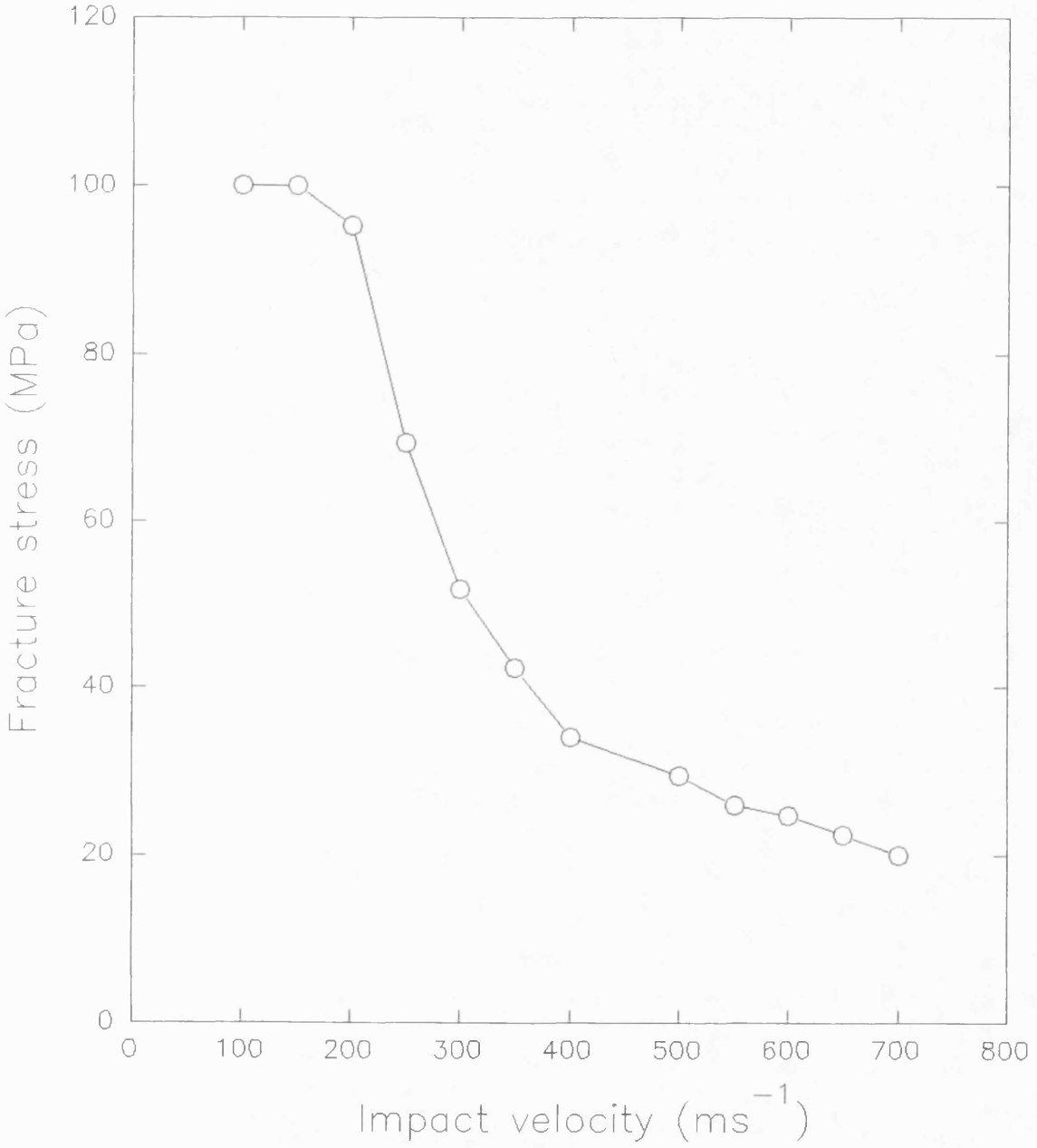

these waves in the initiation of flaws, interaction with pre-present flaws and with each other would be likely to cause the fracture patterns observed here. Although the velocity of the longitudinal wave is by far the greatest and would therefore be assumed to contribute more fully to damage, only the Rayleigh wave is present at the surface of the sample and this must create the greatest amount of damage in combination with the other shock waves and the resultant high pressure regime. More information as to the actual nature of these waves can be found in other literature sources (18,90) and will not be discussed any further as they are outside the scope of this dissertation.

From these single impact studies it can be ascertained that the behaviour of PET exhibits a truly brittle response to the water drop impact, whilst PEEK and to a greater extent PEK exhibit ductile behaviour. It would be beneficial to absorb the energy of impact in ductile/plastic deformation processes in which both the strength reduction and loss of material would be minimised. On the basis of these criteria, the thermoplastics PEEK and PEK would prove more useful than PET or thermosetting resins, but again this will be discussed in more detail.

The type of failure exhibited by PET and PEEK (and to some extent PEK) can be considered in three ways;

(i) Failure in the impact region because of the pressure produced by the impacting water drop, seen as plastic deformation on the surface and the

presence of a half penny crack in the sub-surface.

(ii) Failure as a result of the shearing action of high speed radial flow, which has been observed as the characteristic ring of damage near the point of initial impact and which shows evidence of actual material removal in all three polymers investigated.

(iii) Failure caused by the interaction of stress waves. Where some sites of failure are evident away from the impact zone, for example the formation of the cone crack observed for PET and PEEK and surface analysis reveals radial cracks at some distance from the droplet impact site.

5.1.2. The effects of multiple water droplet impact.

Although the effects of collision with a single water drop are studied to elucidate the damage processes, in order to simulate the conditions encountered by a component in flight multiple impact studies need to be carried out. Despite the fact that the water jet apparatus used in this study is inconvenient for multiple damage assessment, some parameters of this process have been investigated.

Multiple impacts were performed, at velocities lower than the critical velocities where a fall off in properties would occur, to assess fully the effect of repeated impacts without clouding the impact responses with the sub-surface damage that has been shown to occur at the critical velocity. The evaluation of the response of PET to multiple impact at lower velocities was not carried out since as it

has been shown not to offer the same resistance as PEEK or PEK but still behaves in a similar manner. In the case of PEEK, five impacts at 334 m/s were sufficient to cause a reduction in toughness with no differences being observed as to degree of crystallinity, whilst for PEK with 37% crystallinity, five impacts at 900 m/s were required and for PEK with 35% crystallinity, 10 impacts at 900 m/s were sufficient to cause a reduction in toughness. This difference between the polymers has already been seen in the single impact study. Despite the fact that the samples broke during the Ceast impact, the failure was still observed to be governed by a ductile process (plastic deformation) in the PEK samples, while the PEEK samples broke in an intermediate fashion, namely bructile in nature. There is an indication that the less crystalline PEK specimens offer a greater resistance, which is as expected, but with the PEEK specimens there was no difference. This was thought to be a result of the velocity chosen which may have been too severe and not sensitive enough to reveal any differences between crystallinities as observed in the single impact study.

The post-impact loss in properties with increasing number of impacts has also been evaluated with brittle materials by means of the jet technique (7) where the reduction has been seen to occur at lower velocities coupled to the increase in number of impacts, as can be seen in figure 5.4.

The amount of damage visible on the sample surface was also seen to increase, but proved

difficult to measure as a result of the interaction between each new impact site of damage. What became more evident was the increased likelihood of material removal at ten impacts. If the technique lent itself to easier and quicker experimentation, it would have been interesting to have increased the number of impacts in order to evaluate the loss in weight of the samples. It is now understood that the Cavendish Laboratory at Cambridge have developed the jet technique so as to provide apparatus suitable for multiple impact analysis.

In this experiment, at least, it was possible to cause PEK to fracture in the Ceast, so allowing further evaluation by examination of the cross-sections. On examining PEEK and PEK by SEM, a mode of damage different from that under single impacts had occurred in multiple impact loading. No indication of a cone or half penny crack was observed, and instead a 'crumbling' effect was seen extending away from the impact site. It was felt that this effect occurred as a result of the constant pounding produced by the low velocity water drops, where the action of the hydrostatic pressure becomes predominant.

This so called crumbling effect has been used to explain the induction period that has been observed during a whirling arm evaluation of materials (with particular reference to PEEK), where this crumbled zone allows easier material removal (steep rise in weight loss) followed by the conversion of the crumbled zone into a fresh surface (the plateau region), as can be seen more clearly in figure 5.5.

Figure 5.4. Effect of impact velocity on fracture stress for multiple impact of soda lime glass. Jet diameter 0.8mm (7).

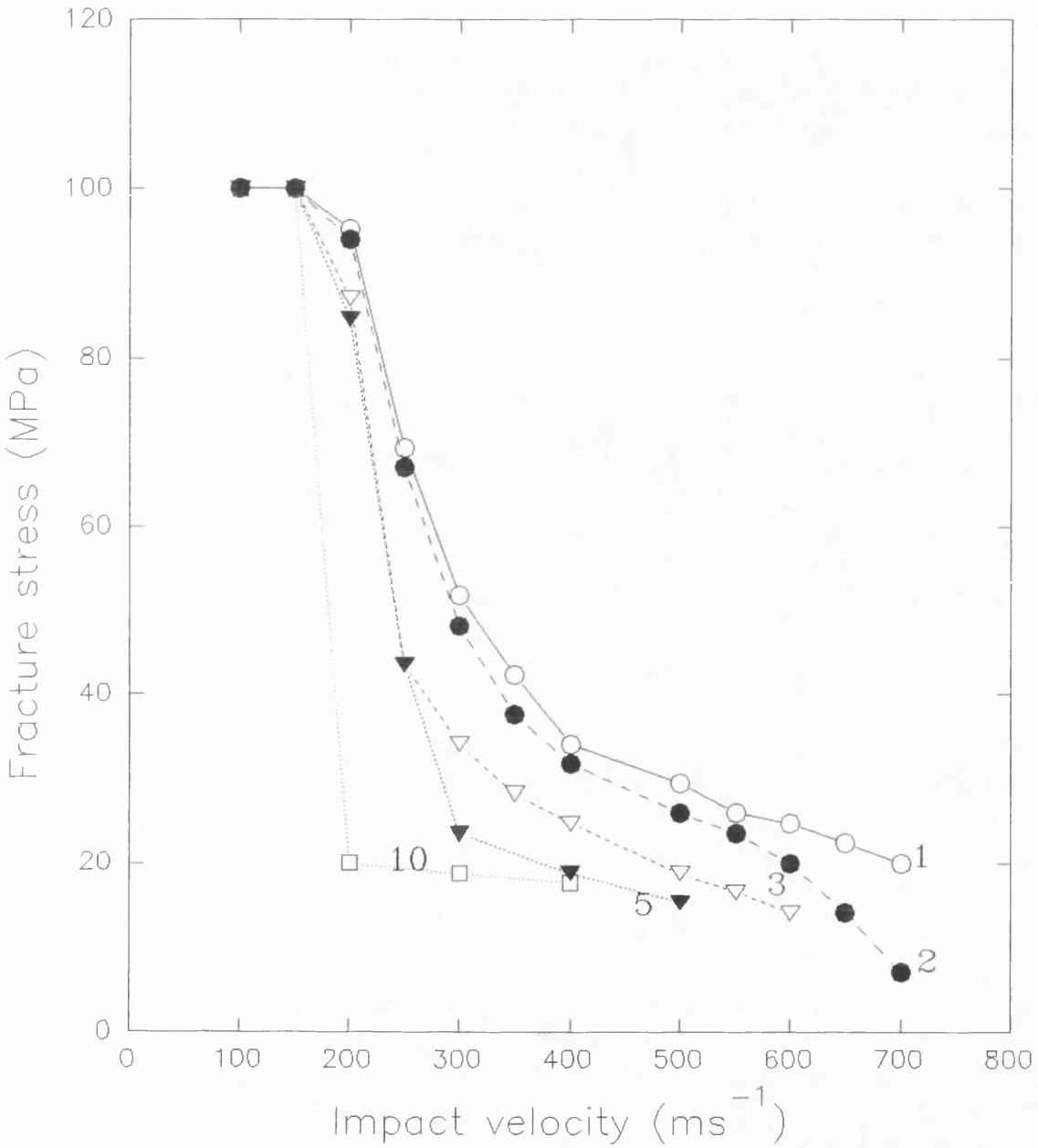

This crumbled zone produced by the multiple impact obviously acts as points for stress concentrations to arise, resulting in the observed fall-off in toughness of the polymers.

Although it has been postulated that this crumbled zone is a result of the pressure of the jet upon impact rather than being seen as the interaction of the stress waves with the flaws that have been initiated by the first impact, it must be explained in greater detail why it is felt that the stress waves are not principally responsible for the damage seen. During the experimental procedure the samples are not cleaned between the impacts in order to ensure that the sample was always impacted at the same place. In not cleaning the sample, a film of water was present between the polymer surface and the incoming jet of water. There would therefore have been a cushioning effect and the shock impulse would be partially dispersed within the film, so impinging over a larger contact area. In consequence, the surface waves would not interact with the sample to the same extent as on meeting a water-free surface. This film of water would be more representative of what would occur in service.

It has been shown that an incubation period also exists in observing rain erosion resistance of metals, where experiments carried out on steam turbine blades reveal an increase in the microhardness of steel. This increase continues until the internal stress has been raised sufficiently so that erosion (deformation and material removal) will proceed (91).

Figure 5.5. Postulated mechanism for material removal during multiple impact, describing the induction period.

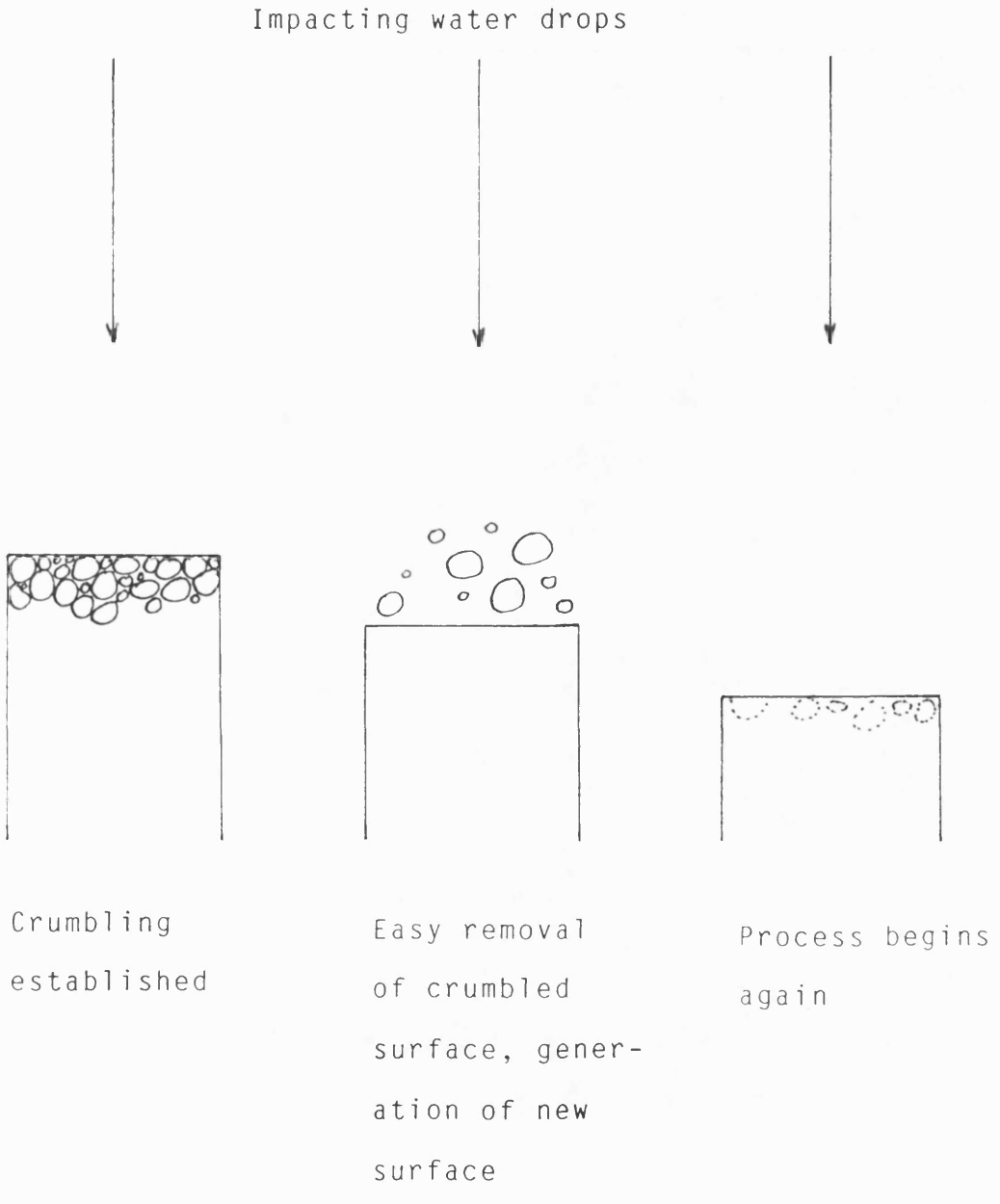

Again a difference between PEEK and PEK has been observed which was not expected. In general multiple water drop impact studies have only been used in the literature to evaluate materials by weight loss measurements, which obviously yields limited information. This approach has shown the loss in toughness of the materials as well as actual material removal with the ability to examine the fractured cross-sections of the samples. Again a similarity in the response of PEEK and PEK with brittle materials exists with a reduction in material toughness on increasing the number of water drop impacts.

5.1.3. Water drop impacts at elevated temperatures.

The physical and mechanical properties of these thermoplastics are significantly affected by temperature, so that it would be reasonable to assume that the rain erosion characteristics would also be affected. There is some indication that marginal improvements occur in rain erosion resistance at temperatures close to the glass transition temperature of the matrix material in question (2).

It has been shown in figure 4.41 that the extent of damage increases with increasing temperature of impact, and that the type of visual surface damage is altered so as to resemble the pressing of a steel ball bearing onto the surface (see plate 4.42). At temperatures above the glass transition of the polymers in question, the formation of a distinctive 'nipple' occurs on the surface of the sample away from the impacting event (ie the rear surface). This is attributed to the reduction of the yield strength

of the material at elevated temperatures resulting in a greater extent of plastic deformation as a result of the hydrostatic compressive pressure.

Although the extent of visual damage is increased as the temperature of water drop impact is increased, no evidence of material cracking or material removal was observed, and the post-impact fracture energy has been shown not to be affected (see figure 4.40), with the samples not breaking and the values returning to un-notched pre-water impact results. This is in accord with the conclusion that no sub-surface damage, such as fissures, was evident so that the response of the material to the pressure of the water drop impact event is to dissipate the energy as plastic deformation.

Single impact studies of PEEK, PES and glasses such as soda lime glass have confirmed that the amount of damage increases with temperature (31), seen as a reduction in the threshold velocity. For brittle materials such as glasses and zinc sulphide impacted at 300°C a variety of flaws developed which were not solely a result of the water impact, but a response to thermal shock, caused by the prolonged contact of cold water after the initial high pressure impact phase. This was confirmed by firing a jet of water from a hypodermic syringe onto the material surface which was at 300°C. At the temperatures investigated in this dissertation, no evidence of thermal shock was observed.

5.1.4. Sample geometry effects.

Two types of sample dimensions were used for the evaluation of the water drop impact process, as discussed in chapter three, where the sample dimensions are also presented;

(i) Standard impact bars
(ii) Disc samples

It was observed that the visual damage was more pronounced with the disc samples, seen as a greater evidence of radial cracks and a more distinct region of circumferential damage at comparable impact velocities. No corrections for sample geometry were used. It was felt that the greater amount of damage was a result of the disc sample being of reduced thickness (3mm as opposed to 6mm for the bars), allowing the interaction of the stress waves to occur more readily. This can be further explained by the fact that in the case of the thicker sample, the compression wave would be attenuated to a greater degree before it returns to the surface as a reflected tensile wave. Therefore, this reflected wave does not interact to the same extent with the impacted surface to create further damage.

5.2.0. Mechanical behaviour.

The increase in the glass transition and crystal melt temperature on going from PET to PEEK and finally to PEK, in the polymer series under investigation, yields information on the increased chain stiffness of the polymer PEK. The high glass

transition temperatures are essential for the thermoplastic to be considered for use at elevated service temperatures whilst retaining mechanical integrity. It has been shown in chapter 2.0 just how similar the crystalline nature and mechanical behaviour of all three polymers are. One would therefore expect that PEEK and PEK would respond to the impingement of a water drop in the same manner, and that any differences would be small. This has not been the case, with PEK showing a significant superiority in resistance to the impact process (be it by liquid or solid impact) than either PEEK or PET.

In molecular terms the extra ether linkage in PEEK would account for the enhanced chain flexibility, resulting in a lower glass transition and melting temperature than PEK, and the effects of the chemical differences are well documented (34,92). If for the moment we ignore the behaviour of PET, the polymers PEEK and PEK have in general been found to be of a very similar structure (both chemically and morphologically) giving rise to similar mechanical responses, see table 2.13. An established difference is that PEK is of a higher molecular weight than PEEK, which would suggest that the polymer would be more difficult to crystallise and that it would result in higher tensile strength and stiffness values. These features were described in chapter 4.0 and it was proposed that the reason that the grade of PEK used in this dissertation did not follow these rules (ie was easier to crystallize and exhibited a large difference in notched impact performance) was a result of the filler package used to assist

processing. To assess fully the mechanical responses of the polymers used, some detailed and varied analyses were used, and they will now be discussed.

5.2.1. Mechanical characterisation.

The behaviour of thermoplastics can best be described as non-linear viscoelastic, so that the modulus, for example, will be dependent upon the magnitude of the applied stress or strain. The viscoelastic response was studied in some detail and in general, by application of the time-temperature equivalence principle, the polymers exhibited a similar modulus response to increased frequency as can be seen in figure 4.15. The master curves follow similar trends, with values of the same order and the only real differences that occur are because of differing crystallinity rather than polymer structure, when the glass transition temperature was used as the reference temperature for calculating a_T. A concern was raised in this study when the dependence of the glass transition temperature (or any other lower order transition temperatures) to frequency and crystallinity was calculated. A general trend was determined, showing the activation energy increasing as one goes from PET to PEEK with PEK exhibiting the highest value (see table 4.13). Increasing the crystallinity of the polymers also resulted in a shift to higher values for Ea, and the results obtained are indicative of the increased chain stiffness, with PEK being the less mobile. Some low order transitions were also observed at around -60°C for PEEK and PEK and about -36°C for PET, with low values of Ea for this low order

process, indicative of a small portion of the main chain being responsible. What has led to some concern is that the calculated values obtained for the glass transition process are of such a high order and that extrapolating the plot back to the origin would yield large values for the pre-exponential factor, A. The absolute top value would be the atomic vibration frequency which would be about 10^{12}. Any value for a molecular response higher than this must be absolutely meaningless. Rough values for A, determined from the data presented herein yield the following ;

PET $10^{58} s^{-1}$

PEEK $10^{98} s^{-1}$

PEK $10^{110} s^{-1}$

An attempt has been made to find some literature on this subject but, although values for the activation energy of the glass transition process have been found, there has been no mention of what the values determined actually indicate, and whether or not the use of the Arrhenius expression holds for the analysis of polymer systems in general. It is felt that some investigation into these processes would be of value, but to address these in this thesis would be unjustifiable.

The similarities of the polymers are also clearly shown in the measurements of the tensile strengths. The values for PEEK and PEK are of the same order and offer a similar response to the application of the tensile loading, namely a ductile response. The stress/strain curves follow the same route for PET although the actual values obtained are

of a lower order. No differences were seen between PEEK and PEK when measuring the tensile behaviour at elevated temperatures (up to the glass transition temperature) with the increased level of crystallinity producing a negligible effect upon the values as the temperature of testing was increased. To obtain a better understanding of the polymer toughness, the response to impact and bending was investigated.

On attempting to measure the fracture toughness of un-notched specimens, it was found that PEEK and PEK samples did not break. This agrees with results found in literature for un-notched specimens (see table 2.13), where the polymers did not fracture under Charpy or Izod impacting conditions. A measure of the rigidity of the samples resulted, where PEK was found to offer a greater resistance to deformation than PEEK, and, increasing the crystallinity created an even greater resistance. The PET specimens did fracture under the conditions used giving a value of the fracture energy of 71 kJm^{-2}. In 3-point bending experiments none of the un-notched samples fractured, illustrating the effect of the magnitude of strain rate upon the final mechanical properties, ie the lower the strain rates used, the more ductile the behaviour of the polymers. To characterise the impact behaviour more closely, notched specimens were also tested in bending.

Under Charpy testing conditions the behaviour of the polymers in response to increased notch depth can be seen in figure 4.24. It is now evident that a difference between PEEK and PEK has been established,

PEK having been shown to be a tougher material than PEEK, offering a greater resistance to the propagation of cracks. The 3-point bend test confirms these findings, the fracture energy of PEK being of a higher order than those of PEEK or PET over the notch depth range studied, as can be seen in table 4.26. The application of fracture mechanics was attempted and values of K_{ic} were calculated. These values are difficult to compare or to draw any conclusions from as can be seen in figure 4.25. The load/displacement curve illustrates a ductile response, so that the conditions for the valid application of fracture mechanics are not obtained (93,94). These ductile responses are a result of several possible effects, such as, for example, plastic deformation at the crack tip leading to unstable fracture. Nevertheless, PET behaved in a truly brittle manner and the values determined are a result of a true propagation of the crack front resulting in a non ductile response. For reasons of simplicity, an attempt to develop an effective fracture analysis for the polymers was not considered.

Even though the analysis of the fracture behaviour of the polymers was not strictly academic, it was still possible to determine the differences in their behaviour from the comparative tests carried out. There was no correlation between the values produced in this work and those obtained from published literature, since many factors are involved, for example, notch tip radius, specimen geometry, impact load, speed of testing etc (95). In chapter 2.0, some discussion of the fracture

toughness of PEEK is presented.

The large difference found in the toughness of PEK compared to PEEK led to some concern as the values found in literature for these two polymers are usually very similar. For example, in table 2.13 the Izod impact strengths, following ASTM D256, for PEEK and PEK were 83 and 85 J/m, respectively. This toughness similarity has also been shown in an ICI product bulletin (96), describing PEEK and PEK, both manufactured by ICI, as having the same impact performance.

As has already been mentioned several times, the grade of PEK used was not a virgin polymer since it has added to it various processing ingredients (then again some discussions concerning Victrex PEEK have shown the addition of nucleating agents to be likely in this case, too). It was felt that the TiO_2 and Al_2O_3 particles could act as nucleating agents, which accounts for the ease of producing PEK at high crystallinities. Moreover, the addition of PTFE as a fine powder (particle size not disclosed), added as a processing aid, is supposed to have a modifying effect upon the mechanical properties.

The level of PTFE used was 0.5% with approximately 4.0% of mineral fillers, Al_2O_3 and TiO_2. The use of the mineral fillers could possibly have the effect of acting as stress concentrators and in doing so lowering the stress at which fracture occurs, but for the case of semi-crystalline polymers this seems highly unlikely, especially at the levels used. It is felt that the use of the fine PTFE

powder could have an overall effect of acting as a rubber toughening agent for brittle plastics, as with the use of butadiene rubber with a glassy styrene network in the case of ABS for example. It is understood that PEEK and PEK are extremely tough in their own right, but as the literature suggests the mechanical similarity leads one to believe that the filler package is having an influence. In general, provided that there is a good bond between the two phases, then an increase in toughness should result as can be seen in figure 5.6 where the variation of G_{ic} with rubber content in an epoxide clearly illustrates the enhanced toughness even at low levels of rubber addition (97).

Even so it does seem unlikely that such a small addition of PTFE could give rise to such a large difference in the fracture toughness and, ultimately, the rain erosion resistance, between PEEK and PEK. The chemical, morphological and mechanical similarities of the polymers lead one to deduce that the modification of the polymer by PTFE is a feasible explanation. In the light of this comment the reader would be justified in asking why no experiment was carried out involving the elimination of the filler package from PEK and/or the addition of the filler package to PEEK. The reasons for not doing so are as follows;

(i) The only grade of PEK available in large enough quantities, manufactured by Raychem Ltd, was with the filler package.

(ii) Processing equipment available involved the use of 10kg minimum quantity of polymer for compounding trials. To carry out a succesful experiment, various

Figure 5.6. Variation in fracture surface energy with rubber content of an epoxide containing carboxy terminated butadiene acrylonitrile (CTBN), (97).

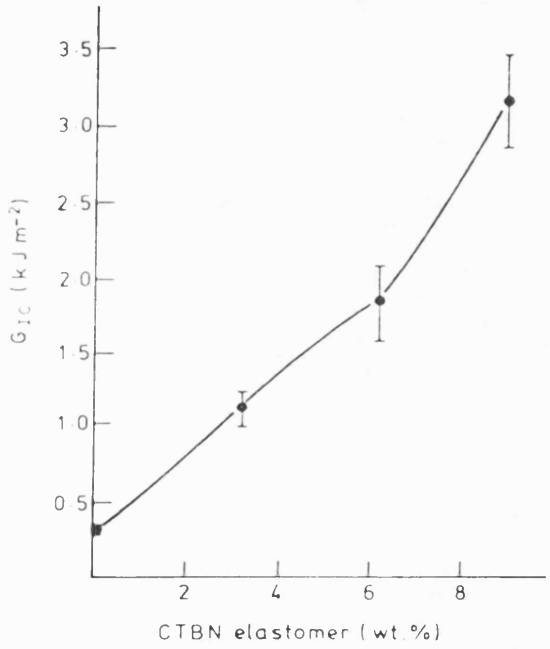

blending procedures would need to have been investigated and the cost of the polymers in question would have made this experiment too expensive with the resources available.

Taking these factors into account, the improved properties of this grade of PEK have been demonstrated and, in particular, this grade had been released for evaluation as a candidate radome material, and so a closer examination was necessary.

To conclude this mechanical characterisation section, some erosion data have been found for virgin PEK as manufactured by ICI Advanced Materials under the tradename Victrex PEK (96). It is clearly evident that the erosion resistance is less than that of PEEK as can be seen in figure 5.7. This gives further justification to the possible influence of the filler package and in particular the addition of PTFE, albeit differing polymerisation routes would have been used.

5.2.2. Correlation of mechanical properties with water droplet impact.

It has already been mentioned that it proves difficult to postulate what aspects of mechanical properties of polymers would influence the resistance to impact by a water drop where an erosion process also develops. It has been suggested that if a polymer has a high modulus and a high impact strength, then it should exhibit good water droplet impact/erosion resistance. From the work carried out here there seems to be no reason to dispute this

Figure 5.7. Rain erosion resistance of materials, tested by the Whirling arm technique at 223 m/s and a rain intensity of 25mm.hr.

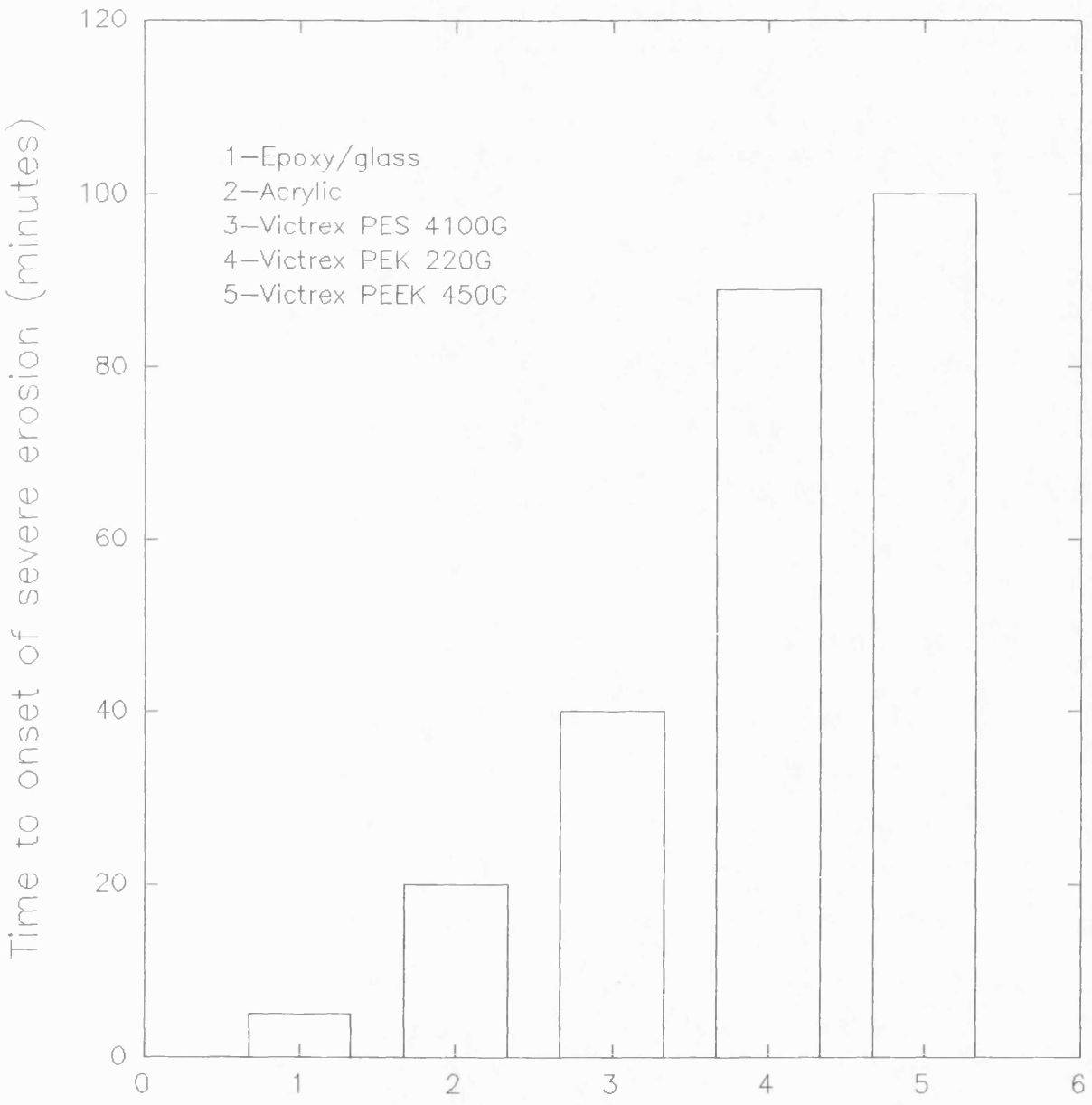

generalised statement, as PEK has been shown to offer the greater resistance, with both the amount of surface (material removal and formation of cracks) and sub-surface damage occurring to a much lesser extent than found for PEEK and PET. The dynamic modulus values for all three polymers, as measured by DMTA, have been shown to be similar, as have their tensile properties, so that these forms of characterisation do not seem to offer any greater understanding.

It has also been suggested that the value of Poisson's ratio of a material can also have a modifying effect. This also seems to be a reasonable statement to make, as in the measurement of the basic elastic constants, namely, Young's modulus, E, the shear modulus, G and the bulk modulus, K, Poisson's ratio, μ , has an overall effect as can be seen from the inter-relationships between these various properties:

$$G = E/\ 2(1+\mu) \qquad 18$$

$$K = E/\ 3(1-2\mu) \qquad 19$$

$$E = 9KG/\ (3K+G) \qquad 20$$

$$\mu = \tfrac{1}{2}\ (3K-2G/3K+G) \qquad 21$$

By altering the value of Poisson's ratio a significant effect upon the constants is achieved. The values of Poisson's ratio for PEEK, PEK and PET are 0.42, 0.395 and 0.43 respectively, indicating a change in response to loading between all the three

polymers concerned. The maximum value for Poisson's ratio that an isotropic material could have would be 0.5, representative of a rubber which would undergo a maximum 'thinning' down and in effect a low shear modulus relative to its bulk modulus. Poisson's ratio is normally about 0.3-0.4. For rubbers (as already mentioned), or liquids, or plastically deforming metals it is 0.5, which means that when you deform the solid you change the shape but not the volume. For normal μ values, elastic extension leads to lateral contraction (the Poisson effect), which may be greater or smaller depending on the value of μ. But to get a volume expansion, μ must be negative and you can only find negative values in materials with strange characteristics, like some foams or cloths, never in homogeneous materials. The values differ only slightly and it is felt that these alone would not account for the dramatic difference in the notched toughness between PEEK and PEK, and the differing resistance to impact by a water droplet.

The ideas on which the fracture mechanics approach is based were first used by Griffith(103). He proposed that the fracture stress, σ_f can be obtained from;

$$\sigma_f = (2E\gamma/\pi c)^{\frac{1}{2}} \qquad 22$$

where c is the crack length, E is Young's modulus and γ is the surface energy (energy required to create a new surface and is the property of the material). The factor 2 appears because fracture forms two new surfaces each requiring a surface energy.

For a given material failing in a brittle fashion, plotting the fracture stress against

increasing crack lengths would produce a curve where at very small crack lengths there is a levelling out at some "intrinsic" crack or defect size, c_o, typical of the material structure or surface. The following analysis is used to try to determine this.

An important difference was observed in the toughness of the polymers and the fracture values were re-plotted from figure 4.24 on a log/log graph as can be seen in figure 5.8. These were used to find the apparent notch/crack lengths of the materials after water droplet impact, by extrapolation. These values can be seen in table 5.9 below.

Table 5.9. Apparent notch depths measured after a water drop impact.

Material	Water drop velocity m/s	No.of impacts	Fracture Energy kJ/m^2	Extrapolated A/W	Apparent notch depth (mm)
PEEK 27%	334	5	158	7.94×10^{-4}	5×10^{-3}
"	334	10	29	1.2×10^{-2}	7×10^{-2}
PEEK 35%	334	5	171	4.79×10^{-4}	3×10^{-3}
"	334	10	87	2.29×10^{-3}	1.4×10^{-2}
PEK 35%	900	5	615	3.98×10^{-4}	2.4×10^{-3}
"	900	10	533	5.01×10^{-4}	3×10^{-3}
PEK 37%	900	5	593	5.25×10^{-4}	3×10^{-3}
"	900	10	494	7.29×10^{-4}	4×10^{-3}
PET 38%	334	3	15	1.99×10^{-2}	1.2×10^{-1}

These notch depths determined from figure 5.8, do not seem to correspond to the amount of damage

observed in the SEM photographs of the post-impact fractured cross-sections, where the damage at the impacted surface seems to extend approximately 400-500 μm into the sample. This could be as a result of the different geometry of the flaws produced as in the notch characterisation, the flaw was manually created using a blade whilst here we are comparing with flaws produced by the water drop impacting process (seen as half penny and cone type cracks). Even so, one can readily determine the evidence that even a crack of small proportions would result in a loss in toughness. What is apparent from the data achieved so far, is that the initiation of flaws or cracks occurs to the same extent for all three polymers concerned as can be observed from the SEM photographs, although to a slightly lesser extent with PEK. It is the propagation of the crack that has been assumed to differ, with PEEK and PET exhibiting a similar brittle response whilst for PEK the propagation is hindered by a greater level of plastic deformation (observed as ductile behaviour from the load/displacement curves of both the Ceast and 3-point bend tests). This again would be contrary to values found in the literature and it is suggested that it is as a result of the addition of PTFE.

The reduced amount of visible damage for PEK as compared with PEEK and PET is not surprising since from the tensile measurements the yield strength of PEK is slightly higher. The presence of surface damage was to be expected as the hydrostatic pressure (≈1.5 GPa) in combination with the shearing action of the water over the sample surface would contribute to

Figure 5.8. Fracture energy values re-plotted from figure 4.24, for the determination of crack depths p after water droplet impact.

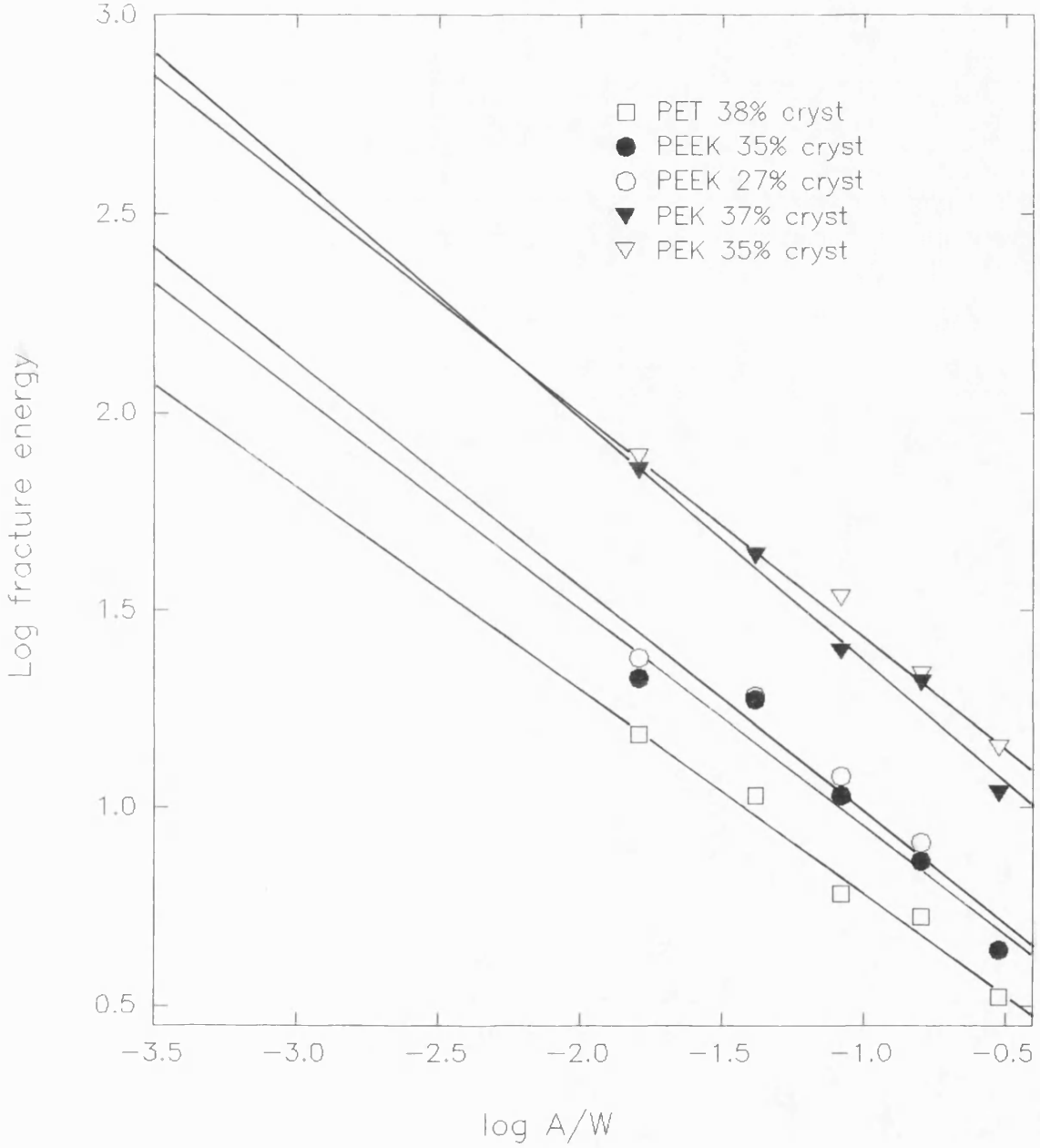

material failure. The reasons as to why PEK exhibits the least amount of damage whilst PET has the greatest amount can therefore be explained in terms of the strengths of the materials.

5.3.0. Concluding remarks.

An attempt has been made in this discussion chapter to offer a greater understanding of the results obtained in chapter 4.0. These results have been discussed in relation to work already carried out in this field and it is hoped that a new approach to analysing the water drop impact event has been established.

From this discussion chapter it has become apparent that a different response to the application of an impact loading is present in the case for PEK, which becomes more pronounced on impact by a water droplet. This difference was not expected as the polymers PEEK and PEK are of a similar chemical, morphological and mechanical nature, and the difference has been linked to the addition of processing additives, especially PTFE. Several conclusions can be determined from these discussions and they will be dealt with in the following chapter.

CHAPTER 6
CONCLUSIONS AND SUGGESTIONS FOR FUTURE WORK

6.1.0. Summary.

The liquid impact properties of three thermoplastic engineering polymers have been investigated by using the liquid jet impact technique, and a method for analysing the impact process quantitatively has been proposed. At the end of this section data will be presented to justify the use of PEK as a candidate radome material.

6.1.1. Quantifying the liquid impact process.

The only means of quantifying the damage caused by the impact of a water drop with a plastic component has been to measure weight loss over a period of time under multiple impact regimes. This involves elaborate test equipment that is not readily available to the materials scientist. A method has been developed here where standard impact specimen bars were used and the liquid jet (corresponding to a water drop) process was carried out to produce flaws in the sample which could further be analysed by impact testing in a Charpy type tester. This now becomes a measure of the polymer toughness, which in behavioural response follow similar trends to ones that are well documented. The results show a fall off in fracture energy with increasing velocity of the water drop impact (as seen with increasing notch depth). Increasing the velocity of the water drop impact produces a more pronounced transition to brittle behaviour.

This method has been applied to the polymers PEEK, PEK and PET, and it has been shown that under

both single and multiple liquid impacts, PEK offers the greater resistance, with PET failing catastrophically at the velocities of impact chosen. Some care needs to be taken during the experimental procedure as on increasing the water drop velocity the amount of damage that is visible becomes more apparent as well as the observed sub-surface fractures. The ring of circumferential cracking can extend towards the edges of the sample resulting in material removal (detected for PET at 334 m/s) or as in the case of PEEK and PEK, which both exhibited a ductile behaviour, a region of plastic deformation was observed which distorted the sample dimensions. Altering the geometry of the specimens would obviously reduce the possibility of this occurring.

It has also been shown that the level of crystallinity has an effect, with less resistance to the impact being offerred on increasing the degree of crystallinity because of the reinforcing nature of the crystallites tending towards a more brittle material response. These findings suggest that improved resistance would be obtained if it was found to be possible to manufacture the component in its amorphous state.

The mechanical and viscoelastic measurements at first yielded information as to the similarities between PEEK and PEK and large differences were only observed when initial investigations into the response to impact by a water drop were carried out. This led to some analysis of the fracture properties of notched specimens where the response of PEK became significantly different from either PEEK or PET.

Reports in the literature have contradicted these findings as there is evidence that there is very little difference in the notched fracture behaviour of PEEK and PEK. It is therefore concluded that the processing filler package used to improve the rheology of PEK had an effect and in particular the addition of PTFE had a modifying influence upon the fracture behaviour, even for the small amounts incorporated. Insufficient experimentation has been carried out for us to be entirely convinced that this statement holds true, but a difference has clearly been established which cannot be ascribed to chemical or morphological changes and so, if the addition of PTFE does offer such improvements to this family of polymers, then a great deal of benefit could be obtained.

6.1.2. Polymer response to single and multiple water drop impacts.

In the experimental procedure outlined in this dissertation two types of failure mode have been observed;

(i) In single impact studies, analysis of the cross sections after fracture following water impact, has revealed the presence of a cone type crack directly underneath the visible surface circumferential damage zone and a central zone of damage resembling a half penny crack as seen by the application of a Vickers diamond indentor. These zones of damage are a result of the shock waves and hydrostatic pressure of the water drop during the impact event.

(ii) In the case of multiple water droplet impact, there is sufficient evidence of a so called 'crumbled' zone which has been postulated to be a result of the interaction and propagation of cracks under the combined effect of numerous high pressure producing water droplets impinging at the sample surface. It has also been concluded that this crumbled zone can be used to explain the formation of an incubation period during weight loss experiments in the whirling arm test procedure.

6.1.3. High temperature effects.

The water drop impact of the polymers at elevated temperatures yielded some surprising results. Firstly, as seen in previous literature the amount of visible damage is seen to increase as the temperature of the specimen is increased. Large areas of plastic deformation were evident as the formation of a pit, once the temperature of the specimen reaches and surpasses the glass transition temperature of the polymer. No evidence of thermal shock was observed at the temperatures chosen for experimentation, and the increase in plastic deformation is a direct result of the reduction of the yield strength of the polymers as the temperature is increased.

Investigation of the fracture properties following water impact has shown that the energy of the water drop impact has been dissipated as plastic deformation and not in the creation of cracks, as can be seen where no fall off in fracture energy occurs even after water impacts at 200°C. The ductilities

of the polymers have obviously increased at elevated temperatures (as can be seen from the stress/strain diagrams), absorbing the energy of water impact more efficiently without a result of sub-surface fracture inherent of a brittle response.

6.2.0. PEK as a candidate radome material.

The best publicized composite matrix material of the polyarylate family has undoubtedly been PEEK. It is recognized on account of its impact performance and environmental resistance which are superior to most other thermoplastic and thermoset matrix polymers. One consequence of this attention has been that other members of the family have been given less detailed consideration and in particular PEK has been shown in this dissertation to compare very favourably with PEEK. To end this Conclusions section, an attempt has been made to compare PEEK and PEK by using results obtained in this work and from other sources to illustrate the potential of PEK as a useful material to select for radome applications.

6.2.1. Fabrication of a PEK radome.

This will be an important process as one must produce a shaped article (radome) cost effectively and technically simple. Injection moulding of PEK has been shown to be relatively easy for preparing non-complex samples for experimentation within this thesis, however direct injection moulding could offer severe limitations in producing a radome as really

only small radomes would be possible of the solid wall design to facilitate dimensional and morphological control.

Attempts have been carried out at Raychem Ltd in two areas;

(i) The injection moulding of fibre-reinforced PEK (with glass and carbon fibre) into moulds of low complexity.

(ii) Production of a PEK yarn which could be interwoven (co-mingled) with a glass or carbon fibre yarn to facilitate mould lay up and the production of components by match mould forming (female and male moulds used to produce large and/or complex parts). The PEK yarn produced was of 0.07mm in diameter with a modulus of 10.3 GPa and an elongation to break of 38%.

Both these routes proved to be succesful in their own right but it is envisaged that the yarn-forming technique would offer greater advantages, ie, control of fibre orientation and distribution, coupled to less complicated plant processing machinery.

6.2.2. Properties.

As has already been discussed in detail in this thesis, the higher toughness of the grade of PEK used, as compared to the PEEK, would lead one to believe that it would offer a greater resistance to water drop impingement. The findings have shown this to be true and also that, regarding the increased

tensile and yield strength characteristics of PEK and its lower value of Poisson's ratio, the actual ability of the water droplet to remove material, ie to erode the PEK would prove more difficult than in the case of PEEK.

For PEK to be succesfully used as a radome material, its mechanical properties are not the only considerations: its electrical properties also need to be understood. The polymer needs to have a low dielectric constant and low loss tangent properties to allow effective passage of electromagnetic waves with minimum interference.

Without going into great detail, the dielectric constant or relative permeability is defined as (98);

$$\text{dielectric constant, } E' = Cs/Co \qquad 22$$

where Cs is the capacitance of a capacitor with a dielectric specimen filling the space between the metallic plates and Co is the capacitance with a vacuum (in practice this medium is air) replacing the material, while the loss tangent (tan δ) is given by;

$$\tan \delta = I_l/Ic \qquad 23$$

With an alternating voltage of a certain frequency, applied to a capacitor with the dielectric material filling the space between the plates, the resulting alternating current will contain the two components, I_l (loss current) and Ic (charging current).

The following table lists results obtained from Plessey Materials, Towcester, Northants, of experiments carried out by Mr F.S.Ward (March 1985). Prior to testing the samples were conditioned at 50% RH @ RT for two days and the measurements were carried out at 9.368 GHz. The slight increase in values for PEK in comparison to PEEK are accounted for by the filler package used and in particular to the use of mineral fillers which are known to reduce the electrical permeability.

Table 6.3. Dielectric measurements on PEEK and PEK.

Temp	PEK		PEEK	
(°C)	E'	tan δ	E'	tan δ
20	3.566	0.0043	3.248	0.0034
65	3.525	0.0049	3.205	0.0040
110	3.502	0.0062	3.178	0.0048
155	3.491	0.0075	3.167	0.0062
200	3.517	0.0112	3.189	0.0103
260	3.623	0.0228	3.293	0.0199

As has already been mentioned in the first chapter, PEK was shown to offer greater resistance to rain erosion than PEEK, when tested in a whirling arm test rig. This has been confirmed by using single impact studies as has already been discussed in this thesis. These results contradict the manufacturers values for a comparison between PEEK and an ICI grade of PEK (96), where PEEK was shown to offer an improved resistance to rain erosion.

The differences described in this thesis were

felt to be a result of the addition of PTFE particles, which were thought to act as rubber reinforcement domains within the matrix of PEK. Tables 6.4 and 6.5 present rain erosion data obtained by the whirling arm technique at R.A.E, Farnborough, by the Materials and Structures Department (99), who commented upon the favourable erosion and dielectric properties of PEK as being potentially very useful.

The conditions of testing carried out for the whirling arm assessment were at a velocity of 223 m/s, a rainfall intensity of 25 mm/hr, a 2 mm nominal drop diameter and an impact angle of 90°.

Table 6.4. Rain erosion data for PEK (as used in this dissertation.

Test time (mins)	weight change (mg)			
	sample 1	sample 2	sample 3	sample 4
-	0	0	0	0
15	0	-5	0	-1
30	0	0	0	0
45	0	0	0	-3
60	0	0	0	0
75	0	-3	0	0
90	-2	-1	0	-8
105	0	-3	-3	0
120	-3	-5	-2	-2
135	-2	-7	-3	0

These compare to weight loss values of 44 mg for PEEK after 110 minutes and 364 mg for PES after 40 minutes.

Table 6.5. Rain erosion data for PEEK and PEK.

Test time (mins)	weight change (mg) PEK sample 1	PEK sample 2	PEEK sample 1	PEEK sample 2
15	-1	-1	-1	+1
30	+1	0	0	0
45	0	+1	+1	-27
60	0	0	-1	large
70	-1	0	0	hole
80	0	+1	0	
90	0	0	0	
100	+1	0	0	
110	+1	-2	+1	
120	-3	-1	-3	
135	0	0	-3	
150	-4	-2	-4	

6.2.3. Concluding remarks.

The above results, in conjunction with the mechanical properties measured in the course of this work, illustrate the usefulness of PEK. The overall radome performance requirements can be listed as follows (100):

a) Structural integrity up to 232°C for 30 minutes.

b) Low dielectric constant and loss tangent properties that are not affected to a great extent by humidity and/or temperature.

c) Resistance to rain/dust/particle erosion.

d) cost effectiveness.

It is considered that PEK does meet these requirements.

6.3.0. Suggestions for future work.

In undertaking a study of this kind, where in the past a great deal of theoretical analysis has been carried out, the use of more practical methods

for understanding the parameters of water droplet impact erosion of engineering plastics has thrown up further questions that require answering rather than producing a thesis with hard and fast conclusions. As has been discussed, the level of crystallinity, fracture properties and strength characterisation all have an influence upon the resistance of the polymer to liquid impact. The following suggestions for further experimentation are presented to assist in providing a deeper understanding of the process.

The use of a Charpy impact testing machine to assess the fracture properties following liquid impact has proved to be successful. It is felt that a whole range of polymers that are currently being used for aircraft components, and any emerging ones, could be placed into context by means of this technique, thereby fully characterising their response to water impact. For example, some preliminary work has been carried out by the author, where materials were investigated which were known to offer less resistance to water droplet impingement damage than PEEK, namely an un-reinforced epoxy thermoset and a thermoplastic, PES. Initial findings (not disclosed), confirmed their inferior properties, with similar failure modes being exhibited, namely, the lower notch fracture energies corresponding to a fall off in fracture properties at lower water drop velocities of impact. It is considered important, therefore, and worthwhile to follow up this method of analysis because under the rates of strain governed by a water drop impact the materials will behave in a brittle manner, resulting in the formation of flaws which will contribute to a drop in fracture

properties.

It has been suggested that the addition of PTFE, even in such small quantities, has led to the polymer PEK behaving as a rubber modified brittle plastic. The data produced have been inconclusive and further research is needed in order to demonstrate whether there is any merit in the addition of PTFE, or other particulate polymers. This should consist of providing adequate dispersion by using modern compounding equipment (such as the twin screw types) and observing the fracture behaviour as detailed in this thesis.

An evaluation of the matrix material in its composite form would also be required. It is already known that the resistance to rain erosion is reduced in a composite in comparison to the matrix alone, but a greater understanding of fibre dispersion, orientation and matrix interaction would be of great benefit. The level of the matrix crystallinity has a modifying effect at reduced levels and incorporating this alongside composite behaviour alone would yield an interesting and informative study.

Some fundamental research is needed with both single and multiple water droplet impacts, especially drop sizes, velocity range and impact angles, and their effect on post-impact fracture properties. Two distinctive modes of damage have been observed between the two regimes and closer examination of initiation and the propagation of these fracture sites would be possible.

A more theoretical approach may be considered, with the interaction of the stress waves with the polymer in question being elucidated. A possibility may exist for developing a model of the damage process in order to find any correlation between the mechanical properties of the polymer and its ability to resist the water impact process. Correlations should be possible between the single and multiple impacts carried out with the jet technique and the more specialised whirling arm technique, since some mathematical correlations relating the threshold velocity to rain erosion resistance from the whirling arm test do exist (101,102). This should involve closer understanding of the material properties as well as of the water drop.

It has also been observed in brief experimentation on the polymers PEEK, PEK and PET, that although undergoing a greater amount of surface damage and deformation, the post-impact fracture properties have remained un-altered when impacting at elevated temperatures. This needs to be investigated more carefully especially when considering composite behaviour. A greater range of velocity and temperature is required to assess the materials fully before it could be concluded that the erosion behaviour (as sub-surface damage) does not influence the strength of the component when subjected to water drops as rain at thermodynamic heating regimes.

Finally, a concern has been raised as to the applicability of the Arrhenius equation when discussing molecular motions. It is apparent that although this technique is used to describe certain

processes it may not be fully understood in relation to events on a polymer molecular scale. It is also felt that a greater understanding is necessary.

CHAPTER 7
REFERENCES

1. Walton J.D. Radome Engineering Handbook. Design and Principles. Marcel Dekker, Inc., New York. 1970.

2. Fyall A.A and King R.B. Guide to Rain Erosion. Royal Aircraft Establishment Technical Memorandum, Mat 266. 14th Jan 1977.

3. Wahl N.E. Investigation of the phenomena of rain erosion at subsonic and supersonic speeds. Tech.rept. AFML-TR-65-330, Oct 1965.

4. Schmitt G.F, Jr. Liquid Impact Erosion- a unique form of wear for aerospace materials. Sampe Journal July/August, 1977.

5. Meades G.F. Domes in search of the delicate balance. Plastics and Rubber Weekly, No. 1046, July 14, 1984.

6. Hall C.K. Continuous fibre reinforced thermoplastics in new generation radomes. Fibre Reinforced Composites, 19.1-19.13, 1984.

7. van der Zwaag, S. Liquid impact and contact damage in brittle solids. Ph.D thesis, University of Cambridge, 1981.

8. Conti D.A. Communications and advanced radome concepts. Paper B12, RPG symposium, Reinforced plastics in electrical and electronic applications. 25-

26th Feb, 1975.

9. Conti D.A and McCartney C. Design aspects of non-metallics in guided weapons and aircraft radomes. British Aerospace PLC, Reinforced Microwave Plastics Group. Workshop on design philosophies with non-metallics. H.M.S Nelson, 22-23rd June, 1982.

10. Jones D.M.A. The shape of raindrops. J.Meteorol., 16, 504, 1959.

11. de Haller P. Schweiz.Bauztg, 101, 243, 260. 1933

12. Cook S.S. Erosion by water hammer. Proc.Roy. Soc.Lond. A 119, 481-488, 1928.

13. Bowden F.P and Brunton J.H. The deformation of solids by liquid impact at supersonic speeds. Proc. Roy.Soc.Lond. A 263, 433-450, 1961.

14. Heymann F.J. High speed impact between a liquid drop and a solid surface. J.Appl. Phys. 40, 5113-5122, 1969.

15. Rochester M.C and Brunton J.H. Pressure distribution during drop impact. Proc.5th.Int.Conf. on erosion by liquid and solid impact, 6.1-6.7, 1979.

16. Pidsley P.H. A numerical investigation of water drop impact. Proc.6th.Int.Conf on erosion by liquid and solid impact,

18.1-18.6, 1983.

17. Campbell A. — Assessment of the rain erosion resistance of composite materials for radome applications. Proc.6th. Int.Conf on erosion by liquid and solid impact, 23.1-23.6, 1983.

18. Bowden F.P and Field J.E. — The brittle fracture of solids by liquid impact, by solid impact and by shock. Proc.Roy.Soc.Lond. A 282, 331-352, 1964.

19. Lawn B.R and Evans A.G. — A model for crack initiation in elastic/plastic indentation fields. J.Mat.Sci, 12, 2195-2199, 1977.

20. Fyall A.A and Strain R.N.C. — A whirling arm test rig for the assessment of the rain erosion of materials. R.A.E.Rept (Chem), No. 509, FCSTI AD 132-133, 1956.

21. Tatnall C.J., Foulke K.W and Schmitt G.F. — Joint Air Force-Navy supersonic rain evaluation of dielectric and other materials. Rept. NADC-AE-6708, 1967.

22. Hurley C.J., Zahavi J and Schmitt G.F. — Rain erosion mechanisms on polyurethane and fluoroelastomer coated composite constructions. Proc.6th. Int.Conf on erosion by liquid and solid impact, 22.1-22.13, 1983.

23. Schmitt Jr, G.F. The subsonic rain erosion response of composite and honeycomb structures. Proc.5th.Int.Conf on erosion by liquid and solid impact, 15.1-15.11, 1979.

24. Schmitt Jr, G.F. Captive carry anf free flight rain erosion considerations for reinforced ablative fluorocarbon radome materials. Sampe Journal, Nov/Dec, 12-16, 1980.

25. King R.B. Rain erosion part IV, An assessment of various materials. R.A.E. rept. (Chem), No.521, 1960.

26. Adler W.F. Single water drop impacts on polymethylmethacrylate. Proc.5th.Int. Conf on erosion by solid and liquid impact, 9.1-9.10, 1979.

27. Gorham D.A., Matthewson M.J and Field J.E. Damage mechanisms in polymers and composites under high-velocity liquid impact. Erosion: Prevention and useful application, ASTM STP 664 , W.F Adler, Ed., American Society for Testing and Materials, 320-342, 1979.

28. Matthewson M.J and Gorham D.J. An investigation of the liquid impact properties of a GFRP radome material. J.Mat.Sci., 16, 1616-1626, 1981.

29. Voss D.L. Urethane-clad polycarbonate. SPE High Performance Plastics. National Tech.Conf, 30-35, 1976.

30. Corney N.S and Pippett J.S. The rain erosion resistance of some radome and irdome materials. Proc. 6th.Int.Conf on erosion by liquid and solid impact, 24.1-24.7, 1983.

31. Hand R.J. Impact and fracture properties of infra-red and optical transmitting materials. PhD thesis, University of Cambridge, 1987.

32. Evans K.E. Tailoring the negative Poisson's ratio. Chemistry and Industry, 654-657, Oct 15th, 1990.

33. Anon. Engineering plastics. European Plastic News, 7-23, Feb, 1979.

34. Billmeyer Jr, F.W. Textbook of Polymer Science, third edition. J.Wiley and Sons Inc, 1984.

35. Brydson J.A. Plastic Materials, fourth edition. Butterworth Scientific, 1982.

36. Rose J.B. British patent 1,414,421, 1975.

37. Marks B.M. US patent 3,442,857, 1969.

38. Dahl K.J. British patent 1,387,303, 1975.

39. Young R.J. Introduction to Polymers. Chapman and Hall Ltd, 1989.

40. Blundell D.J and Osborn B.N. The morphology of poly(aryl-ether-ether-ketone). Polymer, 24, 953-957, 1983.

41. Sharples A. Introduction to polymer crystallization. Edward Arnold (publishers) Ltd, 1966.

42. Waddon A.J., Hill M.J., Keller A and Blundell D.J. On the crystal texture of linear polyaryls (PEEK, PEK and PPS). J.Mat .Sci, 22, 1773-1784, 1987.

43. Hay J.N and Kemmish D.J. The conformation of crystalline poly (aryl ether ketone). Polymer Communications, 30, 77-80, 1989.

44. Fratini A.V., Cross E.M., Whitaker R.B and Adams W.W. Refinement of the structure of PEEK fibre in an orthorhombic unit cell. Polymer, 27, 861-865, 1986.

45. Kumar S., Anderson D.P and Adams W.W. Crystallization and morphology of poly (aryl-ether-ether-ketone). Polymer, 27, 329-336, 1986.

46. Jog J.P and Nadkarni V.M. Crystallization kinetics of polyaryl ether ketones. J.Appl.Poly.Sci, 32, 3317-3322, 1986.

47. Blundell D.J Crystalline morphology of the matrix

and Osborn B.N. of PEEK-Carbon fibre aromatic polymer composites II. Crystallization behaviour. Sampe Quaterly, 17 (1), 1-6, 1985.

48. Lovinger A.J and Davis D.D. Electron microscopic investigation of the morphology of a melt-crystallized polyaryletherketone. J.Appl.Phys, 58(8), 2843-2853, 1985.

49. Wakelyn N.T. On the structure of poly (etherether ketone), PEEK. Polymer Communications, 25, 306-308, 1984.

50. Bassett D.C., Olley R.H and Al Raheil I.A.M. On crystallization phenomena in PEEK. Polymer, 29, 1745-1754, 1988.

51. Blundell D.J., Crick R.A., Fife B., Peacock J., Keller A and Waddon A. Spherulitic morphology of the matrix of thermoplastic PEEK/Carbon fibre aromatic polymer composites. J.Mat. Sci, 24, 2057-2064, 1989.

52. Seferis J.C. Polyetheretherketone (PEEK): Processing, structure and property studies for a matrix in high performance composites. Polymer Composites, 7(3), 158-169, 1986.

53. Deslandes Y., Day M., Sabir N.F and Suprunchuk T. Crystallization of poly(aryl-ether-ether-ketone): Effect of thermal history of the melt on crystallization kinetics. Polymer Composites,

10(5), 360-365, 1989.

54. Cebe P and Hong Su-Don. Crystallization behaviour of poly (ether-ether-ketone). Polymer, 27, 1183-1192, 1986.

55. Hay J.N and Kemmish D.J. The crystallization of PEEK, a poly aryl etherketone: molecular weight effects. Plastics and Rubber: Processing and Applications, 11(1), 29-35, 1989.

56. Choe C.R and Lee K.H. Non-isothermal crystallization kinetics of poly(etheretherketone), PEEK. Polymer Engineering and Science, 29(12), 801-805, 1989.

57. Carpenter J.F. Thermal analysis and crystallization kinetics of high-temperature thermo-plastics. Sampe Journal, 36-39, Jan/Feb, 1988.

58. Mishra A.K and Schultz J.M. Effects of flow rate and temperature on crystallization kinetics, crystallinity index and elastic modulus of PEEK. J.Appl.Poly.Sci, 38, 655-666, 1989.

59. Deslandes Y and Alva Rosa E. Characterization ofpoly(ether-ether -ketone) films by microindentation. Polymer Communications, 31, 269-272, 1990.

60. Jones D.P., Mechanical properties of poly(ether-

Leach D.C and Moore D.R. ether-ketone) for engineering applications. Polymer, 26, 1385-1393, 1985.

61. D'Amore A., Cocchini F., Pompo A., Apicella A and Nicolais L. The effect of physical ageing on long term properties of poly-ether-ether-ketone (PEEK) and PEEK based composites. J.Appl.Poly.Sci, 39, 1163-1174, 1990.

62. Barton J.M., Lloyd J.R., Goodwin A.A and Hay J.N. Thermal and mechanical properties of aryl ketone polymers and their composites. British Polymer Journal 23, 101-109, 1990.

63. Medellin-Rodriguez F.J and Phillips P.J. Crystallization and structure-mechanical property relations in poly(aryletheretherketone)[PEEK]. Polymer Engineering and Science, 30 (14), 860-869, 1990.

64. Karger-Kocsis J and Friedrich K. Temperature and strain rate effects on the fracture toughness of poly (etheretherketone) and its short glass fibre reinforced composite. Polymer, 27, 1753-1760, 1986.

65. Kemmish D.J. Polyetheretherketone. Rapra review report 16, 2(4), 1989.

66. Neuhaeusl E., Linhart J and Control of filling and hold on stages of an injection moulding

Rybnicek L. cycle with respect to quality of thermoplastics injection mouldings. Plasty a Kaucuk, 24(3), 77-82, 1987.

67. Whelan A.F. Injection moulding machines. Barking Elsevier Applied Science Publishers Ltd, 1984.

68. Aggarwal S.L and Tilley G.P. Determination of crystallinity in polyethylene by X-Ray Diffractometer J.Poly.Sci, 18, 17-26, 1955.

69. Chung F.H and Scott R.W. A new approach to the determination of crystallinity of polymers by X-Ray Diffraction. J.Appl.Cryst, 6, 225-230, 1973.

70. Campbell D and White J.R. Polymer characterisation. Physical techniques. Chapman and Hall, 1989.

71. Field J.E., Gorham D.A., Hagan J.T., Matthewson M.J., Swain M.V and van der Zwaag S. Liquid jet impact and damage assessment for brittle solids. Proc 5th.Int.Conf on erosion by solid and liquid impact, 13.1-13.11, 1979.

72. Jenkins D.C. Erosion of surfaces by liquid drops. Nature, 176, 303-304, 1955.

73. Hurley C.J and Schmitt Jr, G.F. Development and calibration of a mach 1.2 rain erosion test apparatus AFML-TR-70-240, AD No. A175-909, Oct 1970.

74. Field J.E., Camus J.-J., Gorham D.A and Rickerby D.G. Impact damage produced by large water drops. Proc.4th.Int.Conf on rain erosion and allied phenomena, 395-419, Meersburg 1974.

75. Gorham D.A and Rickerby D.G. A hydraulic strength test for brittle surfaces. J.Phys. E,8,794-796, 1975.

76. Savadori A. Impact testing of plastics: Present knowledge. Polymer Testing, 5, 209-241, 1985.

77. Hsiung C-M., Cakmak M and White J.L. Crystallization phenomena in the injection moulding of polyether etherketone and its influence on mechanical properties. Polymer Engineering and Science, 30(16), 967-980, 1990.

78. Day M., Suprunchuk T., Deslandes Y and Wiles D.M. The thermal processing of poly(ether etherketone)(PEEK): Some of the factors that influence the crystallization behaviour. 34th Int.Sampe symposium, 1474-1485, 1989.

79. Karger-Kocsis J., Walter R and Friedrich K. Annealing effects in the fatigue crack propogation of injection moulded PEEK and its short fibre composites. J.Poly.Eng, 8(3-4), 221-255, 1988.

80. Talbott M.F., Springer G.S The effects of crystallinity on the mechanical properties of PEEK

and Berglund L.A. polymer and graphite fibre reinforced PEEK. J.Comp.Mat, 21, 1056-1081, 1987.

81. D'Amore A., Pompo A and Nicolais L. Viscoelastic effects in poly(ether etherketone)(PEEK) and PEEK based composites. Composites Science and Technology, 42, 1-23, 1991.

82. Wolfe S.V and Tod D.A. Characterization of engineering polymers by Dynamic Mechanical Analysis. J.Macromol.Sci-Chem., A26(1), 249-272, 1989.

83. Goodwin A.A and Hay J.N. Relaxation spectra of amorphous and crystalline poly(aryl-ether-ether-ketone). Polymer Communications, 30, 288-293, 1989.

84. Brandrup J and Immergut E.H. Polymer Handbook, 3rd Edition. John Wiley and Sons, Inc, 1989.

85. Heijboer J. Dynamic mechanical properties and impact strength. J.Poly.Sci:Pt C (16), 3755-3763, 1968.

86. Berry B.W. Fracture Toughness. ISI Publication 121, The Iron and Steel Institute, 1968.

87. Gorham D.A and Field J.E. The failure of composite materials under high-velocity liquid impact. J.Phys.D: Appl.Phys., 9, 1529-1541, 1976.

88. Fyall A.A and Smith P. Single impact studies of rain erosion. Part 1. Preliminary evaluation. R.A.E, technical report 69086, April 1969.

89. Fyall A.A. Single impact studies with liquids and solids. Proc.2nd.Int.Conf on rain erosion and allied phenomena, 563-591, Meersburg, 1967.

90. Rayleigh Lord. Proc.Lond.Math.Soc, 17, 4, 1885.

91. Perel'man R.G and Denisov Yu.D. The strength of materials under the action of droplet impacts. Problemy Prochnosti, 10, 20-26, 1971.

92. Cowie J.M.G. Polymers: Chemistry and Physics of modern materials. International Textbook Co.Ltd. 1973.

93. Williams J.G and Birch M.W. The impact testing of polymers- A reassessment. Fracture 1977, Vol 1, ICF4, 501-528, 1977.

94. Plati E and Williams J.G. Effect of temperature on the impact fracture toughness of polymers. Polymer, 16, 915-920, 1975.

95. Vincent P.I. Impact tests and service performance of thermoplastics. The Plastics Institute, 1971.

96. Anon. ICI bulletin VP2, Oct 1987.

97. Richardson M.O.W. (editor) Polymer Engineering Composites. Applied Science Publishers Ltd,1977.

98. Baird M.E. Electrical properties of polymeric materials. The Plastics Institute, 1973.

99. Corney N.A. Technical report, R.A.E(F) MT/ 33/4/2. Materials and Structures Department, 1984.

100. Mayor R.A., Welsh E.A and Ossin A. Material selection for cost effective millimeter wave radomes. Sampe Quaterly, 1-7, April 1980.

101. Huth J.H., Thompson J.S and Valkenberg M.E. Some new data on high speed impact phenomena. J.Appl.Mech, 24, 1, 1957.

102. Heymann F.J. A survey of clues to the relationship between erosion rate and impact parameters. Proc.2nd.Int.Conf on rain erosion and allied phenomena. Meersburg, 1967.

103. Ward I.M. Mechanical properties of solid polymers. Second Edition. John Wiley & Sons, 1979.

8.0. Appendix

8.1.0. Introduction.

This appendix has been introduced at the end of the dissertation to explain in more detail some of the procedures used. These could not be discussed fully in the main body of the thesis, but the reader is now given some further information on the following areas;

8.1.1. A discussion of the features of injection moulding and the sample structure resulting from the process.

8.2.0. The background to the use of the Arrhenius equation to describe molecular mobility.

8.3.0. Limitations on the use of fracture mechanics in relation to polymers.

8.1.1. Injection moulding.

8.1.2. Melt flow.

When a thermoplastic polymeric material is heated it will soften and if sufficient pressure is applied it will deform and eventually flow. The science of deformation and flow of materials falls under the general heading of Rheology. Polymer rheology is particularly important since most processing methods rely on deforming a polymer melt into a pre-determined shape and its subsequent solidification in that shape. There are two main types of flow.

(i) Shear flow.

This is the most important process in polymer liquids. These differ from simple liquids in that the shear viscosity is extremely large and secondly that Newton's equation giving a linear relationship between shear stress (τ) and shear rate ($\dot{\gamma}$) with constant shear viscosity (μ), namely:

$$\tau = \mu \dot{\gamma} \qquad (1)$$

does not apply.

As the shear stress increases the polymer liquid yields and this behaviour is known as pseudoplasticity or shear thinning. The conditions of processing equipment are adjusted to make use of this reduction in shear viscosity with increasing shear stress.

(ii) Elongational flow.

This type of flow may be one of three kinds,

viz. tensile, stretching or free surface flow. Elongational flow is important in film processing, fibre forming, blow moulding and vacuum forming. In ideal extensional flow, planes normal to the extension direction remain planes and remain normal to the extension direction, but their areas decrease uniformly.

A difference between extensional flow and shear flow is that when the latter is steady (constant shearing rate) all particles have constant velocity, but when an extensional flow is steady (constant extension rate) all fluid particles are being accelerated with respect to one another. This will have two main effects;

a) In all liquids, if the extension rate is quick enough, the internal effects of the accelerations can effect the shape of a drawn filament for example.

b) In viscoelastic liquids, the accelerating lengths of material lines in the liquid produce an elastic contribution to the equilibrium stress/strain relationship, so that there may be a dependence of the tensile viscosity (tensile stress ÷ extension rate) on the extension rate that is different from the dependence of the same liquid's shearing viscosity on the shearing rate. For many polymers the tensile viscosity increases rapidly with extension rate even when the shearing viscosity is decreasing with the increasing shear rate.

8.1.3. Flow into a mould.

The flow of the molten polymer mass is driven by pressure. The pressure is necessary to cause the

molten polymer to flow through the nozzle, sprue, runner, gate and finally into the mould cavity.

The melt enters the mould (usually maintained at temperatures lower than the melt to ensure solidification) and the material next to the cold mould wall will be the first to solidify, with a moving central core of molten material taking longer to cool (figure 8.1).

The filling process relies on how well the polymer flows and the heat flow to the mould. In the case of semi-crystalline polymers this effect can lead to a skin/core structure as mentioned in chapter 4.0 (page 87) of this thesis. A completely amorphous skin was observed with a highly crystalline core developing at the centre of the moulding. The first sample prepared for experimentation in this dissertation showed a skin core structure , visible to the naked eye. The final processing conditions subsequently used ensured that this was kept to a minimum (until no evidence of a visible skin/core structure was seen). Further annealing of the samples would have altered any skin/core morphology towards a more homogenous structure.

It would have been extremely difficult to obtain moulded samples without any skin/core differences at all, and attempts were made to keep these to an absolute minimum. Scanning electron microscopy of samples damaged by water droplet impact and subsequently fractured in impact tests, illustrate that the cracks extend towards the centre of the moulding by as much as 0.5mm in some cases. This

would mean that if a skin/core structure were present, the effects of the skin were negligible as the damage had definitely extended beyond this. Moreover, the damage patterns observed were comparable to the ones found in the literature, giving weight to the proposition that the skin/core structure and any other moulding peculiarity, did not effect the results).

8.1.4. Orientation and frozen-in stresses.

Examination of moulded samples in general may show a pattern of orientation which can be seen in figure 8.2. The skin layer displays molecular orientation determined by the state of the material laid down from the melt front as the latter passes by the cold mould wall. The next layer displays an orientation consistent with the melt undergoing uni-directional shear while the central core is relatively free from preferred orientation and corresponds to solidification from an undisturbed melt.

Other effects that have been observed are a result of thermal stresses developed in a material solidifying at rest. The final cooling of a moulding that solidifies while significant symmetric temperature gradients exist in the material leads to compressive stresses on the outer skin and tensile stresses in the core. Any asymmetry in these patterns can lead to buckling of the article before or during annealing (not observed for samples prepared for the work in this dissertation).

Figure 8.1. Flow of molten polymer in to a mould.

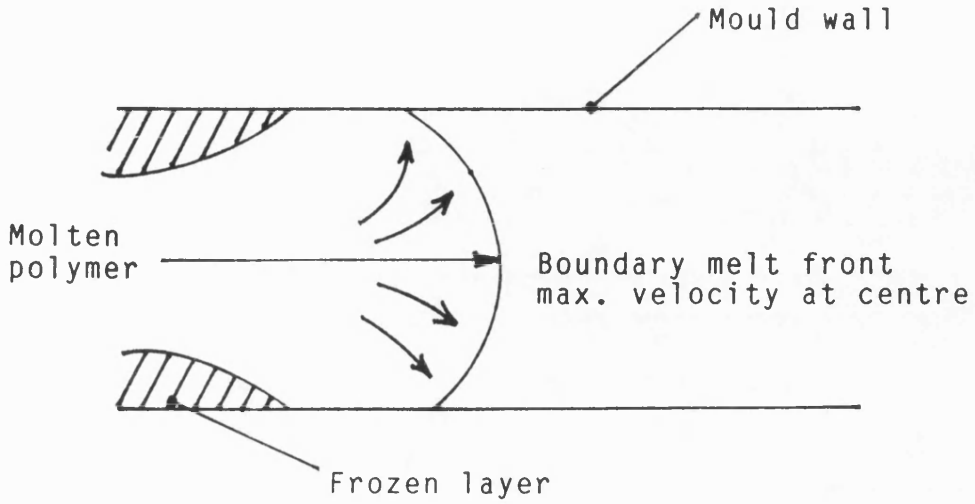

Figure 8.2. The orientation of the moulding.

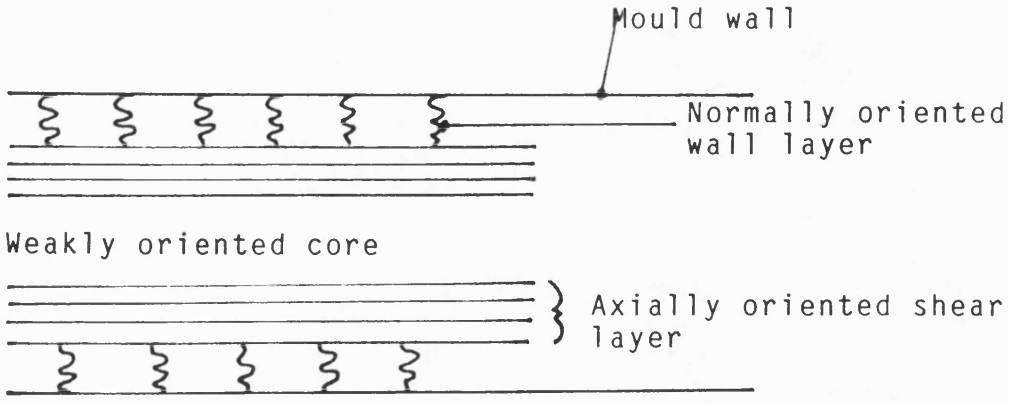

8.1.5. Concluding remarks.

To summarise the information outlined above, it can be said that injection moulding of samples can lead to the production of an article with differing skin/core morphology and molecular orientation together with the presence of internal stresses. It is recognised that these may effect experimental evaluation of materials, but it is felt that these effects did not contribute to a great extent to the results obtained and the damage patterns seen. It must be remembered that the processing conditions for all three polymers were very similar and so any orientation/internal stress effects would have been a constant factor allowing comparison of results between the materials, to be valid.

8.2.0. The Arrhenius expression.

A large class of transformations in materials are temperature-dependent. The rates of these transformations are controlled by the existence and nature of any barriers retarding the reaction.

The Swedish chemist Arrhenius observed that the increase in rate of chemical reactions with increased temperature could be expressed by;

$$\text{rate constant} = \text{constant} \times e^{-Q/RT} \qquad (2)$$

where Q is the 'activation energy', R is the gas constant, T the absolute temperature and the constant being temperature independent. A simple model in which reactants have to surmount an energy barrier of height Q (activation energy) before forming the product, rationilizes the relationship (see figure 8.3)

The dependence of reaction rate with temperature is specified by the activation energy. The exponential dependence of temperature resembles that of a Maxwell-Boltzmann distribution, where the exponential term is proportional to the number of molecules having an energy greater than Q, ie a sufficient energy to overcome the activation energy barrier. The exponential term describes the form of the distribution whilst the pre-exponential term (the Arrhenius constant, A) is described by the Collision Theory and is identified as a collision frequency that can be calculated from kinetic theory;

$$A = P.Z \qquad (3)$$

Figure 8.3. Energy changes in an exothermic reaction.

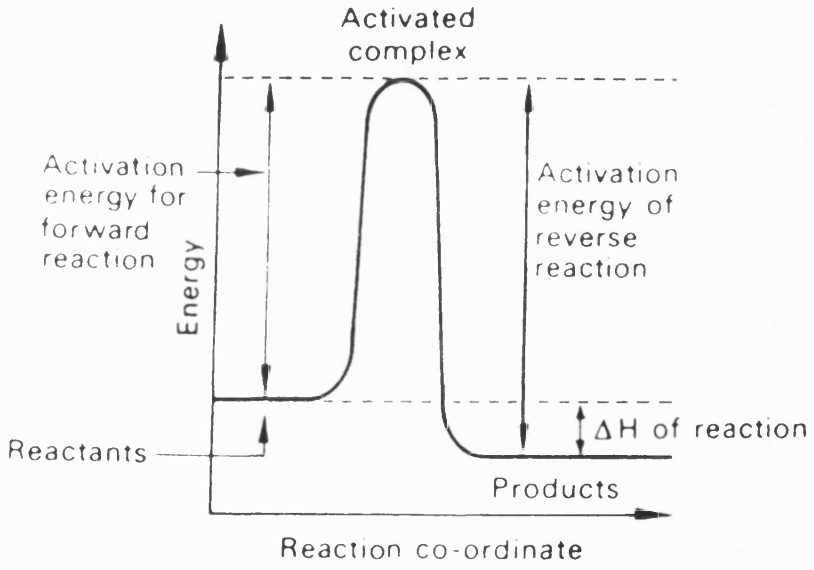

where P is a `probability factor' (collision will lead to a reaction) and Z being the frequency.

Basically if enough thermal energy is available the probability of there being sufficient energy to overcome the barrier is increased.

8.2.1. Motion of polymer chains.

Viscoelastic effects can be regarded as thermally activated movements of molecular segments under an imposed mechanical stress. A simplified description is given for a monoatomic system. Barriers for the atom to move from one equilibrium position to another, are as a result of constraints provided from neighbouring atoms. For the atom to pass between its neighbours, an elastic distortion is required. The probability of achieving the distorted structure is very small. Normally atoms approach their neighbours and are reflected back, but sometimes a thermal fluctuation occurs allowing the atom to pass through the barrier to the neighbouring potential well.

The application of movement within a polymer must take into account the elastic distortion of the surrounding molecules, the availability of a `free' volume for the moving chain segment to occupy and the energy needed to facillitate this molecular motion.

Eyring introduced the concept that upon the application of a shear stress the barrier height for the molecule to pass is modified, so that in the direction of the stress, the rate of segment jumping

becomes fast enough to result in a strain change. In the absence of stress, the frequency of this jumping is the same but on the application of stress, the forwards and reverse jumping occur at differing frequencies resulting in the calculation of the strain rate.

Dynamic mechanical data of polymers are often dealt with in terms of the Arrhenius equation in some form or another. In most cases this is only an approximate treatment due to the limited range of experimental frequencies. In general it has been found that the temperature dependence of the glass transition relaxation behaviour of amorphous and crystalline polymers does not fit a constant activation energy, in contrast to more localized molecular relaxations.

Above the glass transition temperature the free volume increases very rapidly and the associated jump frequency ν can be expressed by the Macedo-Litowitz theory ;

$$\nu \propto \exp - \left(\gamma \frac{V_o}{V_f} \right) \qquad (4)$$

where γ is a numerical factor between 0.5-1.0 to account for the overlap of volumes, V_o the molar volume of jump unit associated with zero free volume and V_f the molar free volume of the jump unit.

When equation 4 is combined with the Arrhenius approach, for the temperature variation of viscosity,

η (and by extension the viscoelastic functions) the following equation is obtained;

$$\eta = A \exp(Q/kT) . \exp(\gamma V_o/V_f) \qquad (5)$$

where k is Boltzmann's constant.

Equation 5 provides a reason as to why the simple Arrhenius relationship is a poor estimate, as the term: $\exp(\gamma V_o V_f)$, is strongly temperature dependent above the glass transition temperature.

8.2.3. Concluding remarks.

The theories behind the use of the Arrhenius expression in describing molecular movement of polymers, have been briefly described. The Arrhenius analysis was used to describe the viscoelastic properties of PEEK, PEK and PET, and the validity of the expression was questioned, with respect to the astronomical values obtained for the pre-exponential factor, A.

To question the validity of the Arrhenius expression is nothing new (see equation 5), as it has been derived to measure molecular motion at the glass transition and this process must be a result of a combination of all molecular movements (segmental motion to small group rotation). This has been cofirmed to some extent within the main text of this thesis, where the activation energy for the glass transition process was calculated at $\approx$ 700 $kJmol^{-1}$ (PEEK), whilst for the lower order transition (cessation of movement of a smaller portion of the

chain) an activation energy of ≈ 47 $kJmol^{-1}$ was measured (see pages 107 and 113). It must be mentioned that the results obtained were calculated over a small temperature range and in so doing would allow for a great deal of error when determining the pre-exponential factor, A (extrapolating back to zero 1/T).

The Arrhenius expression underestimates the temperature effects when analysing molecular motion, it is clearly not valid over a wide temperature range for the reasons outlined above.

8.3.0. Fracture mechanics.

Fracture can be defined simply as the creation of new surfaces within a body through the application of external forces. Brittle solids fracture because the applied stress is amplified by minute cracks of the order of 1μm in size, which occur naturally and are termed Griffith cracks after the originator of the thermodynamic theory of the fracture strength of cracked brittle bodies.

8.3.1. The concept of stress concentration.

Any material which contains a geometrical discontinuity will experience an increase in stress in the vicinity of the discontinuity. This stress concentration effect is caused by the re-distribution of lines of force transmission through the material when they encounter discontinuities such as Griffith cracks, holes, notches or corners. It is implied that as the crack becomes sharper (ie the crack tip radius tends towards 0) then the material containing this crack would not be able to withstand the application of any stress. This is not true and the stress concentration approach is not suitable for allowing for the effects of cracks. This has given rise to the use of fracture mechanics. A simplifying assumption that the cracked body obeys Hooke's law is often made and the fracture analysis based on this assumption, is referred to as ` Linear Elastic Fracture Mechanics ', (LEFM).

8.3.2. LEFM.

To overcome the difficulties associated with sharp cracks, parameters have been defined which relate to the applied stress and the crack size to allow a toughness or resistence to crack propagation to be measured. Basically there are two approaches to the fracture of a material;

a) The microscopic model involves the rupture of atomic or molecular bonds. The force necessary to rupture these bonds is usually many times greater than the measured strength of the material because it does not take into account the stress concentration effect.

b) The continuum model treats the solid as a continuum rather than as an assembly of molecules. It is recognised that failure initiates at defects and the strength predictions are made on the basis of the stress system and the energy release processes around the crack.

8.3.3. Griffith theory.

Griffith based his theory on two propositions. First, rupture produces a new surface area and for rupture to occur the increase in energy required to produce the new surface must be balanced by a decrease in elastically stored energy. Secondly, the elastically stored energy is not distributed uniformly throughout the specimen but is concentrated in the neighbourhood of small cracks. Fracture thus occurs due to the spreading of cracks which originate in pre-present flaws. The fracture stress, σ_f of a plate with a small eliptical crack, which is stressed

at right angles to the axis of the crack can be obtained from;

$$\sigma_f = \left(\frac{2E\gamma}{\pi a}\right)^{0.5} \qquad (6)$$

where a is the crack length, E is Young's modulus and γ is the surface energy.

This approach assumes that for any material the fracture stress is controlled by the size of the flaw present in the material. The strength of the material can be increased by reducing the size of the flaw. However, in practice this rise in strength does not continue indefinitely as the material contains inherent flaws and so the introduction of smaller artificial flaws does not effect the strength.

The surface energy of the material can be calculated from the above equation and results in values very much greater than the actual values of surface energy. This discrepancy arises because the Griffith equation assumes that the material behaves elastically and does not undergo any plastic deformation. It is known that even in brittle materials a small amount of plastic deformation occurs at the tip of the crack. The energy absorbed during this deformation is much higher than the surface energy. Irwin and Orowan modified the Griffith equation to account for this.

$$\sigma_f = \left(\frac{2(\gamma + \gamma_p)E}{\pi a}\right)^{0.5} \qquad (7)$$

where Y_p is the work done in plastic deformation per unit area of crack surface. The term $2(Y + Y_p)$ is denoted by G_c, which is the critical strain energy release rate or crack extension force, so that equation 5, can be written as;

$$\sigma_f = \left(\frac{EG_c}{\pi a}\right)0.5 \qquad (8)$$

This only applies for plane stress conditions (thin sheets). For plane strain (thick sheets) the introduction of Poisson's ratio and G_{ic} (critical value of fracture toughness under plane strain) are required.

In a thick plate, the thickness at the tip of a stressed crack does not decrease by Poisson's contraction (plane strain) while in thin plates the thickness of the plate decreases and plane stress conditions occur at the crack tip.

Irwin further modified these equations and observed that the stresses at the crack tip are inversely proportional to $(\pi a)^{\frac{1}{2}}$. On this basis he defined the the stress intensity factor, K_1 which characterises the elastic stress field around a crack tip. Failure will occur when K_1 reaches a critical value defined as the critical stress intensity factor, K_{ic}.

$$K_{ic} = \sigma_f (\pi a)^{\frac{1}{2}} \qquad (9)$$

This equation needs further modification to allow for the geometry of the sample. In reality bodies have finite dimensions, they can be loaded in

flexure rather than just tension and they may have more than one starting crack. In passing from one loading configuration and geometry to another all that changes is K and so a dimensionless parameter is introduced;

$$K_i = \sigma_f \, Y(a/W) \, a^{\frac{1}{2}} \qquad (10)$$

where Y is the shape factor and W is the sample width.

It is sometimes more convenient to use G_{ic} rather than K_{ic} to characterise the fracture behaviour of materials, especially as G_{ic} is an energy parameter and can be related more easily to energy absorbing fracture processes. If the value of K_{ic} is known then G_{ic} can be determined from;

$$K_{ic} = \left(\frac{EG_{ic}}{1-\mu^2} \right)^{0.5} \qquad (11)$$

where μ is Poisson's ratio.

Care is required as the rate of testing alters the values of E and Y_p, and it is not always obvious which rate of testing is appropriate for the fracture experiment.

8.3.4. Concluding remarks.

The use of fracture mechanics and its limitations have been outlined. It was necessary to discuss this as it has been found in this dissertation that the use of fracture mechanics was not applicable under the conditions used. Altering

the sample geometry, test temperature and rate of testing could all have been employed to analyse the fracture properties more effectively.

It must be remembered that the experiments were carried out for comparative purposes only and to provide base values for subsequent analysis of impact by a water droplet. The rates chosen were arbitary, but constant throughout the experimental procedure and they were chosen to show the comparative toughness of the materials, where it was found that the notched toughness of PEK was superior to PEEK and PET. The use of the 3-Point bend analysis was to add another dimension, as very high rates of impact were being investigated in the Ceast impact and the water drop impact, to allow further comparisons to be drawn (ie was PEEK still inferior to PEK at greatly reduced impact rates).

Appendix References.

J.R.A.Pearson. Mechanics of polymer processing. Elsevier Applied Science Publishers Ltd, 1985.

J.M.McKelvey. Polymer processing. John Wiley & Sons, Inc, 1962.

R.J.Crawford. Plastics Engineering, 2nd Edition. Pergamon Press, 1987.

J.H.Brophy, R.M.Rose and J.Wulff. The structure and properties of materials, Vol 2. Thermodynamics of structure. John Wiley & Sons, Inc, 1964.

N.G.McCrum, C.P.Buckley and C.B.Bucknall. Principles of polymer engineering. Oxford University Press, 1988.

I.M.Ward. Mechanical properties of solid polymers, 2nd Edition. John Wiley & Sons, Inc, 1979.

V.D.H.Kaelble. Physical chemistry of adhesion. John Wiley & Sons, Inc,

G.N.Gilmore. A modern approach to comprehensive chemistry. Stanley Thornes (Publishers) Ltd, 1977.